Synthesis and characterization of nanomaterials for uptake of radio nuclides and toxic metal ions

By

JOYEETA MUKHOPADHYAYA

Enrollment No. CHEM. 01201104025

BHABHA ATOMIC RESEARCH CENTRE, MUMBAI

A thesis submitted to the
Board of Studies in Chemical Sciences
In partial fulfillment of requirements
For the Degree of
DOCTOR OF PHILOSOPHY
of
HOMI BHABHA NATIONAL INSTITUTE

August 2017

Homi Bhabha National Institute[1]

Recommendations of the Viva Voce Committee

As members of the Viva Voce Committee, we certify that we have read the dissertation prepared by **Smt. Joyeeta Mukhopadhyaya** entitled **“Synthesis and characterization of nanomaterials for uptake of radionuclides and toxic metal ions”** and recommend that it may be accepted as fulfilling the thesis requirement for the award of Degree of Doctor of Philosophy.

Sudhir Kapoor 12.12.2017

Chairman : **Prof. S. Kapoor** **Date:**

12.12.2017

Guide / Convener: **Prof. A. K. Tyagi** **Date:**

Co-guide - (if any) **Date:**

RNagarajan 12.12.2017

Examiner : **Prof. R. Nagarajan** **Date:**

Raghunath Acharya

Member : **Dr. R. Acharya** **Date:** 12/12/2017

Sudarsan V

Member : **Dr. V. Sudarsan** **Date:** 12/12/2017

Member : **Dr. (Mrs) J. Ramkumar** **Date:**

Final approval and acceptance of this thesis is contingent upon the candidate’s submission of the final copies of the thesis to HBNI.

I/We hereby certify that I/we have read this thesis prepared under my/our direction and recommend that it may be accepted as fulfilling the thesis requirement.

Date: 12.12.2017

Place: BARC, Mumbai

(Signature)

Guide

डॉ. ए. के. त्यागी/Dr. A. K. Tyagi
अध्यक्ष, नाभिकीय एवं ऊर्जा पदार्थ अनुभाग
Head, Nuclear & Energy Material Section
रसायनिकी प्रभाग/Chemistry Division
भा.प.अ.केंद्र/B.A.R.C.
ट्रॉम्बे, मुंबई-४०००८५./Trombay, Mumbai-400085.

---

[1] This page is to be included only for final submission after successful completion of viva voce.

I was not present during the viva, however I agree with the content of thesis Jayashree 1/1/18

STATEMENT BY AUTHOR

This dissertation has been submitted in partial fulfillment of requirements for an advanced degree at Homi Bhabha National Institute (HBNI) and is deposited in the Library to be made available to borrowers under rules of the HBNI.

Brief quotations from this dissertation are allowable without special permission, provided that accurate acknowledgement of source is made. Requests for permission for extended quotation from or reproduction of this manuscript in whole or in part may be granted by the Competent Authority of HBNI when in his or her judgment the proposed use of the materials in the interests of scholarship. In all other instances, however, permission must be obtained from the author.

Joyeeta Mukhopadhyaya.

(Joyeeta Mukhopadhyaya)

DECLARATION

I, hereby declare that the investigations presented in the thesis have been carried out by me. The work is original and has not been submitted earlier as a whole or in part for a degree / diploma at this or any other Institution / University.

Joyeeta Mukhopadhyaya.

(Joyeeta Mukhopadhyaya)

List of Publications arising from the thesis

Journals

1. Sorption characteristics of nano manganese oxide: efficient sorbent for removal of metal ions from aqueous streams

Joyeeta Mukherjee, Jayshree Ramkumar, S. Chandramouleeswaran, R. Shukla and A. K. Tyagi

J. Radioanal.Nucl. Chem. 297 (2013) 49–57

2. Uptake of Cs and Sr radionuclides within oleic acid coated nanomagnetite - hematite composite

Joyeeta Mukhopadhyay, Pranesh Sengupta, D. Sen, S. Mazumdar and A.K. Tyagi J. Nucl. Mater. 467 (2015) 512-518

3. A comprehensive study on the uptake of dyes, Cu (II) and radioactive ^{137}Cs (I) by sonochemically synthesized strontium / yttrium tungstate and molybdate nanoparticles **Joyeeta Mukherjee**, Dimple P. Dutta, J. Ramakumar and A.K. Tyagi J. Environ. Chem. Eng. 4 (2016) 3050-3064

Conference proceedings

1. Characterization of nano-magnetite developed for environmental clean-up

Joyeeta Mukherjee, Sunita Dafauti, Ruby Singh, Sanjay Kumar Jha, Jayashri Ramkumar, A. K. Tyagi, Geogy Abraham, Pranesh Sengupta, G.K. Dey

International Conference on Electron Microscopy and XXXIV Annual Meeting of Electron Microscope Society of India (EMSI), Kolkata (July 2013)

2. Separation of low concentration of cesium from aqueous solution using silica coated nano- magnetite

Joyeeta Mukherjee, Pranesh Sengupta and A K Tyagi

Theme meeting on Chemistry in Nuclear Technology, CHEMNUT-2015, July 30-31, 2015, Kalpakkam, Chennai.

Dedicated to

My Beloved Maa & Baba

Latika Mukhopadhyay

&

Arup Kumar Mukhopadhyay

Acknowledgements

It feels great satisfaction and joy to present my dissertation work and acknowledge those who have really matters me the most. First and foremost I would like to thank my research guide Dr. A. K. Tyagi, Head, Solid State Chemistry Section, Chemistry Division, BARC, Mumbai from the bottom of my heart for his valuable guidance, rock solid support, encouragement and valuable suggestions throughout my research work. The best part of him is optimistic attitude towards any situations has helped me a lot to overcome any difficulties throughout my research work.

My especial gratitude to Dr. Jayshree Ramkumar, Dr. Pranesh Sengupta, Dr. Dimple P. Dutta, without their guidance, help and support the completion of the thesis would have been difficult. I have learnt a lot from them. Jayshree madam has first introduced me to the world of sorption studies and to work in her laboratory and I will always cherish the moments with her. The experience and knowledge I gained from Dimple maam was always very knowledgeable. The discussions with Pranesh sir were enriching and his active support I will always reminisce.

I would like to thank all the doctoral committee members including respected chairman, Dr. S. Kapoor and earlier chairperson Dr. Shyamala Bharadwaj for their constructive and critical evaluation of my work during the course of the studies. Special thanks for valuable comments are for all the doctoral committee members. I would like to mention Dr. P N Pathak sir who is no more among us for his valuable suggestions.

I am thankful to Dr. D. N. Sharma, Ex Director, and Dr. Pradeep Kumar, Associate Director, Health,Safety and Environmental Group, BARC, Mumbai and Dr. R. M. Tripathi, Head, Health Physics Division, BARC, Mumbai for allowing me to avail all the facilities at the division required for the completion of the work.

It is also my great pleasure to thank Dr Tapas Bandyopadhyay and Dr. (Mrs) Vandana Pulhani for their support in carrying out the research work. My sincere thanks are due to Dr. P. K. Sarkar (Ex-Head, HPD) for granting me permission for doing this work and Dr. Pramila Sawant for her encouragement and giving me permission to work in her lab at any time. Special thanks to my friends' ankita, seemita, moushumi, bholanath for their help. I am very thankful to my colleagues in BARC Vikram Joshi, Sunita Dafauti, Sanu madam, Dr.Rakesh Shukla, Mohsin, Ms. Kruti for helping me a lot. It is with immense gratitude that I acknowledge the comments, suggestions and encouragement rendered by my Doctoral Committee members, for their support and valuable comments.

My gratitude and special thanks goes for the entire HP unit in RRCAT, Indore including Dr. G. Haridas (OIC), Dr. Nayak, Vijay, Sahani, Dimple, Sahu, Vipin, Dilip, Saleem and others for giving me a supporting environment to complete my thesis. I heartily acknowledge the help from P Podder Sir, Anita madam, Vikas, DG Mishra, Shriparna, Dr Sumit Kumar and my teachers. I thank all those who have helped me directly or indirectly in the successful completion of my thesis.

My parents who are no more in this world are always my source of inspiration. Without their vocal tonic and affection, I could not have finished my work. I am always indebted to them for all my achievements in life.,I heartily acknowledge the fact that my lovely sons Turjo and Tojo has endured me in the course of my study. There is no need of formal words to thank my entire family including my sisters Lopamudra Banerjee, Gargi Chatterjee, my only brother Krishnendu Mukherjee for their love and continuous support. Last but not least I would like to specially thank my husband Tushar for his support. I am thankful to the persons who have shown me no interest in my work so that I have become more determined to finish my work anyway. Finally I thank My Almighty for everything.

CONTENTS

SYNOPSIS I

LIST OF FIGURES XI

LIST OF TABLES XIV

Chapter1: Introduction 1-30

1.1 Introduction 2

1. 2 Types of water sources 2

  1.2.1 Ground-water 3

  1.2.2 Surface water 4

1.3 Radionuclide contamination 5

  1.3.1 Low level waste (LLW) 6

  1.3.2 Intermediate level waste (ILW) 7

  1.3.3 High level waste (HLW) 7

1.4 Properties of uranium and its effect on human health 8

1.5 Properties of cesium and its effect on human health 10

1.6 Properties of strontium and its effect on human health 14

1.7 Properties of hexavalent chromium and its effects on human health 17

1.8 Properties of copper and its effect on human health 18

1.9 Common removal techniques used for uranium (VI), cesium (I) and strontium (II) 19

1.10 Literature survey 20

  1.10.1 Literature survey for uranium removal 20

  1.10.2 Literature survey for cesium removal 22

  1.10.3 Literature survey for strontium removal 25

  1.10.4 Literature survey for chromium and copper removal 27

1.11 Scope of the thesis 28

Chapter 2 : Experimental methodology and characterization techniques 31-57

2.1 Introduction 32

2.2 General synthesis methods for preparation of nanomaterials 32

2. 2. 1 Solid state method 33

2. 2. 2 Top down methods 33

2. 2. 3 Bottom up methods 33

2. 2. 3.1 Synthesis of nano manganese oxide by alcoholic hydrolysis method 34

2. 2. 3.2 Co-precipitation method 35

2. 2. 3. 2. 1 Synthesis of nano magnetite 36

2. 2. 3. 2. 2 Importance of encapsulation of nanomaterials for certain applications 37

2. 2. 3. 2. 3 Synthesis of oleic acid coated magnetite 37

2. 2. 3. 2. 4 Synthesis of silica coated magnetite 38

2. 2. 3.3 Sonochemical method 38

2. 2. 3. 3. 1 Synthesis of $SrWO_4$ 39

2. 1. 3. 3. 2 Synthesis of $SrMoO_4$ 40

2. 2. 3. 3. 3 Synthesis of Y_2WO_6 40

2. 2. 3. 3. 4 Synthesis of $Y_2(MoO_4)_3$ 40

2.3 Characterization techniques 40

2. 3. 1 X ray diffraction 41

2. 3. 2 Transmission Electron Microscopy 44

2. 3. 3 Small Angle X Ray Scattering (SAXS) 44

2. 3. 4 Fourier Transform - Infra Red Spectroscopy

2. 3. 5 BET surface area analyzer 45

2. 3. 6 Dynamic Light Scattering for Zeta potential analyzer 46

2. 3. 7 Vibrating-Sample Magnetometer (VSM)

2. 3. 8 Gamma spectrometry using NaI (Tl) detector

2. 3. 9 UV-Vis absorption spectroscopy 47

2. 3. 10 Atomic absorption spectroscopy (AAS) 48

2. 3. 11 Inductively coupled Plasma-Atomic Emission Spectroscopy (ICP-AES) 48

2.4 Sorption Studies 50

2. 4. 1 Sorption isotherms 50

2. 4. 1. 1 Langmuir isotherm

2. 4. 1. 2 Freundlich isotherm 51

2. 4. 1. 3 Temkin isotherm 52
2 .4. 1. 4 Dubinin-Redushkevich isotherm 52
2. 4. 1. 5 Redlich-Peterson isotherm 53
2. 4. 1. 6 Sips isotherm 53
2.4.2 Sorption kinetics 54
2. 4. 2. 1 Pseudo first-order kinetic model 54
2. 4. 2. 2 Pseudo second-order kinetic model 54
2. 4. 2. 3 Elovich model 55
2. 4. 2. 4 Intraparticle diffusion model 55
2.5 Error Analysis 55
2.6 Conclusion 57

Chapter 3: Sorption of uranyl and other metal ions using nanocrystalline manganese oxide (MnO_2) sorbent 58-78

3.1 Introduction 59
3.2 Synthesis and characterization of nano manganese oxide 59
3.3 Sorption experiments 59
3.4 Results and discussions 59
3. 4. 1 Characterization of nano manganese oxide 62
3. 4. 2 Sorption studies 63
3. 4. 3 Modeling of the data 71
3. 4. 3. 1 Two parameter isotherms 71
3. 4. 3. 2 Three parameter isotherms 73
3. 4. 4 Sorption mechanism 77
3.5 Conclusions 78

Chapter 4: Sorption of radioactive cesium and strontium on nanocrystalline magnetite based sorbents 80-117

4.1 Introduction 81
4.2 Synthesis and characterization of magnetites 83
4.3 Sorption experiments 84
4.4 Results and discussion 84
4. 4. 1 Structural and micro-structural studies 84
4. 4. 2 Small angle X-ray scattering studies 87
4. 4. 3 Zeta potential study for surface charge 89

4. 4. 4 Magnetic properties study 91
4. 4. 5 Iron-leaching studies 92
4. 4. 6 BET sorption Isotherm study 93
4.5 Sorption studies 94
4. 5. 1 Effect of pH on cesium (I) and strontium (II) ion uptake 94
4. 5. 2 Effect of initial concentration on cesium (I) and strontium (II) ion uptake 96
4. 5. 3 Theoretical modelling of sorption data for cesium (I) and strontium (II) ion uptake 98
4. 5. 4 Non linear regression analysis of equilibrium isotherm models for cesium(I) sorption on magnetites 108
4.5.4.1 Calculation of error function 109
4.6 Sorption kinetics 113
4. 6. 1 Effect of time on uptake of cesium (I) and strontium (II) ion on magnetites 113
4.7 Conclusions 117
Chapter 5: Sorption of cesium(I), strontium(II) and chromium(VI) ions on MnO_2 118-129
5. 1 Introduction 119
5. 2 Synthesis and characterization of nano Manganese Di oxide 120
5. 3 Results and discussion 120
5. 3. 1 Characterization results 120
5. 3. 2 Sorption studies 121
5. 3. 2. 1 Effect of pH on cesium (I) and strontium (II) ion uptake 121
5. 3. 2. 2 Effect of initial concentration on cesium (I) and strontium (II) ion uptake 122
5. 3. 2. 3 Theoretical modeling of sorption data for cesium (I) and strontium (II) ion uptake 124
5. 3. 2. 3. 1 Sorption isotherms 124
5. 3. 2. 3. 2 Sorption kinetics 126
5. 4 Conclusion 129

Chapter 6 : Nanocrystalline molybdates and tungstates - potential 130-156 sorbents for removal of radio-nuclides,toxic metal ions and other species

6. 1 Introduction 131

6. 2 Synthesis and characterization 133

6. 3 Sorption studies 133

- 6. 3. 1 Copper removal experiments 133
- 6. 3. 2 ^{137}Cs uptake experiments 134
- 6. 3. 3 Dye sorption studies 134

6. 4 Results and discussion 134

- 6. 4. 1 Characterization results 134
- 6. 4. 2 Sorption of Cu (II) ions 139
- 6. 4. 3 Sorption of ^{137}Cs ions 141
- 6. 4. 4 Sorption of Dyes 142
    - 6. 4. 4. 1 Influence of pH 145
    - 6. 4. 4. 2 Influence of initial concentration of dye 146
    - 6. 4. 4. 3 Influence of weight of sorbent 146
    - 6. 4. 4. 4 Selective sorption of RhB by $SrWO_4$ 146
- 6. 4. 5 Isotherm studies 147
- 6. 4. 6 Kinetic modeling 149
- 6. 4. 7 Insight of sorption mechanism based on sorbent structure 153
- 6. 4. 8 Regeneration of sorbents 155

6. 5 Conclusion 155

Chapter 7: Summary and Future Scope 157-162

References 163-184

Synopsis

Rapidly growing urbanization of the global scenario and related living standard of present time drives human beings to use a smarter way to deal with the related environmental problems. One major problem with the technological upgradation of this century is ever increasing need to supply decontaminated ground water and surface water as well as other unconventional sources of waters which are generated due to anthropogenic activities. The challenges ahead for the mankind are accentuated global warming, pollution of total environment and hence related health hazards. For industrial sources it is mainly toxic metal ion contamination and for nuclear industry it is radiological waste. In this scenario, nanotechnology has vast potential for the removal of toxic metal ions and low level radiological waste treatment. Recently Fukushima nuclear accident showed the direct application of nanomaterials by using magnetic nanomaterials for area decontamination due to cesium radioactivity **[1, 2]**. About 130000 Bq of cesium activity contaminations were reported according to Tokyo Electric Power Company (TEPCO) **[3]**. Maximum radioactive cesium decontamination of the affected area was done by encapsulated magnetite. At the nanoscale level the advantages over conventional materials are high surface area to volume ratio, increased porosity, regeneration of the same materials, cost effectiveness and high efficiency for the waste water purification and subsequent treatment **[4-7]**. Although, there are several other removal techniques such as ion exchange method, membrane filtration, chemical precipitation electrochemical deposition, coagulation-flocculation, flotation **[8,9]** etc. Sorption by nanomaterials is gaining the importance due to their superior powder properties. Among the various types of nanomaterials, oxide-based nanomaterials have been used for adsorption studies of heavy metal ions **[10-12].**

Nanomaterials are defined as the materials as smaller than 100 nm in size at least in one dimension **[13]**. However, if the size becomes very small (e.g. less than 10 nm), the surface energy becomes very high, which results in agglomeration and in turn the high efficiency of nanomaterials is decreased. To overcome this problem, encapsulation (capping) of the nanomaterials is required to lower the surface energy **[14]**.

In nuclear reactors, ^{137}Cs and ^{90}Sr are produced as fission products. ^{137}Cs is highly gamma radioactive with a half life 30 years. It emits high gamma energy of 662 keV. ^{90}Sr is a fission product having a half-life of 28 years which is generated in the nuclear fuel cycle and has to be separated from nuclear waste. Similarly, most of the tannery industries discharge hexavalent chromium in wastewater, whereas copper and hexavalent chromium are among the list of toxic metals by-products from metal plating industry. Higher concentration level of heavy metals, more than the safe permissible limit, is lethal and detrimental for living beings. Thus the treatment of heavy metals is of special concern due to their recalcitrance and persistence in the environment **[15]**.The worst example of chromium contamination in groundwater in history till date happened in California, USA. **[16]**. Epidemiological data of cancer patients surrounding the contaminated area of California, USA is still higher than the background data **[17]**. Objective of the present study includes synthesis and characterization of porous high surface area nanomaterials and their sorption study for radionuclide (cesium- 137, strontium- 90 and uranium) and toxic metal ions (hexavalent chromium and divalent copper).

In this study, the simple metal nano-oxides as well as encapsulated nano-oxides have been synthesized for uptake study. Convenient bottom-up methods such as co - precipitation, alcoholic hydrolysis and sonochemical method were employed for synthesis of various nanomaterials. The synthesized nanomaterials such as manganese dioxide, magnetite, oleic acid coated haematite-magnetite composite materials, silica coated magnetite, strontium molybdate, strontium tungstate, yttrium tungstate and yttrium molybdate were characterized by FT-IR spectroscopy, Transmission Electron Microscopy, X-Ray Diffraction, BET surface area analyzer and Dynamic Light Scattering for zeta potential analyzer. Finally, uptake studies were performed using all this nanomaterials. Inductively Coupled Plasma –Atomic Emission Spectroscopy , Atomic Absorption Spectroscopy and UV-Vis Spectrophotometric techniques were employed for analyte’s concentration determination.

The studies carried out in the present work have been presented in different chapters. A brief overview of each chapter is given below.

Chapter1: Introduction

This introductory chapter gives an overview about the different sources of water like surface and groundwater, their contamination and radiological waste water treatment procedure for radio nuclides like cesium, strontium and uranium. The industrial effluent like hexavalent chromium and divalent copper contamination and their removal techniques have also been discussed. Among all the reported methods the sorption technique has been widely used for uptake studies of the above species. The chapter will give an insight into the different removal methods of cesium(I), strontium(II), uranium(VI), hexavalent chromium and copper(II) which have been used in literature. It will be emphasized that why it is necessary to remove these species from the waste water matrices. Different nanomaterials used by the earlier workers, their advantage and disadvantages over the other separation methods have also been discussed.

Chapter 2: Experimental Methodology and Characterization Techniques

In this chapter, different methodologies for synthesis and characterization of the nanomaterials have been discussed. Different oxide nanomaterials in powder form have been synthesized via co-precipitation, alcoholic hydrolysis, and sonochemical method. The detailed methodology of these synthesis processes has been discussed. For characterization of the synthesized materials, X-ray diffraction (XRD), Fourier Transform - Infra Red Spectroscopy, Transmission electron Microscopy, BET surface area analysis, Dynamic Light Scattering for Zeta potential analysis techniques have been employed. Basic theory and methodology of these characterization techniques have been elaborately discussed also. The sorption behaviors of nanomaterials are investigated by measuring remaining concentration of metal ions in solution after the uptake for a specified time. For this purpose, Atomic absorption spectroscopy (AAS), inductively coupled Plasma-Atomic Emission Spectroscopy (ICP-AES), UV-Vis absorption spectroscopy has been used. The detailed description of these analytical techniques has been discussed. Standard Radioanalytical technique of analysis has been used for analysis of the sorption of radioactive cesium(I) ions onto various synthesized nano-sorbents. The activity at fixed time intervals was measured by gamma spectrometry using NaI(Tl) detector. The analytical techniques and instrumentation used for the radiochemical assay was based on standard procedures as described in USEPA. **[18].** Basic theory behind the gamma spectrometry has also provided here.

Chapter 3: Sorption of uranyl ions using nanocrystalline manganese oxide (MnO_2) sorbent

In this chapter, sorption of uranyl along with interference of transition metal ions using nano manganese oxide (MnO_2) has been discussed **[19]**. Nanocrystalline manganese oxide was prepared and characterized using various techniques such as XRD, surface area analyzer and zeta potential measurements. Nanocrystalline manganese oxide was prepared by the hydrolysis of $KMnO_4$ and it was found to have a size of about 8 nm and surface area of 145 m^2/g. The sorption characteristics with respect to uptake of various metal ions including uranyl ions have been evaluated. Various experimental conditions which affect the sorption characteristics have been studied. Due to the high surface area, the sorption property of the nano MnO_2 was found to be excellent. Effect of pH, initial ion concentration and time for equilibration has been studied in batch mode sorption experiments. It has been observed that maximum uptake for the different metal ions differ significantly, thus providing a means for separating the metal ions from one another. At lower pH values, the uptake is low and with increasing pH, it increases and reaches a maximum at the particular pH. It was found that the quantitative sorption was achieved at different pH values and with varying time of equilibration. Thus it is seen that the kinetics was an important aspect for the separation of metal ions. The kinetic and equilibrium modeling of the data was performed to establish the above fact.

Chapter 4: Sorption of radioactive cesium(I) and strontium(II) on nanocrystalline magnetite based sorbents

This chapter discusses the sorption of cesium(I) and strontium(II) onto magnetite and encapsulated magnetites **[20]**. Magnetite, silica coated magnetite and oleic acid coated magnetites have been used for cesium and strontium uptake studies. Nano-sized magnetic composite comprising of nanomagnetite - nano hematite (oleic acid coated magnetite) has been synthesized for uptake of cesium(I) and strontium(II) ions from low level environmental effluents in effective decontamination from waste water. Synthesis of material was based on co-precipitation route and *in situ* coating of oleic acid/or tetra ethyl ortho silicate (TEOS) for silica coating on magnetite nanocomposite was imparted. Magnetic properties were studied for both the uncoated as-prepared and coated nanocomposite materials. The magnetization curves showed no hysteresis or remnant magnetization. All the materials exhibited super-paramagnetism. Saturation magnetization of the coated nanocomposites were found to be 30 emu/g whereas for as-prepared nanocomposite it was 64 emu/g. Detailed characterization of the materials was carried out by X ray diffraction , transmission electron microscopic techniques and zeta potential analyzer. The grain sizes were found to vary between 10 and 15 nm range. Sorption experiments on cesium(I) and strontium(II) were carried out by batch mode equilibrium study. The uptake studies were performed by Atomic Absorption Spectroscopy for cesium ions and Inductively Coupled Plasma Atomic Emission Spectroscopy (ICP-AES) for strontium ions. Size distribution of the particles was measured using Small Angle X ray Scattering (SAXS) technique. Shifting in weak repulsive potential facilitates to enhanced sorption for a longer period of time under stable conditions in comparison to the uncoated nanocomposite which tends to form larger aggregates.

Chapter 5: Sorption of cesium(I), strontium(II) and hexavalent chromium ions on MnO_2

This chapter has been divided by two sections. The first section contains sorption of hexavalent chromium onto nano manganese di oxide. The other section contains sorption of cesium(I) and strontium(II) onto nano manganese oxide.

Hexavalent chromium, Cr (VI) is a known carcinogenic heavy metal ion which is present in industrial waste water and effluent treatment plants. Porous nanomaterial cerium oxide (nano ceria) and manganese di oxide were used for effective removal of hexavalent chromium from synthetic aqueous solutions. The effect of various experimental parameters such as pH, initial concentrations, and contact time. The removal was found to be pH dependent. Different isotherm models like Langmuir, Freundlich, Temkin, Redlich- Peterson, Dubinin–Radushkevich and Sips models were tested to describe the equilibrium isotherms. All the model parameters have been reported for the sorption models used.

Nano crystalline MnO_2 was prepared, as discussed earlier. Sorption experiments for cesium(I) and strontium(II) show good removal efficiency in reasonable time (1 hr). Selective removal of cesium(I) at pH 6 and Strontium(II) at pH 4 has been observed. The experimental results of equilibrium and kinetic parameters for cesium and strontium sorption have been presented in this chapter.

Chapter 6: Nanocrystalline molybdates and tungstates: Potential sorbents for removal of radio-nuclides, toxic metal ions and other species

Several samples such as $SrWO_4$, $SrMoO_4$, Y_2WO_6 and $Y_2Mo_3O_{12}$ nanoparticles have been synthesized via a facile sonochemical route. The samples obtained have been extensively characterized using powder XRD and TEM. The surface area and surface charge of the nanoparticles have been determined from BET adsorption isotherm of N_2 and zeta potential studies, respectively. Sorption characteristics of all the samples have been analyzed for uptake of heavy metal Cu(II) ion, radioactive ^{137}Cs (I) ,and cationic dye (Rhodamine B, Methylene blue [**21**]. The effect of pH, concentration of dye and loading of sorbent on the process of adsorption has been investigated. $SrWO_4$ could be used for the selective removal of RhB from a mixture of RhB and MB dyes. The dye sorption process for all samples has been discussed using Langmuir and Freundlich models. Kinetic studies indicate that the adsorption behavior obey the pseudo second order rate law. The rate determining step has been elucidated from the Webber Morris and Boyd plots. Thermal regeneration of the dye loaded sorbents is easily possible and similar adsorption efficiency up to six consecutive cycles has been demonstrated. For the Cu (II)/Cs (I) loaded samples, pH variation leads to efficient regeneration of the sorbents. A comparative study on the uptake properties of all four sorbents for dyes and toxic heavy metal ions indicates that the efficiency of the sorption process depends on the surface charge as well the inherent crystal structures of the materials. It could be inferred that sonochemically synthesized $Y_2Mo_3O_{12}$ nanoparticles exhibits superior sorption characteristics for uptake of dyes, heavy metal ions like Cu(II) and radioactive ^{137}Cs(I) ions.

Chapter 7: Summary and future scope

Uranium, radioactive cesium and strontium, hexavalent chromium and copper removal from synthetic low level liquid waste were carried by a series of nano materials. Suitable convenient bottom-up methods such as combustion, co -precipitation, and sonochemical method were employed for synthesis of various nanomaterials. However, other method of synthesis can be used for a better size tuning properties. Further work can be done on the reproducibility factor of synthesis. The powder form can be modified to an extent so that it can be used in column experiment also with a varied range of pH.

References

1. C Thammawong, P.Opaprakasit, P.Tangboriboonrat, et al. J.Nanopart Res 15(2013): 1689.
2. Yoshihisa Namiki, Toshihiko Ueyama, Takayuki Yoshida, Ryoei Watanabe, Shigeo Koido& Tamami Namiki , Scientific Reports 6 (2016) 19937
3. http://www.tepco.co.jp/nu-news/2014/1234259_5878.html
4. A . Agrawal, K. K. Sahu, J hazard. Mater.137 (2006) 915-924

5. T Pradeep, Anshup, Thin Solid Films 517(2009)6441-6478
6. M A Sayed, Acc chem. Res. 34 (2001) 257-264
7. Guixia Zhao, Xilin Wu, Xiaoli Tan and Xiangke Wang,The Open Colloid Science Journal, 4(2011)19-31
8 . Y. Lin, G. E Fryxell, H Wu.& M Engelhard, Environ.Sci. Technol. **35**(2001)3962–3966
9. R Chen, et al. Electrochim. Acta**87**(2013)119–125
10. H. I. Adegoke and F. A. Adekola , ISSN 1061933X, Colloid Journal, 74 (2012) 420–426.
11. Ming Hua,Shujuan Zhang, Bingcai Pan, Weiming Zhang, Lu Lv, Quanxing Zhang J. Hazardous Mater. 211– 212 (2012) 317– 331
12. Jamal Al Abdullah & Abdul G. Al Lafi&Wafa'a Al Masri&Yusr Amin & TasneemAlnama, Water Air Soil Pollut227(2016)241
13. XiaoleiQu, Pedro J.J. Alvarez, Qilin Li, Water research 47 (2013), 3931-3946.
14. Book entitled as "Synthesis, properties, and Applications of Oxide nanomaterials", Edited by Jose A .Rodriguez and Markos Fernandez-Garcia
15. F Fu , Q Wang J Environ Management; 92 (2011) 407-18.,
16. PG&E Hinkley, Chromium Cleanup California Environmental Protection Agency, 9/10/08
17. Schwartz, Naoki (2010-12-13), The Boston GlobeDec 13, 2010
18. Multi Agency Radiological Laboratory Analytical Protocols Manual," Volume II: Chapter 10- 17 and Appendix F, EPA/402/B-04/001B/ (NUREG-1576), 2004.
19. Joyeeta Mukherjee , JayshreeRamkumar ,S. Chandramouleeswaran , R. Shukla , A. K. Tyagi, J. Radioanal.Nucl.Chem. 297(2013) 49–57

20. J. Mukhopadhyay, Pranesh Sengupta , D. Sen , S. Mazumdar , A. K. Tyagi , J. Nucl.Mater. 467 (2015) 512-518
21. Joyeeta Mukherjee, Dimple P. Dutta, JayshreeRamakumar, A. K. Tyagi , Journal of Environmental Chemical Engineering 4(2016) 3050-3064

LIST OF FIGURES

Fig. No.	Figure caption	Pg. No.
Fig. 1.1	Earth's water contents	3
Fig.1. 2	India's nuclear power capacity as a function of time	5
Fig. 1. 3	pH speciation graph with percent concentration of uranium	10
Fig. 2. 1	Schematic depiction of top down and bottom up methods for preparing nano structured materials	34
Fig. 2. 2	Schematic representation of nano magnetite synthesis and encapsulation by two different surfactants	37
Fig. 2. 3	Schematic diagram of a general procedure for sorption reaction	50
Fig. 3. 1. (a) & (b)	XRD pattern & TEM micrograph of nano manganese dioxide	62
Fig.3.2	Variation of surface charge with pH	63
Fig. 3.3	Effect of pH on the amountof metal ions (U(VI), Cu(II), Ni(II), Co(II), Zn(II) taken up at optimized time of equilibration	66
Fig. 3.4	Effect of initial metal concentration on the amount taken up	67
Fig.3.5	Langmuir isotherm model	74
Fig. 3.6	Effect of initial metal ion concentration on the Langmuir isotherm model parameter	74
Fig. 3.7	Freundlich isotherm model	75
Fig. 3.8	Dubinin–Radushkevich isotherm model	75
Fig. 3. 9	Redlich–Peterson isotherm model	76
Fig. 3.10	Sips isotherm model for various metal ions	76
Fig. 4.1	XRD pattern of (a) bare magnetite (b) oleic acid coated magnetite-haematite composite material	85
Fig. 4.1 (c)	XRD pattern of silica coated magnetite	86
Fig. 4.2 (a)	TEM images of bare magnetite	86
Fig. 4.2 (b)	TEM image of oleic acid coated magnetite- haematite composite material	87
Fig. 4.2 (c)	TEM images of silica coated magnetite	87

Fig. 4.3	SAXS scattering data obtained for as prepared and coated nanocomposites.	89
Fig. 4.4	Magnetization curve of all the three magnetite at 50 K	92
Fig.4.5	Effect of pH on percentage removal of (a) Cs (I) & (b) Sr (II)	95
Fig. 4.6(a)	Effect of initial concentration on sorbed Cs(I) quantity	97
Fig. 4.6(b)	Effect of initial concentration on sorbed Sr (II) quantity	98
Fig.4.7(a)	Langmuir isotherm plot for Cs (I) sorption	99
Fig.4.7(b)	Langmuir isotherm plot for Sr (II) sorption	100
Fig. 4.8(a) and (b)	Effect of initial metal ion concentration on the Langmuir isotherm model parameter of (a) Cs (I) & (b) Sr (II)	100
Fig.4.9	Freundlich isotherm model of cesium(I) sorption	102
Fig. 4.10(a) & (b)	D-R Isotherm model for (a)Cs (I) & (b)Sr (II) respectively from left to right	103
Fig. 4.11	Temkin isotherm model for cesium Sorption	104
Fig.4.12	Fig. 4.12(a) R-P model and(b) Sips model for cesium(I) strontium sorption	105
Fig. 4.13	Effect of time on uptake (a) cesium & (b) strontium	113
Fig. 4.14	Pseudo second order kinetic model for (a)cesium and (b) strontium uptake	114
Fig.5.2	Effect of pH on the amount taken up for Cs (I) and Sr (II)	122
Fig. 5.2	Effect of pH on Cr (VI) removal	122
Fig. 5.3	Effect of initial concentration on the amount taken up	123
Fig. 5.4	comparative uptake study with varying initial concentration of three metal ions (CS(I)/Sr(II)/Cr(VI)) on MnO_2	124
Fig.3.5	(a) & (b): Langmuir isotherm plot for Sr (II) sorption &Variation of separation factor (R_L) as a function of initial concentration of Sr (II	125
Fig. 5.6	Sorption isotherms for Cr (VI) sorption studies	125
Fig. 5.7	Pseudo second order kinetic models for Cs(I) and Sr(II) sorption on MnO_2	127
Fig. 5.8	Pseudo second order kinetic model of Cr (VI) sorption byMnO_2	127
Fig. 5.9	Comparative intraparticle model for sorption of Cs (I) and Sr (II) onto MnO_2	128
Fig. 6.1	(a),(b)Powder XRD patterns of $SrWO_4$,$SrMoO_4$ respectively	135

Fig. 6.2 (a),(b)Powder XRD patterns of Y_2WO_6 and $Y_2(MoO_4)_3$ heated for 1h at 300°C and 750°C, respectively 136
Fig. 6.3 TEM of (a) $SrWO_4$ (b) $SrMoO_4$ (c) Y_2WO_6 and (d) $Y_2Mo_3O_{12}$ 137
Fig. 6.4 BET N_2 adsorption-desorption isotherm of (a) $SrWO_4$, (b) $SrMoO_4$, (c) Y_2WO_6 and (d) $Y_2Mo_3O_{12}$ 138
Fig. 6.5 (a) Amount of Cu(II) and Cs(I) taken up by $Y_2Mo_3O_{12}$
(b) maximum Cu(II) sorption exhibited by all four sorbents
(c) time taken for maximum sorption by all four sorbents and
(d) effect of weight of $Y_2Mo_3O_{12}$ on Cs(I) uptake 140
Fig.6.6 Effect of pH on the sorption of 20ppm solution of (a) RhB and (b) MB dye. 142
Fig. 6.7 Effect of initial concentration of (a) RhB and (b) MB dye on the time taken for sorption, (c) Effect of weight of sorbent on time taken for maximum uptake and (d) selective sorption of RhB dye by sonochemically synthesized $SrWO_4$ nanoparticles 143
Fig. 6.8 TEM Micrograph of non sonicated Y2WO6 and Y2Mo3O12 147
Fig. 6.9 Freundlich isotherm for (a) RhB and (b) MB sorption by $SrWO_4$, $SrMoO_4$, Y_2WO_6 and $Y_2Mo_3O_{12}$ nanosorbents 148
Fig.6.10 Webber Morris plot for (a) RhB sorption on Y_2WO_6, (b) RhB sorption on $SrWO_4$ and (c) MB sorption on $SrWO_4$. Also Boyd plot for (d) RhB sorption on Y_2WO_6 and (e) MB sorption on $SrWO_4$ 151
Fig. 6.11 Structure of
(a) Rhodamine B
(b) Methylene blue
(c) FTIR of unloaded $Y_2Mo_3O_{12}$ and RhB loaded $Y_2Mo_3O_{12}$ and
(d) regeneration efficiency of all four sorbents for 20ppm RhB sorption 154

LIST OF TABLES

Table No.	Table Caption	Pg. No.
Table 1.1	A few common radionuclides, their half-lives and mode of decay along with energy (MeV)	13
Table 3.1	Physical characteristics of nano and commercially available MnO_2	61
Table 3.2	Experimental factors for various single ion studies to get maximum uptake	65
Table 3.3	Uptake studies using binary mixtures containing uranyl ionand the various other ions in varying concentration levels	68
Table 3.4	Uptake studies using mixtures containing uranyl ion and thevarious other ions in varying concentration levels	70
Table 3.5	Parameters calculated from the different equilibrium models	77
Table 4.1	SAXS data for as prepared and coated nanocomposites	89
Table 4.2	Zeta potential measurement for three different magnetites at different pH	91
Table 4. 3	Summary of specific surface area, pore volume and pore size distribution of magnetite and oleic acid magnetite	93
Table 4. 4	Langmuir effect of initial metal ion concentration on the Langmuir isotherm model parameter for Cs (R_L stands for separation factor)	101
Table 4. 5	Isotherm parameters for adsorption of Cs (I) on magnetite, oleic acid magnetite and silica magnetite at 25^0C	106
Table 4. 6	Parameters describing the Langmuir equilibrium isotherm model for Sr	107
Table 4. 7	Langmuir effect of initial metal ion concentration on the Langmuir isotherm model parameter for Sr	108
Table 4. 8	Error deviation data for different equilibrium isotherm models related to the cesium sorption onto silica capped nano magnetite using most commonly used error functions	110

Table 4. 9 Error deviation data for different equilibrium isotherm models related to the cesium sorption onto nano magnetite using most commonly used error functions 111

Table 4.10 Error deviation data for different equilibrium isotherm models related to the cesium sorption onto oleic acidcapped nano magnetite using most commonly used error functions 112

Table 4. 11 Fitted parameters of Sr (II) adsorption kinetics and diffusion on magnetite, oleic acid magnetite and silica magnetite at 25^0C 115

Table 4. 12 Fitted parameters of Cs (I) adsorption kinetics and diffusion on magnetite, oleic acid magnetite and silica magnetite at 25^0C 116

Table 5.1 Different isotherm parameters for adsorption of strontium (II), cesium (I) and chromium (VI) on manganese oxide at 25^oC 126

Table 5. 2 Different fitted parameters of strontium (II), cesium (I) and chromium (VI) adsorption kinetics and diffusion on manganese oxide at 25 ^{0}C 129

Table 6.1 Summary of specific surface area, pore volume and pore size distribution of $SrWO_4$, $SrMoO_4$, Y_2WO_6 and Y_2 $(MoO_4)_3$ 139

Table 6. 2 Comparison of Dye sorption property of (a) $SrWO_4$, (b) $SrMoO_4$, (c) Y_2WO_6 and (d) $Y_2Mo_3O_{12}$ nano particles with commercial activated carbon (CAC) 144

Table 6. 3 Zeta potential measurements for sonochemically synthesized $SrWO_4$, $SrMoO_4$, Y_2WO_6 and $Y_2(MoO_4)_3$ samples with RhB and MB dyes at various pH 143

Table 6. 4 Freundlich isotherm constants and correlation coefficients of $SrWO_4$, $SrMoO_4$, Y_2WO_6 and $Y_2(MoO_4)_3$ nanoparticles for RhB and MB dyes 149

Table 6. 5 Pseudo-first order and Pseudo-second order kinetic models for dye sorption on $SrWO_4$ and Y_2WO_6 nano particles (10 mg sorbent, pH 2) 150

Scheme 1. 1 Formation ^{137}Cs and ^{90}Sr in the nuclear fission reaction in the nuclear reactor 12
Scheme 1. 2 Decay scheme of ^{137}Cs 13
Scheme 1. 3 Decay scheme of ^{90}Sr 15

Chapter 1

Introduction

1.1 Introduction

We do not inherit the Earth from our Ancestors; we borrow it from our Children. This ancient American Indian proverb correctly warns the human kind about the future of rapid urbanization of the global scenario for sustaining in a clean environment and pollution free surroundings. One major problem with the technological upgradation of this century is, ever increasing need to supply decontaminated ground water and surface water as well as other unconventional sources of waters which are generated due to anthropogenic activities.

1.2 Types of water sources

Broadly, there are two main types of water sources, namely ground-water and surface water. Ground-water is the water present below the ground surface that saturates the pore space in the subsurface. It is formed by recharge of the saturated zone of earth through precipitation. The layer of soil near the land surface, which has still not yet completely saturated by the infiltrated water, is the other zone, called the unsaturated zone or vadose zone from which vegetation takes up most of the water. In this zone, the majority of soil pore spaces are filled by air. Below the unsaturated zone, where all the pore spaces between geologic materials are filled with water, is called the saturated zone, and the term '**ground-water**' is generally used to describe this water-filled region **[1]**. Shiklomanov **[2]** in 1998 on behalf of the United Nations Educational, Scientific and Cultural Organization has published an article on Earth's water content, this states that freshwater in the form of ground-water contributes to 30.1% and surface water contributes to only 0.3% of the total freshwater on Earth. Earth's total water contents have been shown in diagrammatical representation in **Fig.1.1.** Surface water, though in less percentage of the total freshwater, fulfills the 80 % of the world water need **[2].**

1.2.1 Ground-water is a part of natural water cycle. It can spread throughout the cycle and if contaminated, can cause damage to aquatic and human health. As it is formed from the infiltration of surface water; it is therefore a strong possible scenario of pollution of surface water also. For example, Fitts **[3]** documented that ground-water can be polluted by chemical fertilizers and pesticides used by farmers on the crops, a leaking underground pipeline or tank, a spill into a drain at a factory, or leaking of waste chemicals. In addition, ground-water is limited so over extraction of ground-water will lead to geological and ecological problems.

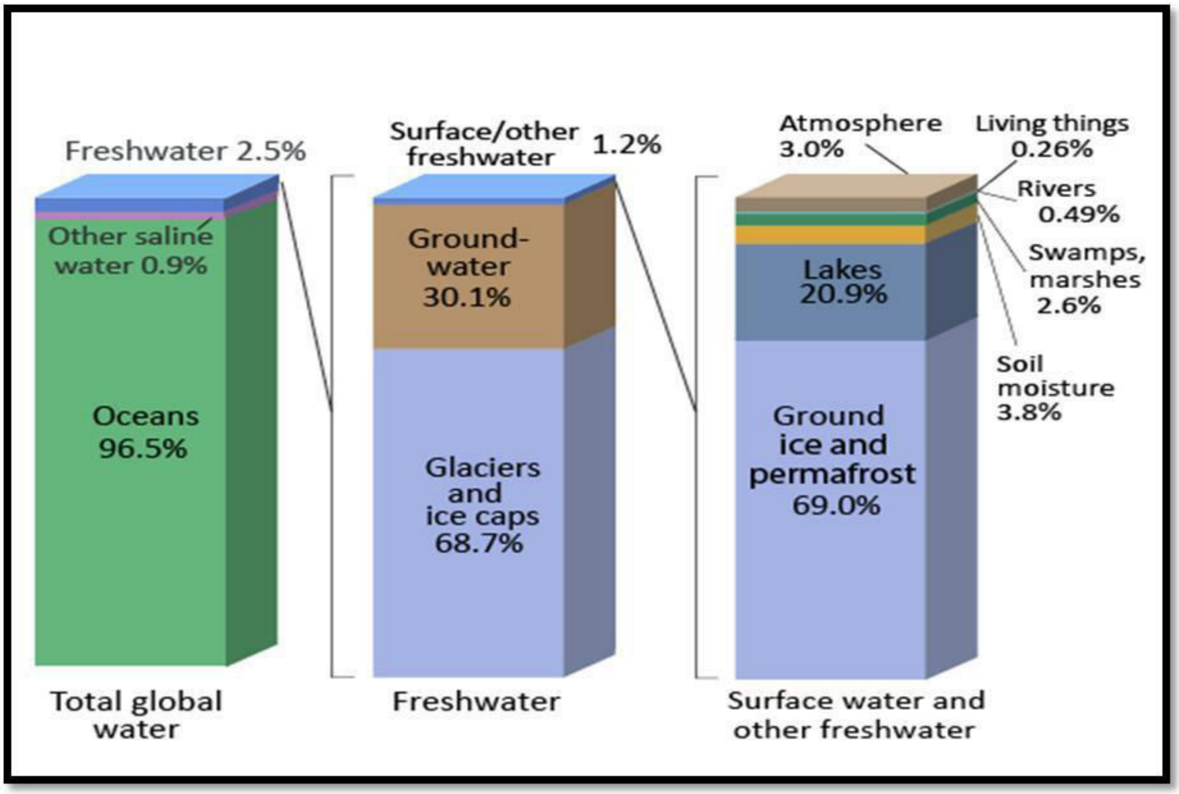

Fig.1.1: Earth's water contents [2]

All the ground-water used for the provision of fresh water for human use is extracted from the aquifer, which is an underground layer capable of yielding ample ground-water. The aquifers are recharged continuously by water infiltrating downwards through the vadose zone. Therefore, depletion of ground-water may never happen theoretically **[4]**.

1.2.2 Surface water charging happens through precipitation and melting of snow and glaciers, but discharging occurs when evaporation and infiltration into the ground-water takes place. Surface water consists of the water on the Earth's surface, like in rivers, lakes, oceans, or artificial reservoirs.

Numerous human activities and natural processes are the main source of ground-water pollution where different industries largely contribute for the same **[5]**.**Contaminations** found in the ground-water cover a broad range of physical, chemical, pathological (due to bacteria, pathogens) and radiological contaminants which can change the water quality parameters. Waste from different industrial area is often dumped near the factories, which percolates through rainwater and reaches the ground-water level. The running water picks up maximum dissolved constituents and reaches the aquifer system and contaminates the ground-water **[6].** According to World Health Organization (WHO) **[7]**, safe drinking-water, should not have significant risk to health over a lifetime of consumption, including different sensitivities that may occur between life stages and it should be free from any toxic elements, living and nonliving organism and excessive amount of minerals which are hazardous to health. The quality of ground-water depends on a large number of individual hydrological, physical, chemical and biological factors. Generally as higher proportions of dissolved constituents are found in ground-water than in surface water because of greater interaction of ground water with various materials in geologic strata, ground-water contamination is comparatively more studied than surface water contamination. Even the heavy metals like chromium, copper though essential to human beings, but large quantities of them in ground-water may cause severe physiological disorders. The toxicity, non-degradable behavior and their accumulation in living organism in Environment make them harmful for human being. Toxic metal ion contamination is mostly related to various industrial sources. These challenges ahead for the humankind are accentuated global warming, pollution of total environment and hence related health concern for present and the future generations to come.

1.3 Radionuclide contamination

With the ongoing demand for power generation, nuclear power has taken a key role for generating power production. Various nuclear power plants are operating throughout the world to supply the power need. India is also operating 21units of nuclear power plants for power generation and several units are under construction. Power generation profile from the start of the nuclear programme in India as of now **[8]** is shown in **Fig.1.2.**

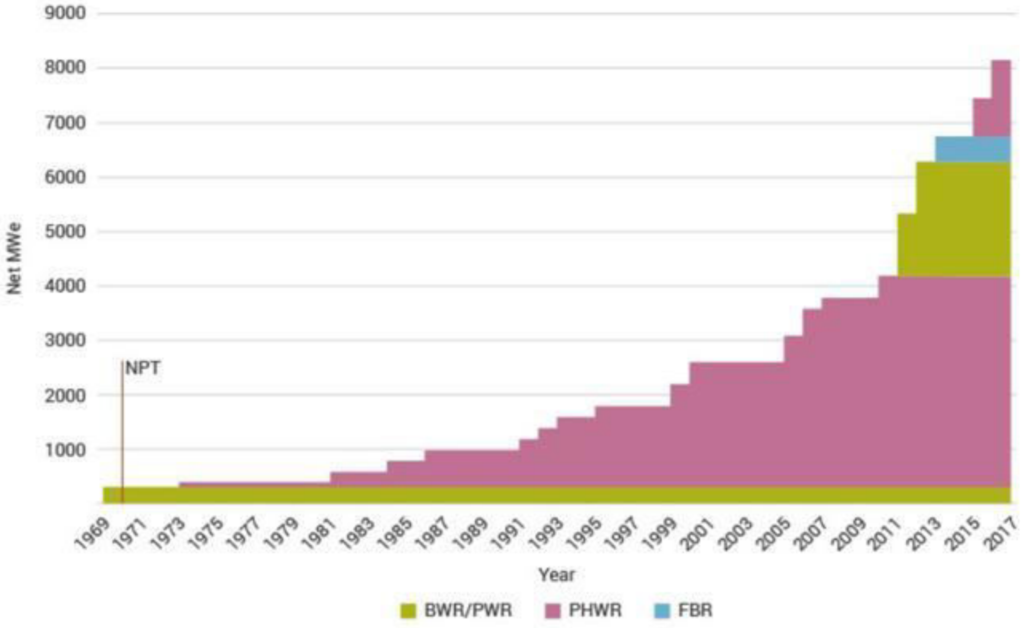

Fig.1.2. India's nuclear power capacity as a function of time [8]

Nuclear power plants produce radioactive waste in the form of solid, liquid or gas. The increasing growth of power generation by nuclear industry and use of radio nuclides for other applications are the source of radioactive waste **[9]**. The primary source of radioactive waste in nuclear industry are the mining and milling of uranium, enrichment, fuel fabrication, spent fuel reprocessing, operation of nuclear power plants, decontamination and decommissioning of nuclear facilities. Institutional uses like in the field of medicine, industry, agriculture, research reactors and test facilities also play some role in the production of radioactive waste **[10, 11].** To safeguard the public health of present and future generations, the proper method of radioactive waste management has been given by the International Atomic Energy Agency (IAEA). Different methods which have been used for the radioactive liquid waste treatment include volume reduction of liquid waste to concentrate and to convert it to a solid form and also removal of radioactive ions from the solution by chemical precipitation, sedimentation, ion exchange, thermal evaporation, membrane permeation etc. **[12-14].** It may be noted that nuclear power is a large-scale energy-producing technology which takes full responsibility for all its wastes. The amount of radioactive wastes is very small relative to wastes produced in other industry and nuclear wastes are neither particularly hazardous nor hard to manage relative to other toxic industrial wastes **[15]**.

In India, along with IAEA categorization, radioactive waste has been categorized depending upon the level of concentration of radioactivity **[16, 17],** such as:

1.3.1 Low level waste (LLW)

The waste containing radioactivity of less than millicurie/L is called low level waste (LLW). It does not require shielding during handling and transport and is suitable for shallow land burial. Before disposal, the waste is usually compacted or incinerated in order to reduce its volume. It comprises some 90% of the volume but only 1% of the radioactivity of all radioactive waste.

1.3.2. Intermediate level waste (ILW)

Intermediate level as the name suggests, contains higher radioactivity than low level waste but not greater than high level waste. Intermediate level waste (ILW) is the category of nuclear waste which contains the radioactivity in the range of millicuries/L to curie/L. As a waste management procedure it is concentrated in solid matrices and stored in shallow trenches. Mainly used ion exchange resins falls in this category.

1.3.3 High level waste (HLW)

The nuclear waste containing radioactivity of greater than curie/L called high level waste (HLW). It contains the fission products and transuranic elements, generated in the reactor core. It is highly radioactive, generates considerable amount of heat and requires interim cooling as well as special shielding. HLW consists of 95% of the total radioactivity produced in the process of nuclear power plant operation. There are two distinct kinds of HLW, viz., used fuel itself and separated waste from spent fuel reprocessing.

HLW contains both long-lived and short-lived radioisotopes depending on the length of time it takes for its radioactivity of a particular radionuclide to decrease to the level that is considered non-hazardous to the people and to the surrounding Environment. The separation of short-lived fission products from long-lived actinides is considered as the primary step for waste management and disposal of HLW. Generally, vitrification, ion exchange, and chemical precipitations are the conditioning processes adopted for the high, intermediate and low level waste management respectively **[18, 19]**. All the power plants operate on a closed or open fuel cycle depending on the reprocessing or direct disposal of the used fuel. Some countries like United States of America (USA) and few European countries had contemplated to adopt deep geological repository facility for direct waste disposal without reprocessing the used fuel and

India had adopted fuel reprocessing method for further recovery of radioisotopes in future application **[15].** During the spent fuel reprocessing stage maximum radioactivity containing waste is generated.Aqueous radioactive waste containing low activity with short half lived nuclide are stored up to 6-7 half-lives to diminish their decay heat and subsequently on decay to exclusion limit, they are discharged in the environmental pathways according to concerned regulatory authorities guidelines. The highly radioactive nuclides and/or long-lived nuclides are treated by different chemical treatment, viz. chemical precipitation, filtration, ion exchange, reverse osmosis, solvent extraction etc. The most important isotopes which have Environmental and severe radiological significance found in the radioactive waste effluents during reprocessing of fuel are cesium, strontium and uranium **[20]**. Among them, the two fission products, viz. ^{137}Cs and ^{90}Sr and the actinide uranium are the most studied radionuclides due to their characteristic chemical and radiological toxic properties.

1.4 Properties of uranium and its effect on human health

Uranium is a radioactive metallic element and its compounds are more chemically toxic than its radio toxicity. Biological effects due to uranium are similar to that of heavy metals. As it is more chemically toxic due to its chemical stability of oxidation state so it is nephrotoxic. Its toxicity due to radioactivity is less than its chemical toxicity, however, if ingested it may have a radiological effect on other tissues of deposition also **[21]**. The chemical toxicity of soluble uranium compounds such as uranyl cations can even surmount the potential radiotoxic effects. Greatest health risk occurs due to severe damage to kidneys. Accumulation of uranium in bones occurs and in humans if accidentally ingested, 99% excretion from the body occurs through urine and fecal but if inhaled or absorbed through skin, it causes nausea, headache, severe diarrhea **[22]** and even lung cancer. The World Health Organization (WHO) **[23]** considers it as a human carcinogen and limit the maximum uranium concentration in drinking waters should be less than 15 µgL^{-1} whereas Environmental Protection Agency (EPA), USA **[24]** has set the maximum level of uranium in drinking water as 30µgL^{-1}. The permissible discharge levels for nuclear industries range from 0.1 to 0.5mgL^{-1}**[25]**. During the production of yellow cake (U_3O_8) which is the final product in the extraction of uranium from its ores and its subsequent milling and chemical processing produces large amounts of solid and radioactive liquid waste. Hazardous elements such as uranium and daughter products of uranium decay chains are the main waste from these, which eventually leach in the ground-water in concentration which exceeds the normal protection standards **[26].** Natural uranium is a mixture of three isotopes, viz., ^{238}U (99.27%), ^{235}U (0.71%) and ^{234}U (0.004%). Abiotic and biotic environmental forms e.g. in soils, rocks, seas, oceans and microorganisms contains uranium which is naturally occurring, ubiquitous, lithophilic in nature **[27].** Its physical appearance is heavy, silvery-white and ductile. In terms of radioactivity it is weak radioactive and has very long half-life of nearly 4.5 billion years. It is strongly electropositive and slightly paramagnetic metal exhibiting poor electrical conductivity. Uranium can exist in five oxidation states viz., 2+, 3+, 4+, 5+ and 6+. The stable naturally occurring form of uranium is U_3O_8. In presence of air uranium metal becomes coated with a layer of oxide. Under reducing aquatic environment, 4+ state of uranium is the most found in its ores but lead to low concentration due to formation of its low solubility aqueous complexes whereas in oxidized aqueous medium+6 state mainly occurs as uranyl cations **[28]**. This is quite evident from the pH speciation graph **[29]** stated in **Fig. 1.3.**

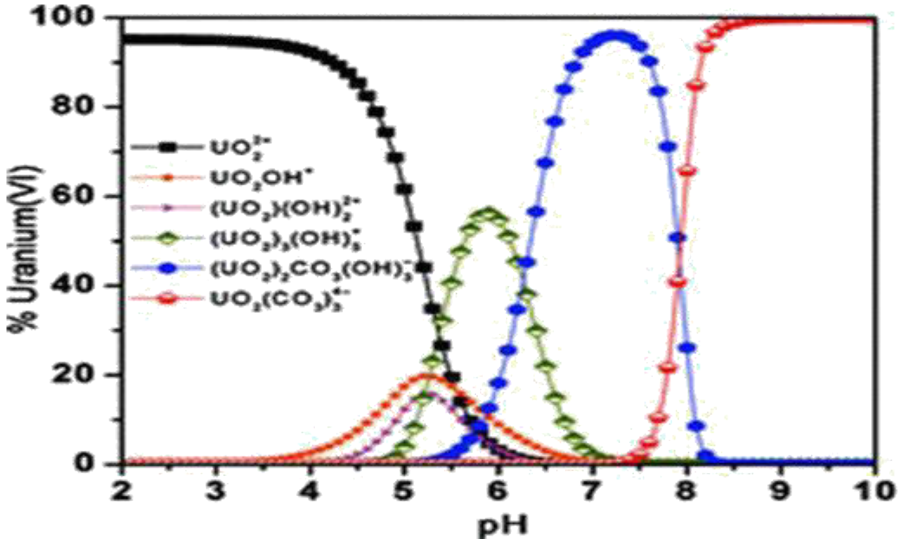

Fig.1.3: pH speciation graph with percent concentration of uranium ["Reprinted (adapted) with permission from [29], Copyright (2008) American Chemical Society."]

The abundance of uranium in the Earth's crust is 4 x10^{-4} percent by mass **[30]**. Uranium (III) is reasonably stable and forms series of hydroxides, hydrated fluorides and phosphates of low solubility. In the near surface zone it can migrate considerably due to the stability of hexavalent uranium in aqueous environment. However, it is precipitated through reduction to tetravalent form or in the form of minerals of uranium, mainly phosphates, vanadates, silicates, arsenates, and oxyhydroxides, large amount of which may occur simultaneously at the same locality. Solubility and dissolution of these complexes will be the main deciding factor about the amount of uranium released to ground or surface waters from these secondary sources which is heavily dependent on pH and water composition **[31].**

1.5 Properties of cesium and its effect on human health

The most common product of nuclear fission is **cesium-137 (Scheme 1.1.).** Radio cesium in the environment is likely to be present mostly due to nuclear accidental fallout. The nuclear accidents of 'Three mile Island' in 1976**[32]**, 'Chernobyl' accident in 1986 [**33]** and recently 'Fukushima daichhi 'accident in 2011 in Japan **[34, 35]** have also contributed in increasing the level of radionuclide concentration in soil and aquatic water system. ^{137}Cs emits beta in the first step of its decay mode to produce ^{137}Ba which emits relatively strong gamma radiation of energy 662 KeV (**Scheme 1.2.**) with half-life of 30.4 years (**Table 1.1**). Serious environmental public health threat for ^{137}Cs is due to its highly water solubility, property, high transportability via the atmosphere, long half-life, easy movability within aqueous media, large bioavailability, readily distributable property in the body, especially in the muscle tissues and readily assimilated by terrestrial and aquatic organism **[36,37].** EPA, USA has established a maximum radioactive contaminant level of 4 millirem per year for man-made radionuclides′ in drinking water. ^{137}Cs would be considered under this Maximum Concentration Level (MCL) **[38].** Physical appearance wise cesium-133 is soft, silvery white-gray. The natural source, providing the greatest quantity of cesium, is the rare mineral pollucite **[39]**. Cesium is a metal but which melts at a relatively room temperature and/or low temperature of 28 ℃. Therefore, like mercury, it is liquid at moderate temperatures and as most of the alkali metals; it reacts explosively in contact with cold water.

The concentration of cesium in the earth’s crust found to be 1.9 mg kg^{-1}, and the concentration in seawater is nearly 0.5µgkg^{-1}. Naturally occurring cesium is entirely non-radioactive. It is a highly electropositive, and in turn forms ionic bonds with nearly all inorganic and organic counters on ions. Cesium exposure can be through ingestion and inhalation. The biological half-life is 110 days which means that half of the ^{137}Cs will be excreted after 110 days. Excess water intake to the body will reduce excretion time to some extent but if ingestion occurs, due to the water soluble property of cesium it will reach digestive tract through blood stream and remain there for a long period and potentially irradiate living tissues with high gamma energy of 662 KeV. Due to chemical similarity with potassium **[40-42]** it affects the potassium levels which are an integral part of human body, in addition to its radiation effects on the various body tissues. It may exchange potassium with radio cesium in the body, thus creating imbalances in the system. A high dose of radioactive ^{137}Cs can induce medullar dystrophy and disorders of reproductive function **[43].** Essentially, all ingested cesium is first absorbed into the blood stream through the intestines, so damage to the related organ start by initiating radiation induced chemical reactions in the tissues which lead to negative health effects including carcinoma of the liver, kidney, bladder, renal functions, cardiovascular disease and gastrointestinal distress **[44, 45].** Several diseases have been reported due to the adverse effect of cesium radio toxicity. Therefore, its removal from the waste streams is the main priority for any radioactive waste management's system, before discharging it to the water body for minimizing water pollution and safety to the public health.

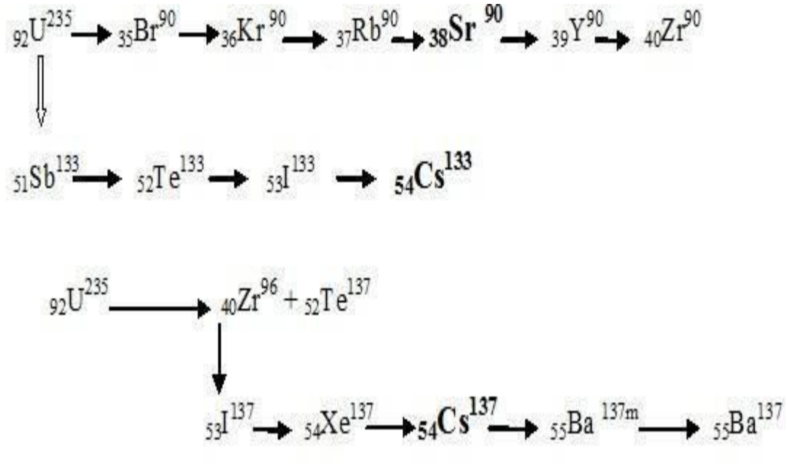

Scheme 1.1: Formation ^{137}Cs and ^{90}Sr in the nuclear fission reaction in the nuclear reactor

Table1.1: A few common radionuclides, their half-lives and mode of decay along with energy (MeV)

Radionuclide	Half life	Mode of decay and energy (MeV)
^{89}Sr	54days	β(1.46),γ(0.390)
^{90}Sr	28.8 years	β(0.546)
^{134}Cs	2.2 years	γ(0.604),0,795
^{137}Cs	30.1 years	β(0.52),γ(0.662)

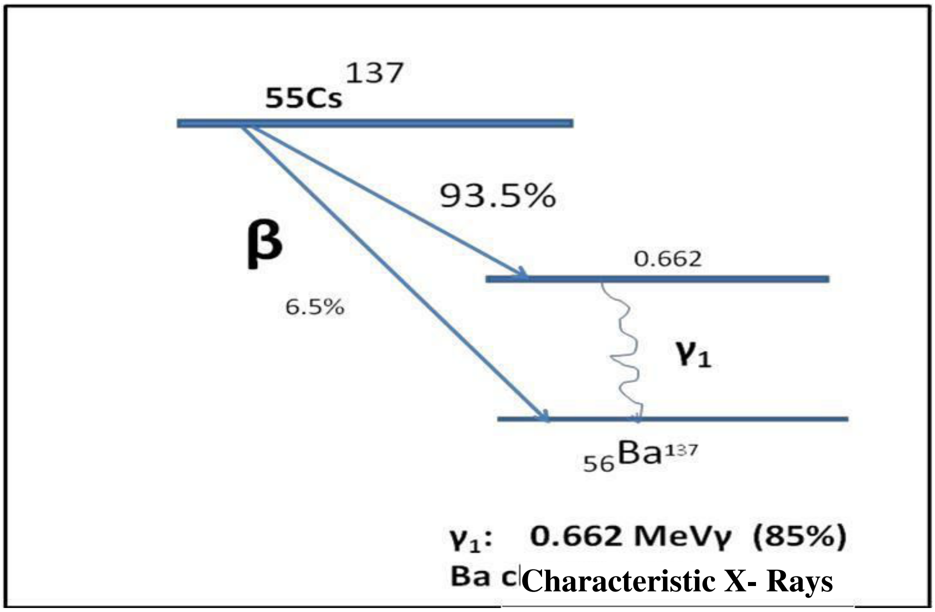

Scheme 1.2: Decay scheme of ^{137}Cs [46]

1.6 Properties of strontium and its effect on human health

Another most important fission product from nuclear waste normally considered by the EPA, USA **[47, 48]** detrimental to the environment is **strontium-90.** In the environment higher percentage of ^{90}Sr is present due to above-ground nuclear test explosions carried out during the 1950s and 1960s. Other than this, the application of highly energetic radiation in space vehicles, commercial use in certain optical materials, pyrotechnic devices etc also play a part in total global strontium contamination **[49].** ^{90}Sr has a half-life of 28.7 years and it is a strong β-emitter of 0.546 MeV energy (**Table 1.1**). Its progeny (^{90}Y, decay energy 2.28 MeV) has the radiating effect of ionization for 100 years **[50, 51]**. It has high fission yield of 5-6% from slow neutron fission of ^{235}U.The chemical properties of strontium-90 are similar to calcium **[52,53],** so when entering into the human body, due to the chemical similarity of alkaline earth metal **[54]**, strontium-90 can easily replace calcium, an essential part of bone structure **[55]**. Normal pathway for strontium absorption by the human body is through alimentary canal and it accumulates in the liver, lung and kidney **[56-59].** ^{90}Sr decays to radioactive yttrium (**Scheme 1.3**), which stays in hypophysis and ovaries and thus disrupting hormonal development and growth in infant. In a nutshell, long half-life, high solubility and biotoxicity of strontium attract special attention for immediate separation and removal of strontium from the waste solution.

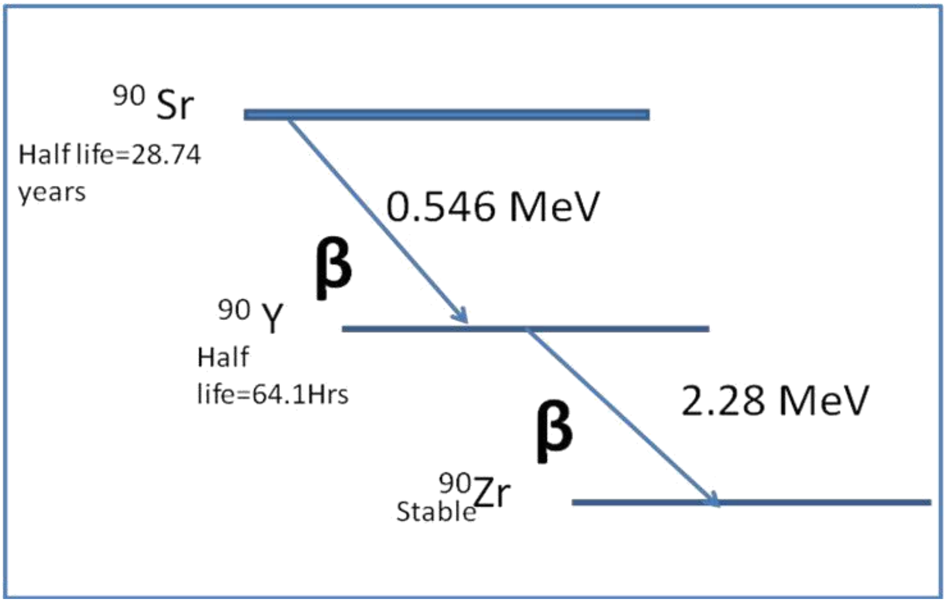

Scheme 1.3: Decay scheme of ^{90}Sr

Physical appearance wise strontium is a soft, silver-yellow, alkaline-earth metal which has three allotropic crystalline forms and it has similar physical and chemical properties like other alkaline earth metals such as calcium and barium. It reacts with water within a second and also quickly reacts in air, so air and water contamination is strictly avoided for its proper storage. Strontium when in contact with air burst into flame. As it is extremely reactive to air, this element always naturally occurs combined with other elements and compounds. Its high-energy radiation has been used to generate an electric current in space vehicles, remote weather stations and navigation buoys. The sulfate mineral celestite ($SrSO_4$) and the carbonate strontianite ($SrCO_3$) are the two most common form of natural strontium **[60]**. The human body contains approximately 4.6 ppm, seawater contains 8 ppm strontium on an average where as river water generally contains about 50 ppb of strontium. When dissolved in water strontium mainly occurs as hydrated Sr^{2+}ion or hydrated $SrOH^{+}$ion. It slowly reacts with water, but faster than calcium and slower than barium to form strontium hydroxide and hydrogen gas. It can exist in two oxidation states, viz., 0 and +2. Under normal environmental conditions, only the +2 oxidation state is stable which readily reacts with both water and oxygen **[61, 62]**. There are 26 isotopes of strontium, out of which four occur naturally. These four stable isotopes, viz., ^{84}Sr, ^{86}Sr, ^{87}Sr, and ^{88}Sr, are commonly referred to as stable strontium. The most important radioactive isotopes, viz., ^{89}Sr and ^{90}Sr are formed during nuclear reactor operations and during nuclear explosions by the nuclear fission of ^{235}U or ^{239}Pu **[63].** ^{235}U is split into smaller atomic mass fragments such as ^{90}Sr by a nuclear chain reaction initiated by high energy neutrons of energy approximately 1 MeV (**Scheme 1.1**).

According to EPA, USA the average concentration of strontium-90 which is assumed to yield 4 mrem/year is 8 picocuries per liter. If other radionuclides which emit beta particles and photon radioactivities are present, the sum of the annual dose from all the radio nuclides must not exceed 4 mrem/year.

Apart from the radioactive waste from nuclear industry, there are industrial sources of toxic metal ion pollutants which are detrimental to the human being. Most of the tannery industries discharge hexavalent chromium in wastewater, whereas copper and hexavalent chromium are among the list of toxic metals by-products from metal plating industry. Higher level of heavy metals concentration, more than the safe permissible limit, is lethal and detrimental for living beings. Thus the treatment of heavy metals is of special concern due to their recalcitrance and persistence in the environment **[64]**. The worst example of chromium contamination in ground-water in history till date happened in California, USA **[65]**. The epidemiological data of cancer patients surrounding the contaminated area is still higher than the background data **[66]**.The heavy metals is a general term used to address group of metals and metalloids, naturally abundant in earth crust with atomic density greater than 4000 kg/m^3 or five times more than water **[67]** or elements having atomic weights between 63.5 and 200.6, and with a specific gravity greater than 5.0 **[68].** Exposure to heavy metals, even at trace level, is believed to be a risk for human beings **[69-71].** In developing countries heavy metal waste water are directly or indirectly discharged into the water body and from water body contamination happens through drinking water route and intake of food chain. Various industries such as leather and tannery , chemical handling industries like ceramics , electroplating, paints, fertilizer industry generate heavy metal such as chromium, lead, cadmium, arsenic, copper, iron, manganese, nickel, mercury, and cobalt among others. Tanneries discharge chromium in wastewater; metal plating industries produce copper, chromium, zinc, and cadmium; the production of electrical equipment and mining, smelting, and fossil fuel combustion contribute to mercury pollution; and lead is discharged from a number of industrial and mining sources. Most of the wastewaters contain higher concentration level of heavy metal than the safe permissible limit that might result in lethal for public. These metals are not bio degradable and so accumulate in the living organism. Among the several heavy metal ions hexavalent chromium and copper removal has been studied in the present thesis.

1.7 Properties of hexavalent chromium and its effects on human health

Chromium is a naturally occurring element found in rocks, animals, plants, soil, and in volcanic dust and gases. Chromium is present in the environment in several different forms. The most common forms are chromium (0), trivalent (or chromium (III)), and hexavalent (or chromium (VI)). Chromium (III), however, is an essential nutrient for humans. It has no taste or odor, neither it is readily soluble in water nor does it bind to soil. It has high potential for accumulation in aquatic life. **Cr (VI)** is more toxic than Cr (III). Cr (VI) affects human physiology, accumulates in the food chain and causes severe health problems ranging from simple skin irritation to lung carcinoma **[72].** The essential heavy metals viz. Cu, In, Fe, Mn and Mo play biochemical and physiological functions in plants and animals. Two major functions of essential heavy metals are: (a) Participation in redox reaction, and (b) Direct participation, being an integral part of several enzymes. Major sources of chromium contamination are electroplating, corrosion control, leather tanning industries, paints and pigments industry, photography, fungicide industry and ceramics or glass manufacturing **[73, 74].** The hexavalent form, reported to be five hundred times more toxic than the trivalent one **[75],** is classified as a known human carcinogen that modifies the DNA transcription process causing important chromosomal aberrations **[76, 77].** Also, it can cause kidney and gastric damage and epidermal irritation. The structural similarity of Cr(VI) anions to biologically important inorganic anions, such as SO_4^{2-} and PO_4^{3-} may lead it to easily transverse cell membranes via the sulfate transport system. Less carcinogenic if ingested, since stomach acids may convert it to nontoxic form whereas short-term exposure can cause skin irritation or ulceration. Long-term exposure at levels above the Maximum Concentration Level (MCL) can cause damage to liver, kidney circulatory and nerve tissues, and skin irritation. Direct eye contact with chromic acid or chromate dusts can cause permanent eye damage. Hexavalent chromium can irritate the nose, throat, and lungs. Repeated or prolonged exposure can damage the mucous membranes of the nasal passages and result in ulcers. In severe cases, exposure causes perforation of the nasal septum. EPA has stipulated maximum level of hexavalent chromium for drinking water purpose is $0.1 mgL^{-1}$. Hexavalent chromium is the substance against which Erin Brockovich campaigned extensively in the recent past.

1.8 Properties of copper and its effect on human health

Another heavy metal ions studied in the present thesis is **copper**. Copper occurs in 0, +1 and +2 states. Among them the +2 state i.e.; cupric ion is the most toxic species of copper. Though copper is essential for good health as a micronutrient, but higher doses are harmful. Long-term exposures to copper dust irritate nose, mouth, and eyes, which cause headaches, dizziness, nausea, and diarrhea. Higher level of copper intake can cause nausea, vomiting, stomach cramps, or diarrhea. In aerobic alkaline system $CuCO_3$ is the dominant soluble species where as in anaerobic environments CuS will form in presence of sulfur **[78].** The soil natural concentration of copper is 2-100 mgL^{-1} where as normal range in plants it is 5-30mgL^{-1}. USEPA has given a MCL limit of copper in water as 1.3 mgL^{-1}**[79].**

1.9 Common removal techniques used for uranium (VI), cesium (I) and strontium (II)

Various techniques **[80]** have been used for removal of radionuclide such as uranium, cesium and strontium. Several methods such as physical adsorption, reactive adsorption, ion exchange, precipitation, and reverse osmosis have been used to treat the ground-water contaminated with uranium. Treatment of radioactive contaminants in ground-water broadly falls into a few categories.

Ion exchange

In this technology, the (water-soluble) contaminants are captured by ion exchange onto a solid support, made of natural or synthetic material.

Precipitation

This approach is mainly practiced above ground where precipitation occurs after the addition of alkali to raise the pH for precipitate of the oxide or hydroxide. Coprecipitations also play a part in this separation method by applying a benign material.

Reverse osmosis

In reverse osmosis, clean water is transported with the help of a high-pressure gradient through a membrane that is essentially non-permeable to the contaminants

Stripping

This method is applied generally for volatile contaminants such a radon. Clean air (or other gas) is contacted with the contaminated water, stripping out the volatiles. WHO recommended a limit based on a sustained effective dose of 0.1 mSv per year from drinking 2 liters of water per day for contamination of uranium. Most of the processes for removal of radionuclides from ground-water are based on sorption phenomena. In adsorption processes, the contaminant is adsorbed on the surface of a solid particle or within the pores of the particles**.**

1.10 Literature survey

1.10.1 Literature survey for uranium removal

A lot of study has been done on the removal of uranium by ion exchange resin and solvent extraction methods. Organic materials have been widely used for resin exchange and solvent extraction process such as liquid–liquid extraction and separation studies of uranium have been carried out from sodium salicylate media using cyanex 272 in toluene **[81].** Alamine 336 has been used for solvent extraction of uranium from vanadium **[82],** silica gel loaded with *p-tert*-butylcalixarene as a new solid phase extractor for determination of trace level of uranium **[83].** However, traditional liquid–liquid extraction continues to have disadvantages such as the use of toxic or flammable solvents, the formation of emulsions, and the generation of large volumes of secondary hazardous organic wastes. In that respect adsorption is the better alternative. In sorption process the design and development of the sorption system and proper tuning of the sorbent surface can be done according to the sorbate system. Secondly, the regeneration of the sorbent is possible with the help of acidification which is favorable for design and development of large scale removal process from the cost effective point of view and the advantage of nano materials usage for sorption is again a boost for sorption process to apply in uptake study. **Nanomaterials** are defined as the materials as smaller than 100 nm in size at least in one dimension **[84]**. Dimension wise, nanomaterials can be nanoscale in one dimension like nano tubes, nano rods, and two dimensions like thin films or three dimensions like nano particles. They can exist in single, fused, aggregated or agglomerated forms with spherical, tubular, and irregular shapes **[85].** Ordinary macroscopic material follow Newtonian mechanics as in heat transfer, conductivity optical properties but in the nano scale, quantum mechanics plays a pivotal role to dictate their property. As the particle size decreases, the atomic behavior changes due to the influence of the structural characteristics of lattice symmetry, cell parameters **[86].** In this condition, bulk and surface atoms differ in their thermodynamic property, tending to thermodynamically unstable state consequently increases entropy and thus become highly reactive. Thus, nanomaterials are chemically more active than macroscopic materials due to their relatively greater surface area to volume ratio. The quantum effect in nanomaterials becomes prominent for magnetic behavior where the magnetic properties changes due to nano scale. There are extrinsic strain also, related to nano materials stability in terms of which synthesis process used. This is generally diminished by annealing or calcinations **[87].** However, if the size becomes very small (e.g. less than 10 nm), the surface energy becomes very high, which results in agglomeration and in turn the high efficiency of nanomaterials is decreased. To overcome this problem, encapsulation (capping) of the nanomaterials is required to lower the surface energy. Here, in this work, nanomaterials mainly oxide nanomaterials have been used for sorption study of radionuclide and heavy metal ions. The synthesis techniques used here for different nano materials and their characterization techniques used have been elaborated in Chapter 2**.**

Inorganic metal oxides such as TiO_2 and ZrO_2 have been used for high radiolytic stability and low solubility property in aqueous environment **[88-90].** Even mixed oxide of TiO_2 and ZrO_2 has also been used for uranyl sorption process **[91].** However, in an actual situation of very low concentration of uranium as in environmental system, uranium remains with metal ions. These ions and uranyl cation have to be specifically removed from the solution as part of environmental radioactive analysis. Simona Regenspung et al. **[92]** have used iron (II) minerals for uranium removal in presence of bicarbonate environment, but in the presence of other heavy metal ions, alkali and alkaline metal ions, the specificity of sorption has been compromised. Further, to get a high uptake factor for uranium, functionalized nanomaterials have been used in literature **[93].** The aim of using nano MnO_2 as a sorbent for uranium removal in presence of other metal ions was to use it without any functionalization and thus avoid the additional step of surface modification and to see if there was a possibility of achieving removal at room temperature.

1.10.2 Literature survey for cesium removal

The earliest known method of cesium removal from spent fuel used is liquid-liquid extraction. Formations of extractable metal-organic complexes are the main step in this process. Based on the solubility product of the organic solution, the cesium metal ions are separated **[94].** Though it can be applied for a large scale industrial application, the major drawback of this process is number of which need steps are to be followed and generation of large amount of secondary waste which is also to be managed according to the norms of public safety. Then the modified fractional extraction method, stripping method was also adopted, but the same disadvantages persisted. In search for less number of chemical steps used and environmental friendly approach, physically amenable sorption method was adopted. For sorption and consequent removal of cesium from nuclear waste, ammonium molybdophosphate (AMP) has been effectively used widely **[95].** However, AMP becomes soluble in solutions with pH >4, and therefore, AMP is only applicable to acidic solutions of nuclear waste system. Cesium can be eluted from AMP with concentrated ammonium salt solutions (NH_4NO_3, NH_4Cl etc.) or the cesium and ammonium molybdophosphate complexes can be dissolved in caustic to separate the active exchanger material from an inert binder material, such as PAN **[96]**. Though, in actual scenario, acidic as well as basic environment is there for radioactive waste matrices. As mentioned earlier, nanosized sorbents are quite attractive due to their larger effective surface area and they can be used over a wide range of pH. The regeneration of the nanosorbents is quite simple as compared to the number of steps involved using AMP. Ion exchange chromatography uses AMP but this also has limitation of clogging of column filtration. Therefore, granulated form or embedded in a macroscopic support may be incorporated in this method. Again, nano sorbents are more preferred than granulated form for better surface area to volume ratio than granulated ones. Several nano materials like zeolite **[97],** inorganic sorbents **[98],** potassium hexacyano ferrate (II) **[99, 100],** calixarene **[101],** series of crown ether **[102, 103, 37]** have been used for the separation and removal of cesium. Shylesh et al. **[104]** have shown that difficulties associated with the recovery of sorbed nanomaterials. In this respect, the nano magnetic unique property has been used for separation of cesium. Nanomagnetite, being a super paramagnetic material has been used for instant separation just by applying even a low field magnet. It may be noted here, that magnetism is highly volume dependent because it arises from the collective interactions of atomic magnetic dipoles. If the magnetic particles size reduce to a critical size of few nano meters, the magnetic susceptibility increases many fold as the magnetic domain changes from multiple to single domain. Thus further decrease in size will make the particles into super paramagnetic, where permanent magnetic moment will lose. This property will allow rapid separation from solution. Several functionalized magnetite, bare magnetite, iron ferrite and even inorganic organic nano magnetic composite material have been used **[105-108]** for sorption of cesium and in medicinal drug delivery system. Recently in Fukushima accident magnetic nano materials have been used for large area decontamination **[109,110]**. Here, in the present work three different nano magnetite viz. bare magnetite, oleic acid coated magnetite, silica coated magnetite, nano MnO_2, Y_2WO_6 and $Y_2Mo_3O_{12}$ have been used for cesium(I) sorption potential. The metal tungstates and molybdates are two important classes of inorganic materials finding applications in the area of optoelectronics, luminescence, magnetic materials, scintillating materials, catalysis, etc. However, to best of our knowledge there are no reports on their sorption properties. Hence it was of interest to study the sorption properties of tungstates and molybdates with divalent strontium ions and compare it with tungstates and molybdates of trivalent yttrium ions. The efficiency of the sorption process is dependent on the surface charge as well as inherent crystal structure of the various metal tungstates and molybdates. The metal atoms attached to the tungstate/molybdate tetrahedra via the oxygen atoms play a crucial role in the resultant crystal structure and can affect the sorption properties. The detailed synthesis and sorption study of all these nanomaterials have been given in the relevant chapter of present thesis. A theoretical calculation has been shown for the three different type of magnetites to compare the linear and non-linear methods used for checking the compliance of the experimental data corresponding to the isotherm models (Langmuir, Freundlich, Temkin, Dubunin-Radushkevich, Sips, and Redlich–Peterson) for optimization of the isotherm parameter. This optimization method will facilitate decision making for successful design and development of sorption system for cesium removal in large scale application. The detail of nonlinear regression method has been described in chapter 2.

1.10.3 Literature survey for strontium removal

Various processes have been used for separation of strontium from radioactive waste streams. Most common method used for strontium removal is ion exchange method. Natural mineral compounds such as different clay minerals e.g.; vermiculite, zeolite, bentonite, clinoptilolite have been used in ion exchange methods. Natural zeolite was earliest known material first used for ion exchange processes. It is a common practice to use clay minerals as backfill or buffer materials for radioactive waste disposal sites due to their ion exchange properties, low permeability and easy workability **[111]**. However, due to the limitation of their physical property of restricted flow through column operation clays are not used in ion exchange processes **[112].** The main drawback for ion exchange process is adverse effect on performance by high salt content, choking hazard and difficulty in regeneration and recycling **[113].** Still many researchers have successfully used modified methods in ion exchange processes in lab scale experiment for strontium removal **[114-116].** The other techniques used are chemical precipitation. Rao et al. **[117]** have used chemical precipitation followed by ultra-filtration method to separate cesium and strontium from aqueous waste. The efficiency of chemical precipitation method depends on the solid–liquid separation steps, this makes cumbersome job for the wide applicability of this process for practical purposes in spite of its advantage over ion exchange are withstanding power in high salt content waste and suitability for large volume of waste. Other methods used are membrane separation **[118,119],** ultra filtration solvent extraction **[117],** electro coagulation **[120],** thermal treatment etc. Solvent extraction generates aqueous and organic secondary waste which causes environmental hazards for society. In ultra-filtration method the organic membranes undergo radiation damage other than their high cost and low efficiency. Apart from these methods, Radiochemical Analysis (RCA) is the most widely used method for separation of strontium-90 from effluent treatment plant in waste management system. RCA is based on selective precipitation and complex formation. Series of selective precipitations reactions have to be performed for the separation of Sr^{2+} from the other alkaline earth metals ions, daughter product yttrium and several other interferences **[121].** Among all the methods, sorption is one of the most commonly used, highly efficient, comparatively low cost and reproducible method for removal of strontium from waste water stream. Mostly studied adsorbents are silica materials and/or magnetic composite, syntheticzeolite **[122]** materials apart from activated carbon **[123]** or multiwall carbon tube **[124]**, layered metal sulphide **[125].** Functionalization of the magnetic materials with biomaterials like saw dust has been used by Zihong Cheng et al, **[126]** or magnetic chitosan beads by Yuwei Chen, [**127**] has been shown to be very effective for strontium removal process due to the excellent magnetic property. Lalhmunsiama **[56]** has used silica based natural clay followed by acid activation for strontium removal from aqueous solution. Valsala et al. [**17**] have used hydrous manganese dioxide for lab scale uptake study in column matrices. They have used a composite ion exchange material consisting of hydrous manganese oxide and poly methyl methacrylate (PMMA) for removal of strontium(II) from aqueous radioactive waste. Here, in present work nano manganese dioxide, without any functionalisation has been used for Sr uptake study. The urge for simple and cost effective yet very efficient and rapid sorption method gives the idea of using magnetite with functionalization of silica or long chain fatty acid. Apart from magnetite, silica coated magnetite and oleic acid coated magnetite, nano manganese dioxide has also been used for strontium removal process. Other than nano magnetic material's unique property stated earlier, the inert coating of silica or long chain fatty acid like oleic acid on the surface of these particles will prevent nano aggregation in liquids and also enhance the chemical stability as well as chemical activity with their presence of many hydroxyl ions on the surface of silica or –COOH group on oleic acid, which will consequently attach to form metal chelates for effective removal. This is the advantage of using surface modification to magnetite nano materials which will shorten the preconcentration and separation steps. The regenerated nano material can also be used for further uptake study. The synthesis, characterization and detailed sorption study has been described in the relevant chapters.

1.10.4 Literature survey for chromium and copper removal

In recent past, several techniques have been used for heavy metal detoxification by uptake studies including but not limited to ion exchange, membrane filtration, chemical treatment, adsorption, bio sorption, oxidation and electrochemical processes [**128-131**]**.** Among them sorption ions application of nanomaterials has been mainly used for their flexibility in design and operation, regeneration, low maintenance cost, ease of operation and their high removal efficiency. Therefore, it is in the forefront of heavy metal removal technological application. The nano materials, most commonly used are metal oxide because of their large surface area and highly selective chemical activities viz. aluminum oxide **[132]**, titanium oxide **[133],** magnesium oxide, manganese oxide **[134],** cerium oxide **[135],** ferric oxide **[136]**. For hexavalent chromium uptake, Joshi et al., 2011**[137**] have demonstrated pH-dependent photo catalytic degradation of Cr (VI) from wastewater using porous TiO_2, ZnO, and CdS nanomaterials. Adegoke et al., **[138]** have reported the sorption of Cr (VI) from aqueous solution with synthetic hematite. They have observed that acidic pH (2-3) and moderate temperature (35-40^{O}C) favors the adsorption process.

Few sorption studies have been reported [**139,140**] where morphology changes of ceria after sorption of hexavalent chromium have been studied. Some researchers have used nano manganese dioxide with surface modified with functional group or nano manganese composite material or beads for the Cr (VI) sorption study. For example, Mallik et al. **[141]** have used manganese nodule leached residue obtained from NH_3–SO_2 leaching for adsorption of hexavalent chromium whereas Gupta et al. **[142]** have used ceria and nano manganese dioxide composite materials for the same**.** Here in present work, nano manganese dioxide without any functionalisation has been used for hexavalent chromium removal study to ensure a low cost easy preparation method. In search for heavy metal remediation from aqueous solution, copper removal has also been shown by transition metal vanadate and tungstate viz. Copper was chosen for the heavy metal sorption studies since copper toxicity is prevalent nowadays due to widespread use of copper in utensils, fungicides, hot water pipes, etc. [**143**].The detailed study for Cr (VI) and copper sorption has been described in respective chapters. Dye removal by $SrWO_4$, $SrMoO_4$, Y_2WO_6 and $Y_2Mo_3O_{12}$ has also been studied in an attempt to further extend the applicability of the above nanomaterials as sorbent.

1.11 Scope of the thesis

A detailed extensive survey for the uptake study for radionuclide such as uranium(VI), cesium(I), and strontium(II), heavy metal ions [Cr (VI) and Cu(II)] has been elaborated with reference to their effect on human civilization and for the future generations to come. The health effect, their remediation techniques using different methods and particularly nanomaterial application in sorption process has also been documented.

The use of nanomaterials for sorption methods, their advantage over the other conventional techniques for uptake studies along with their disadvantages has been discussed. The conventional techniques have been described as reference background for using nanomaterials over these synthesized materials. Though, solvent extraction and ion exchange have wide applicability in industrial scale, but their production of secondary waste, clogging of the column, cost effectiveness puts nanomaterials at their best for application in near future.

In this context, manganese dioxide, nano molybdate and tungstate of strontium and yttrium, bare magnetite, oleic acid coated magnetite, silica coated magnetite nano materials have been synthesized and characterized for uptake studies of radionuclide's and heavy metal ions.

Nano molybdates and nano tungstates of strontium and yttrium have been used for cesium(I) and copper(II) uptake studies. These transition metal molybdate and tungstate samples have also been used for extended application of dye removal. Nano manganese dioxide as a sorbent for uranium (VI) in a mixture of heavy metal ions namely Cu(II),Ni(II),Co(II),Zn(II),Na(I),K(I) and Ba(II) has been used in a series of experiments . Nano MnO_2 has also been extensively studied for its application in cesium (I), strontium (II) and Cr (VI) removal from aqueous solution.

Magnetite, very well known for biomedical applications, has been used, as a bare magnetite, as well as surface functionalized magnetite for cesium (I), strontium (II) uptake studies. A nonlinear regression model has been discussed in relation to the optimization of isotherm parameters for all the three nanomaterials for effective design and development of sorption system for cesium uptake study.

The main objective of this thesis work is to study the potential use of these nano sorbents for removal of radionuclide, viz. uranium(VI), cesium(I) and strontium(II) as well as uptake study of heavy metal ion particularly hexavalent chromium and divalent copper. The effects of various experimental conditions on the sorption efficiency, kinetics, mechanism of the sorption process have been studied for successful design and development of sorption system for practical purpose of radioactive waste management.

In summary, this PhD thesis is dedicated to synthesis, detailed characterization of several nano materials for uptake of radionuclide and heavy metal ions. The results will be discussed in subsequent chapters.

Chapter 2

Experimental methodology and characterization techniques

2.1 Introduction

Different metal oxide nano materials such as MnO_2, Fe_3O_4 and encapsulated Fe_3O_4 along with tungstates and molybdates of divalent strontium ions and trivalent yttrium ions namely $SrWO_4$, $SrMoO_4$,Y_2WO_6 and $Y_2(MoO_4)_3$ have been synthesized using various bottom up methods for potential applications of uptake study for radionuclides *viz.* uranium (VI), cesium (I) and strontium (II) as well as heavy metal ions namely Cr (VI) and Cu (II).This chapter describes the synthesis methodology of nanomaterial, different characterization techniques used in present study for them and theoretical background of general sorption procedure, reaction mechanism, and kinetics and equilibrium isotherm studies. Error analysis techniques for optimization of equilibrium isotherm parameters using non-linear regression method have also been discussed towards the end of this chapter. This Chapter is divided in three segments namely synthesis methods, characterization techniques and sorption studies.

2.2 General synthesis methods for preparation of nanomaterials

The main challenge for synthesis of nano materials is to prepare them in uniform size in with reasonable porosity specifically for use as sorbents. A variety of methods have been used for the synthesis of nanomaterials depending on the material of interest. The main objective behind the use of nanomaterials instead of using bulk materials for sorption studies is that nanomaterials have high surface to volume ratio, which often leads to porous materials. Agglomeration of particles can be prevented by using suitable inert solvent or surface encapsulation so that the surface activity enhances for sorption does not deteriorate. A variety of nano metals, metal oxides, sulfides, polymers and composite nanomaterials have been synthesized by using different synthesis routes. All these synthetic techniques have been broadly classified into two categories, namely solid state method and soft chemical method **[144].**

2.2.1 Solid state method: It is a conventional method for preparation of polycrystalline materials where mechanical mixing of the constituents is required followed by repeated grindings and calcination at higher temperature for long duration is performed. This method is not suitable for preparing nanomaterials. It is diffusion controlled process and in turn it is kinetically slow. The major problem with this method is and variation in local stochiometry. Also the products obtained by this route are in micrometer range rather than nano meter range. This can be overcome by soft chemical approach **[145]** of synthesizing nano materials.

2.2.2 Top down methods: In these methods bulk method is subjected to mechanical energy to obtain finer particles in nano dimension. These include laser ablation method, high energy ball milling and inert gas condensation just to name a few.

2.2.3 Bottom up methods

These methods are based on to the building-up of materials from the bottom, atom by atom, molecule by molecule or cluster by cluster which leads to nano structures. Bottom up approach has several advantages as it leads to nanomaterials with fewer defects, more homogeneous chemical composition. On the other hand, top down methods lead to better control over size uniformity of the product. Depending on the application of the nanomaterials, various bottom up methods have been widely used for synthesis of oxide nanomaterials by controlling chemical reaction, nucleation and growth process. Some of these methods are sol gel method, hydrothermal method, solvothermal method, coprecipitation method, sonochemical method, combustion method, spray pyrolysis, micro emulsion, just to name a few. In bottom up methods, the desired precursors are mixed in a controlled manner. The reaction is mainly driven by the reduction of Gibb’s free energy so that the materials produced reaches close to a thermodynamic equilibrium state. In subsequent sections detailed description of these synthesis procedures which have been used in this work for different synthesis of nano materials have been elaborated.

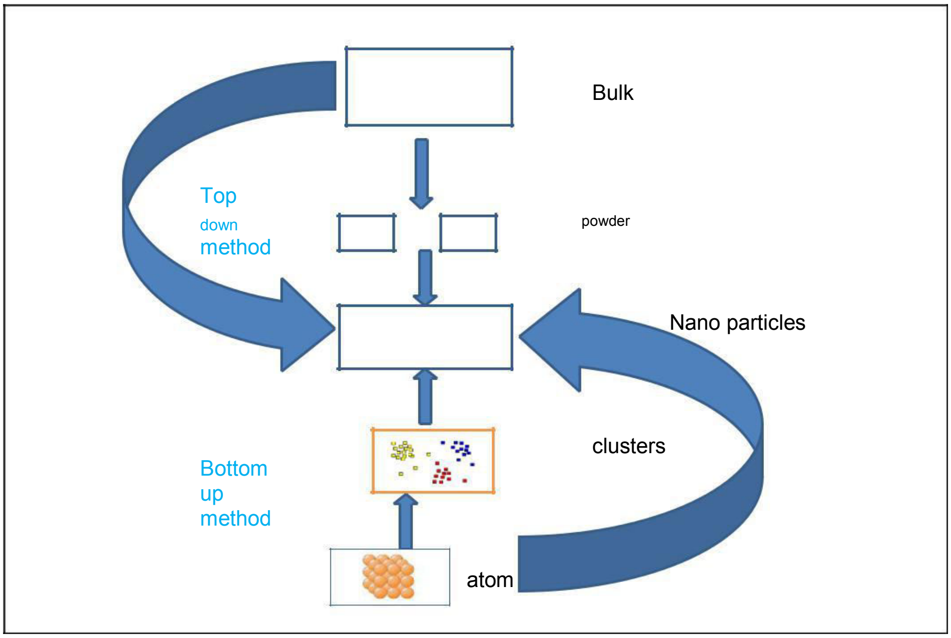

Fig.2.1: Schematic depiction of top down and bottom up methods for preparing nano structured materials

2.2.3.1 Synthesis of nano manganese oxide by alcoholic hydrolysis method:

Manganese (IV) oxide was prepared at room temperature by the alcoholic hydrolysis of aqueous solution of $KMnO_4$. In a typical experiment 2.5 g of $KMnO_4$ was dissolved in minimum volume of de-ionized water. Excess of ethanol was added drop-wise with constant stirring at ~50^{O}C to the aqueous solution of $KMnO_4$ **[146].** The resulting solution was kept on continuous stirring for 3 h at 50^{O}C. The reaction can be represented as follows:

$$KMnO_4 + CH_3CH_2OH \rightarrow CH_3COOK + MnO_2 + KOH + H_2O \qquad \textbf{(2.1)}$$

With time brownish precipitate of MnO_2 was observed and the color of potassium permanganate disappeared. The precipitate was then filtered and washed extensively with de-ionized water and then dried at 100^{O}C. The excess of KOH in the medium was washed completely.

2.2.3.2 Co-precipitation method

This method is the most popular among all the soft chemical methods for nanomaterials synthesis because of its ease of handling, large scale production and its cheap raw materials. Aqueous hydrolysis is more preferred because it can produce fine, spherical particles with higher chemical purity, homogeneity and controlled particle size. Co-precipitation synthesis proceeds in two steps as follows:

I) First required salt precursors are dissolved in aqueous medium.

II) Precipitation of desired material commences with adjustment of pH to desired level.

The co-precipitation technique is widely used for the preparation of ceramics and metal oxide powders. It produces nanomaterials without application of high temperature, with much simplicity and atomic mixing of the constituents yields a final product of near-perfect stoichiometry. Magnetite nanomaterials have been synthesized by this method in this work.

2.2.3.2.1 Synthesis of nano magnetite

In the present study, nano magnetite was prepared via co-precipitation route **[147].** A typical reaction for synthesis of magnetite is as follows:

$$Fe^{2+} + 2\,Fe^{3+} + 8OH^{-} \rightarrow Fe_3O_4 + 4H_2O \qquad \textbf{(2.2)}$$

The synthesis has been carried out under inert atmospheric condition and analytical grade chemicals (from Sigma Aldrich) e.g. ferric chloride hexahydrate, ammonium ferrous sulphate, sodium hydroxide and ethyl alcohol were used. In a typical experiment 6.5 g of ferric chloride ($FeCl_3$) and 7.86 g of ammonium ferrous sulphate, [$(NH_4)_2Fe(SO_4)_2$] were dissolved (as per stoichiometry Fe^{2+}: Fe^{3+} = 1:2) in 100 ml deionised water and transferred to a three neck flask, immersed in room temperature water bath. Boiling solution of 0.5M NaOH was added drop wise (1ml/min) into the 100 mL main solution under constant stirring. The solution was mechanically stirred at 250 rpm at $80^{O}C$ for 2 hours and subsequently centrifuged and washed with water and ethyl alcohol. Nanomagnetite was formed by conversion of metal salts into hydroxides, which took place immediately, and transformation of hydroxides into ferrites. Following these steps, the sample was air dried for overnight and then at $100^{O}C$ for 24 hours.

2.2.3.2.2 Importance of encapsulation of nanomaterials for certain applications

Sometimes, capping agents are used for nanomaterials to get the desired configuration of size and shape, better dispersivity for optimum performance of chemical activity. In addition often it provides chemical stability over coalescing, agglomeration, oxidation or growing large cluster formation. The magnetite nanoparticles surface is hydrophobic and hence they tend towards agglomeration in aqueous solution. Thus to avoid aggregation, surface functionalization or surface coating was provided with a surfactant which has either a polar head and hydrocarbon chain like oleic acid or cage like structure like tetraethyl orthosilicate to stabilise the surface. In case of oleic acid the polar head will be attached with the surface of the nano particle and the hydrocarbon chain will be free to move in surrounding mediaas it is shown in schematic (**Fig 2.3)** .Surface encapsulation thus chemically enhance the surface activity where the external surface is the main participant for sorption of metal ions. Therefore, encapsulating agent mostly enclose the materials, retaining its magnetic property arising due to nano scale.

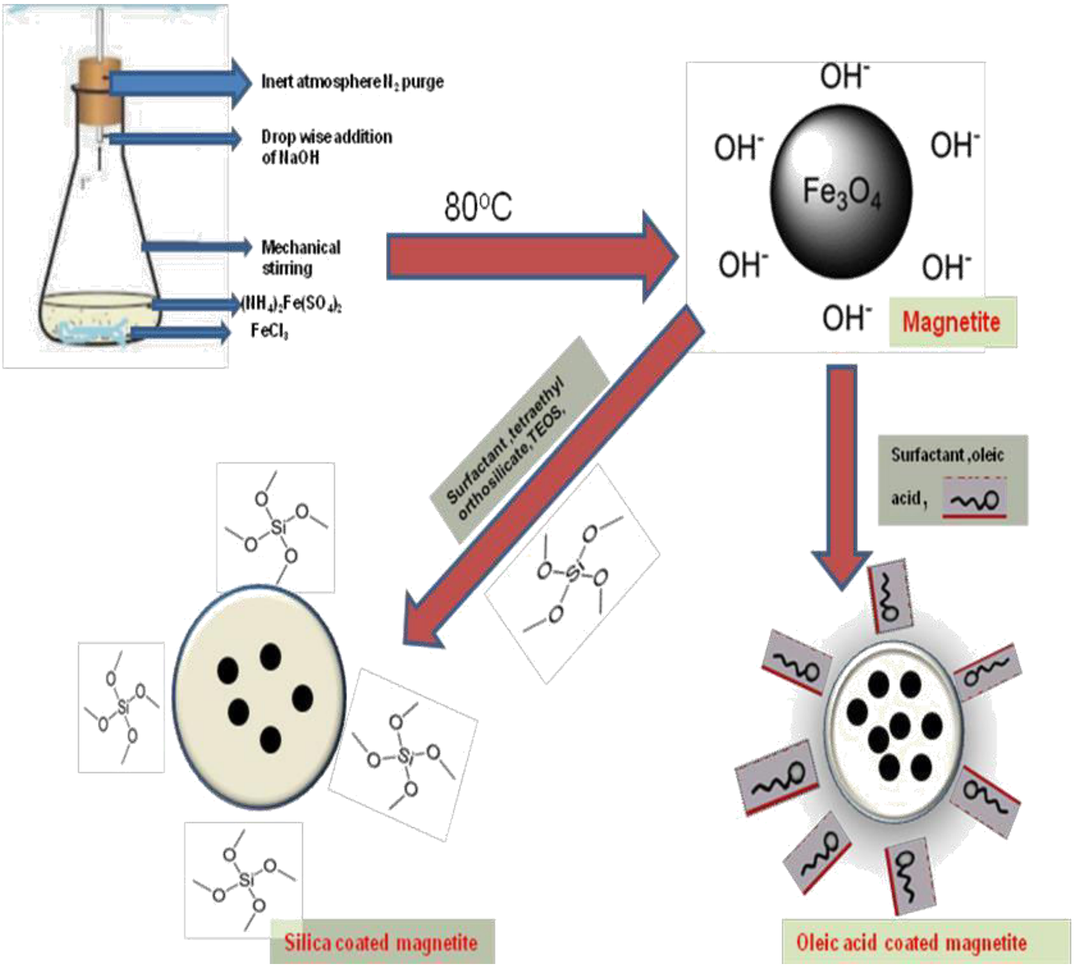

Fig. 2.2: Schematic representation of nano magnetite synthesis and encapsulation by two different surfactants

2.2.3.2.3 Synthesis of oleic acid coated magnetite

For preparation of oleic acid ($CH_3(CH_2)_7CH=CH(CH_2)_7COOH$) coated nano magnetite/composite, 0.8 ml oleic acid was added to Fe_3O_4 in alkaline medium and kept for stirring for 20 hours. It was then washed with alcohol, dried in hot air oven and finally oleic acid coated nanocomposite was obtained. Oleic acid modifies the surface so the magnetic poles will repel each other which favor morphological stability.

2.2.3.2.4 Synthesis of silica coated magnetite

For preparation of silica coated nano magnetite, bare magnetite obtained earlier was added to water, alcohol and liquid ammonia mixture following a modified Stober method **[148].** Then this dispersion was homogenized by ultrasonication in water bath. In next step, under continuous mechanical stirring, 1.6ml tetraethyl orthosilicate (TEOS) was added slowly to this solution. After continuous stirring for 12 h, silica was formed on the surface of magnetite nano materials by hydrolysis and condensation reaction of TEOS.

Further washing of the as-prepared material thrice with alcohol and followed by drying in air resulted in the final product silica coated magnetite. The silica coated magnetite has several advantages such as, screening of the magnetic dipolar attraction between magnetic nanoparticles favoring the dispersion of magnetic nanoparticles in liquid media and preventing them from leaching in an acidic environment. Acidic environment is very common phenomena in separation of radioactive cesium and strontium in nuclear industry. In addition, due to the presence of so many silanol groups (Si–O–H) on the silica layer, silica-coated magnetic nanoparticles will be active for sorption of metal ions on their surface. The most important advantage for silica coated magnetite is that the silica layer provides a chemically inert surface for magnetic nanomaterials **[149]**.

2.2.3.3 Sonochemical method

Sonochemistry is a process where molecules undergo a chemical reaction by application of powerful ultrasound radiation in the frequency range of 20 KHz-10MHz.This method involves high energy and pressure on a short time scale. Sonochemical synthesis is based on acoustic cavitations resulting from the continuous formation, growth and implosive collapse of the bubbles in a liquid **[150].** Cavitations are a process in which mechanical activation destroys the attractive phase of the molecules in liquid phase. By applying ultrasound, compression of the liquid is followed by rare fraction in which sudden pressure drops which forms small oscillation bubbles of gaseous substances. The growth of the bubble occurs through the diffusion of solute vapor into the volume of the bubble. The bubbles expand with each cycle until they reach on unstable size, they can collide and/or violently collapse. According to the hot spot mechanism, very high temperatures (5000–25,000 K) **[151]** are obtained upon the collapse of the bubble. Since this collapse occurs in less than a nanosecond **[152]**, very high cooling rates are also obtained. This high cooling rate hinders the organization and crystallization of the products. Since cavitation can only occur in liquids chemical reactions, this is not seen in the ultra sonic irradiation of solid or solid gas systems. In present work, all the syntheses have been carried out in the absence of any capping agent therefore it is also a surfactant free and template free technique which ensures easy recovery of the final product. Nano materials are finally formed because the fast kinetics does not permit the growth of the nuclei, and in each collapsing bubble a few nucleation centers are formed whose growth is limited by the short collapse.

The synthesis of four material such as $SrWO_4$, $SrMoO_4$, Y_2WO_6 and $Y_2 (MoO_4)_3$ was carried out in aqueous media under air at room temperature and pressure by the sono chemical method. Analytical Reagent grade strontium nitrate [$Sr(NO_3)_2$], yttrium nitrate [$Y(NO_3)_3.6H_2O$], sodium tungstate [$Na_2WO_4.2H_2O$] and sodium molybdate [$Na_2MoO_4.2H_2O$] of high purity (99%) were obtained from commercial sources.

2.2.3.3.1 Synthesis of $SrWO_4$

To an aqueous solution (25ml) of [$Sr(NO_3)_2$] (3.50 g, 16.54 mmol, 25ml aqueous solution of [$Na_2WO_4.2H_2O$] (5.46 g, 16.54 mmol) was added drop wise under pulse sonication. After the addition was complete, the reactants in the beaker was sonicated (100 W/cm^2) under air for

30min. using an ultrasonicator (Oscar Ultrasonic's) operating at 40 kHz. The resulting precipitate was washed with water repeatedly and centrifuged. The white precipitate obtained was dried in air.

2.2.3.3.2 Synthesis of $SrMoO_4$

An aqueous solution (25ml) of $[Sr(NO_3)_2]$ (3.01 g, 14.26 mmol) was pulse sonicated and 25ml of $[Na_2MoO_4.2H_2O]$ (3.45 g, 14.26 mmol) was added to it drop wise. Immediate precipitation was observed. The ultrasonication was continued for 30min and the resultant solution was centrifuged to separate the precipitate. The white precipitate was washed thrice with distilled water and air dried.

2.2.3.3.3 Synthesis of Y_2WO_6

$[Y(NO_3)_3.6H_2O]$ (2.26 g, 5.90 mmol) was dissolved in 20ml of water. To it 25ml of an aqueous solution of $[Na_2WO_4.2H_2O]$ (1.95 g, 5.90 mmol) was added under sonication (100 W/cm^2). The reactants were sonicated for 90min.The white precipitate formed was centrifuged out and washed repeatedly. The product obtained was heated in a muffle furnace at 300°C for 1h.

2.2.3.3.4 Synthesis of $Y_2(MoO_4)_3$

$[Na_2MoO_4.2H_2O]$ (1.72 g, 7.10 mmol) solution in 25ml of water was added slowly to a 20ml solution of $[Y (NO_3)_3.6H_2O]$ (2.72 g, 7.10 mmol). The mixture was sonicated for 90min using an ultrasonicator operating at $100W/cm^2$. The precipitate obtained was washed repeatedly with distilled water and centrifuged out. It was dried in air and heated in a muffle furnace at 750°C for 1h.

2.3 Characterization techniques

A number of techniques have been used for the physical as well as chemical characterization of the synthesized nano materials and for the analytical purposes of the sorbed metal ions. These are

X-ray diffraction (XRD), Fourier Transform - Infra Red Spectroscopy, Transmission electron Microscopy, BET surface area analyzer, Dynamic Light Scattering for Zeta potential analyzer, Vibrating-sample magnetometer(VSM), Small Angle X-ray Scattering (SAXS), Gamma spectrometry using NaI (Tl) detector,UV-Vis absorption spectroscopy, Atomic absorption spectroscopy (AAS) and Inductively coupled Plasma-Atomic Emission Spectroscopy (ICP-AES).Detailed descriptions are given below. These techniques are briefly described in subsequent sections.

2.3.1 X ray diffraction

For the characterization of nanomaterials the first step is the materials structure determination that is whether the crystalline material is in nano range or not. The materials building blocks are atoms and the atomic arrangements in the crystal is the main source of information for diffraction study and further study of sorption process. In a simple method of diffraction study an incident x-ray wave is directed into a material and a detector is typically moved about to record the directions and intensities of the outgoing diffracted waves. Each material has a set of unique d-spacings, which allow the identification of the material. This property makes the diffraction experiment more powerful tools for characterization X-rays are invisible, electrically neutral and electromagnetic radiations wave length ranges from about 0.04 angstrom to 1000 angstrom. X rays are generated from the inner shell electronic transitions in an atom that is termed as characteristics X rays. The higher energy X rays are produced when all the kinetic energy of the incident particles are converted to X rays. When an electromagnetic ray is incident on a solid material, coherent or incoherent scattering or absorbance can occur. The constructive interference will occur for a coherently scattered X rays based on their particular angle when the path difference between the two rays differ by an integral number of wavelengths. Thus coherent scattering is the basic requirement for X ray diffraction to occur **[153].**The classical Braggs law of diffraction that relates the possibility of constructive interference to the inter planar separations is given as

$$n\,\lambda = 2\, d_{hkl} \sin\theta \qquad \textbf{(2.3)}$$

where λ is the wavelength of X rays, θ is the glancing angle or Bragg's angle, d_{hkl} is the inter planner distance between the crystal planes that cause constructive interference and n is the order of diffraction which is a positive integer. This principle of X ray diffraction has been extended for qualitative and quantitative information viz phase identification, crystal structure determination crystallite size determination for a crystalline materials. As the crystal lattice consists of parallel rows of atoms equivalent to the parallel lines of the diffraction grating, the inter-planar spacing could be successfully determined from the separations of bright fringes of the diffraction pattern formed is due to constructive interference**[154]** using the Bragg's equation. A typical X ray Diffraction experimental set up consists of

1. X-ray Tube that is the source of X Rays. During the generation of X rays, the target element gets heated and hence it requires a continuous cooling. The CuKά (λ = 1.5406Å) from sealed tube was used as the incident beam. The X-ray tube rating was maintained at 30 kV and 20 mA.

2. Incident-beam optical instruments which condition the X-ray beam before it hits the sample. These includes beta filter, soller slits and divergence slits. The x rays are produced in all direction so to diverge the X ray beams the divergent slits are used and then the rays passed to the Be window. Also, the background and beta radiation are filtered using beta filters, which must have low absorption for the characteristic radiation.

3. The goniometer which holds and moves the sample. It has been calibrated for correct zero position using silicon standard.

4. Receiving-side optical facility which condition the X-ray beam after it has encountered the sample and these include anti scatter slit, receiving slits and soller slits

5. Monochromator which separates out the stray wavelength radiation as well as any fluorescent radiation emitted by the sample. Here a curved graphite single crystal has been used for this purpose.

6. Detector which counts the number of X Rays scattered by the sample. It is a proportional counter (Argon filled) or GM counter. By sweeping the detector from one angle to the other, the diffracted rays are scanned and the angle where the Bragg's law is satisfied, a constructive interference among the diffracted x-rays occur which results in the sharp rise in the intensity (peak). Generally the scan in the 2θ ranges from 10 degree to 70 degree with a step width of 0.02°, and scan rate of 1° per minute which is sufficient for identification of a well crystalline inorganic material. Here, the observed diffraction pattern were compared with JCPDS-ICDD (Joint Committee on Powder Diffraction Standards- International Centre For Diffraction Data, 1974) **[155]** files available for reported crystalline samples. The average crystallite size of the nano materials synthesized has been estimated from the full width at half maximum (FWHM) of the principle peak in the XRD pattern using the Scherer's formula as **[156]**

$$t= 0.9\lambda/B \cos \theta_B \qquad \textbf{(2.4)}$$

t= thickness of the crystal (Å)

λ is the x ray wave length and theta B is the Bragg angle.

The Line broadening B is measured from the extra peak width at half the peak height and is calculated from Warren formula as

$$B^2 = B_M^2 - B_S^2 \qquad \textbf{(2.5)}$$

B_M= the measured peak width in radians at half peak height

Bs=the measured peak width of a peak of a standard material (silicon)

2.3.2 Transmission Electron Microscopy

The another powerful optical microscopic technique for characterization of nanomaterials is Transmission Electron Microscope (TEM) which is a technique where a beam of electrons is transmitted through a ultra thin specimen and subsequently a image is formed as a result of the interaction of the electrons transmitted through the specimen, finally the image is magnified many a times with a powerful lenses and focused onto an imaging device of fluorescent screen to get a detailed morphology of the sample.

The different parts of a TEM instrument involve:

1. Electron Source which Produces highly energetic and highly coherence electron beams
2. Condenser lenses and aperture which controls spot size and illumination area on sample
3. Sample of interest
5. Objective lens and aperture which takes the images of the sample
6. Projector lenses which Changes modes from diffraction to imaging
7. Fluorescent Screen to detect the final output.

In this work, TEM results were analyzed by using JSM-7600F JEOL JEM-2100F FEG TEM operating with a 100 kV accelerating voltage. In order to get the diffraction pattern, lattice spacing and particle size, 1-2 milligram nanomaterial were dispersed in isopropanol, dropped onto a carbon-coated copper grid and air dried for final sample to be used in TEM.

2.3.3 Small Angle X Ray Scattering (SAXS)

The Small Angle X ray Scattering (SAXS) is often used when it is required to detect large lattice spacing of the order of tens or hundreds of interatomic distances [**157**].This technique is mainly used for detecting in homogeneities on the scale of 10 to 1000Å. In this work, biphasic existence in oleic acid coated magnetite was studied by this technique.SAXS measurements were carried out using a laboratory based SAXS facility with CuKά source. The diameter of the incident photon beam on the sample was taken as 0.4 mm. The SAXS detector was mounted at a sample-to-detector distance of 1.07 m, corresponding to a 2θ range of 0.1–3.5 degrees.

2.3.4 Fourier Transform - Infra Red Spectroscopy

The basic theory behind the Infrared Spectroscopy involves the measurement of change of dipole moment due to the vibration of chemical bonds of materials as a result of absorption of infrared radiation. To improve the signal to noise ratio, numerical iteration method like Fourier transformation are applied. The improved spectroscopic method is now termed as Fourier Transformation IR Spectroscopy (FTIR). In this method, all the frequencies are used simultaneously to excite all the vibrational modes of different types of bonds which again minimize the time of experimentation. In this work, a Bomem MB102 FTIR machine having a range of 200-4000 cm^{-1} and with a resolution of 4 cm^{-1} has been used. IR radiation was generated from globar source of silicon carbide rod. The instrument used CsI single crystal, as the beam splitter and deuterated triglycine sulphate (DTGS) as detector. Prior to IR measurements, the samples were ground thoroughly by mixing with dry KBr powder, made in the form of a thin transparent pellet and introduced into the sample chamber of the instrument to record the spectra.

2.3.5 BET surface area analyzer

For sorption purposes, the surface properties like surface area and porosity of the materials are the main contributor for on efficient sorption process to occur. A high surface area implies a larger number of adsorption sites consequently higher total adsorbate loadings as well as faster sorption kinetics. When the quantity of adsorbate on a surface is measured over a wide range of relative pressures at constant temperature, the result is an adsorption isotherm. The adsorption is obtained point-by-point in the Autosorb-1 by admitting to the adsorbent, successive known volumes of adsorbate, by measuring the equilibrium pressure **[158].** The most common Brunauer-Emmett-Teller (BET) surface area of all the samples were determined by N_2 adsorption-desorption measurement, using Quantachrome Autosorb Automated Gas Sorption System. The samples were out-gassed at high temperature in vacuum, before the measurement.

2.3.6 Dynamic Light Scattering for Zeta potential analyzer

Zeta potential of the samples was determined using a Malvern Zetasizer nano ZS instrument. 1ml of the sample of interest in aqueous solution was taken in the transparent cell for carrying out the zeta potential measurements. Zeta potential is a measure of the magnitude of the electrostatic or charge repulsion/attraction between particles, and is one of the fundamental parameters known to affect stability. Its measurement brings detailed insight into the causes of dispersion, aggregation or flocculation, and can be applied to improve the formulation of dispersions, emulsions and suspensions.

2.3.7 Vibrating-Sample Magnetometer (VSM)

Vibrating Sample Magnetometer measures the electromotive force induced by magnetic moment of a materials when it is vibrating at a constant frequency that is vibration frequency, under the presence of a static and uniform magnetic field which is proportional to the magnetic moment, vibration amplitude and vibration frequency. The instrument displays the magnetic moment in electromagnetic unit (emu) units. The magnetic properties of the samples were measured by Vibrating Sample Magnetometer (Lakeshore, VSM – 7410). The room temperature field dependent magnetic measurements (M vs. H) were carried out on powder samples mounted tightly in the sample holder by varying the magnetic field. The magnetization vs. temperature (M *vs*. T) was measured by VSM-7410 under a constant applied magnetic field to obtain the Curie temperature (Tc) of the sample. The temperature dependent magnetization under zero-field cooled (ZFC) and field-cooled (FC) conditions in a constant applied field were measured. In the ZFC measurements, the samples were cooled from 305 to 5 K without applying an external field. After reaching 5 K, a field was applied and the magnetic moments were recorded as the temperature increased. For FC measurements, the samples were cooled from 305 K under an applied field; then the magnetic moments were recorded as the temperature increased.

2.3.8 Gamma spectrometry using NaI (Tl) detector

The detection of ionizing radiation by the scintillation light produced in certain materials is one of the oldest methods. This method is non destructive method and accurate in small amount also **[159].** The scintillation use the fact that certain materials when interact with a nuclear radiation, emits a small flash of light i.e., scintillation. This scintillation when coupled with an amplifying device such as a photo multiplier tube to convert into electrical pulses, and connected in an amplifier circuit that multiplies gives the electrical signal which is analyzed and counted electronically to give the information about the incident radiation. The scintillating material generally used is NaI(Tl). As the radiation passed through the scintillator, excitation of the atoms and molecules actuates light to be emitted. This light is transmitted to the Photo Multiplier tube (PMT) where it is converted into a weak current of photoelectrons, which is then further amplified by an electron multiplier system consisting of preamplifier and amplifier. The resulting electric current signal is then analyzed by an electronic system of Multi channel analyzer.

2.3.9 UV-Vis absorption spectroscopy

The principle of UV-visible absorption spectroscopy is based on the “Beer-Lambert’s Law”, which states that “A beam of light passing through a solution of absorbing molecules transfers energy to the molecules, as it proceeds, and, therefore, decreases progressively in intensity. The decrease in the intensity, or irradiance, (dI), over the course of a small volume element is proportional to the irradiance of the light entering the element, the concentration of absorbers (C), and the length of the path through the element, (dl). Mathematically, it can be expressed as:

$A = \varepsilon \times b \times c$ **(2.6)** where, ε is the wavelength-dependent molar absorptivity coefficient, *b* is the path length, and *c* is the concentration When the energy of the incident photon matches with the energy of the excited state of an atom, a molecule, radical or an ion the resonance occurs, and the intensity of the transmitted light is decreased. Depending on the energies of the excited states and the absorbed photons a sorption band is observed. In the present studies, UV-visible optical absorption spectra have been recorded, employing a JASCO Model 605 spectrometer.

2.3.10 Atomic absorption spectroscopy (AAS)

The basic theory behind the Atomic Absorption Spectroscopy involves that if the light of properly selected wavelength falls on a ground state atom, the atom followed by an excitation will absorb the light. This involves a particular wavelength for each material which is a unique property for a particular atom. This specific selection of wavelength followed by absorption/emission is the basis for absorption/emission spectroscopy. By measuring the amount of light absorbed by a particular atom will give the, quantitative determination of the amount of analyte element present in the solution. The use of special light sources and careful selection of wavelength allow the specific quantitative determination of individual elements in the presence of others [**160**].

2.3.11 Inductively Coupled Plasma-Atomic Emission Spectroscopy (ICP-AES)

Inductively Coupled Plasma (ICP) uses a high-frequency alternating field to transfer energy to a flowing inert gas like argon to form plasma of ions and electrons. The plasma is propagated when ionization of metal atoms occurs as a result of collisions with the ions and electrons. The ICP sample was prepared by dissolving 1 mg particles in hydrochloric acid and the solution volume made up 10 mL. The accurate concentration of metal ions in the sample was determined by comparing the intensity of each line with the previously measured intensities of known concentrations of the elements and their concentrations are then computed by interpolation along the calibration lines.

2.4 Sorption studies: The sorption process involves a solid phase that is sorbent, here nano materials and a liquid phase which contains the dissolved metal ions to be sorbed. Sorption studies has been carried out by adding a fixed amount of the sorbent (m) of 0.1 g of synthesized nanomaterials into different test tubes which contain a fixed volume (V) of 10 mL of the sorbate solution of varying concentrations. After mechanical shaking for a fixed time, once the equilibrium between sorbent and sorbate is established, the separation of the sorbed phase carried out. To analyze the sorbed quantity by spectroscopic methods a small portion of the aqueous phase was taken. The uptake of metal ion can be calculated as

$$\textbf{Sorption (\%)} = ((C_0-C_e)/C_0)*100 \qquad \textbf{(2.7)}$$

Equilibrium sorption capacity, qe, was determined as

$$(q_e, \text{mg/g}) = ((C_0-C_e)/m)\ V \qquad \textbf{(2.8)}$$

Where, C_o and C_e are the initial and the equilibrium concentrations of the sorbate in the solution respectively. The typical sorption experiment has been schematically depicted in **Fig. 2.8.**

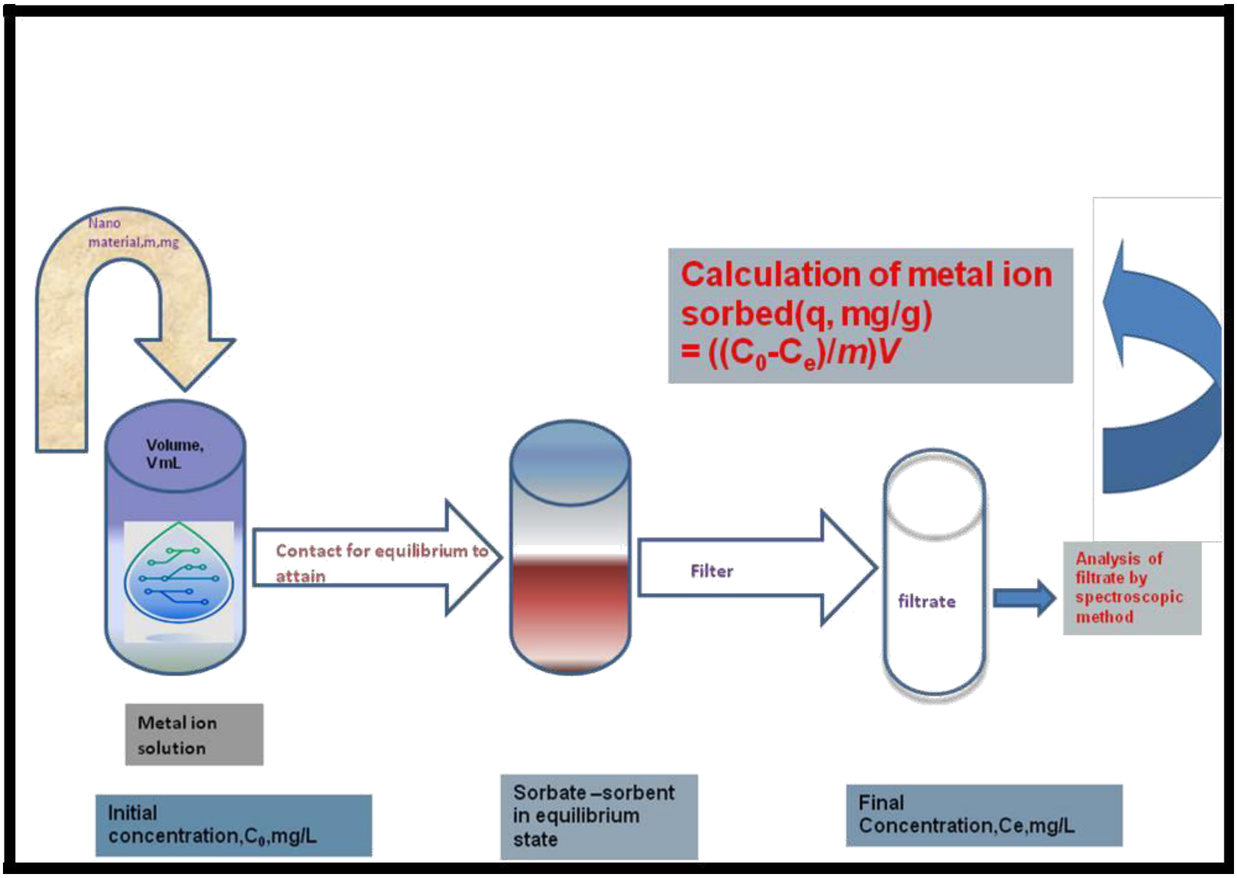

Fig. 2.3: Schematic diagram of a general procedure for sorption reaction

2.4.1 Sorption isotherms

2.4.1.1 Langmuir isotherm

Langmuir **[161]** adsorption isotherm was originally used for gas- solid phase adsorption onto activated carbon. This was the first coherent theory of sorption onto a flat surface based on a kinetic viewpoint. The Langmuir equation initially was formulated on the basis of a dynamic equilibrium between the sorbent and the sorbate, that is, the rate of sorption is equal to the rate of desorption from the surface. The assumptions of the Langmuir model are:

1. Surface is homogeneous, that is, sorption energy is constant over all the sites.
2. Sorption on the surface is localized, that is, atoms or molecules are sorbed at definite, localized sites.

3. Each site can accommodate only one molecule, or atom.

The assumptions of this model are that adsorption is monolayer and occurs at finite defined localized identical and equivalent sites with no hindrance from each other. The mathematical expression of Langmuir isotherm is given by Equation.2.9.q_e is the amount of adsorbate in the adsorbent at equilibrium

$$C_e/ q_e =1/b*q_m + C_e/ q_m \qquad \textbf{(2.9)}$$

C_e – equilibrium concentration

q_m – Maximum capacity of adsorption at equilibrium

b – Langmuir isotherm constant

The main aspect of Langmuir isotherm can be expressed by R_L, a constant known as the constant separation factor or equilibrium parameter which can be used to predict if an adsorption system is "favorable" or "unfavorable". The separation factor, R_L is defined by Equation 2.10, where C_o is the initial solute concentration (mg/L) and b is the Langmuir adsorption equilibrium constant (L/ mg). The value of R_L value indicates the adsorption nature; it can be unfavorable ($R_L> 1$), linear ($R_L = 1$), favorable ($0 < R_L< 1$) or irreversible ($R_L = 0$)

$$\mathbf{R_L, Separation\ factor}=1/1+b\ C_0 \qquad \textbf{(2.10)}$$

2.4.1.2 Freundlich isotherm

The Freundlich isotherm **[162]** is the earliest known relationship that describes the non-ideal and reversible adsorption and can be applied to multilayer adsorption, not restricted to only mono layer as in Langmuir isotherm. The linear form of the equation is given in Equation

$$\log q_e =\log k_F+1/n \log C_e \qquad \textbf{(2.11)}$$

k_F – Freundlich constants

n – Adsorption intensity

The slope gives the value of n which is a measure of sorption intensity or surface heterogeneity and the sorption is termed chemisorptions when the value is between 0 and 1. The value of n if within the range of 1-10, indicates favorable sorption.

2.4.1.3 Temkin isotherm

Temkin isotherm **[163]** considers a heterogeneous surface, where no molecular interaction exists. It is based on Langmuir sorption isotherm. However, like Langmuir model, it does not take into account the lateral interaction between the sorbates. Temkin isotherm assumes that the decrease in the heat of sorption as a function of temperature is linear rather than logarithmic. The heat of sorption of all the molecules in the layer would decrease linearly with coverage due to sorbate-sorbent interactions. The linear form of the Temkin model is given as,

$$q_e = (RT/b)\ln A + (RT/b)\ln C_e \qquad \textbf{(2.12)}$$

A((L mg^{-1}) – Tempkin isotherm equilibrium binding constant

b – Tempkin isotherm constant is dimensionless, R is the gas constant

T is the absolute temperature. A linear plot of q_e *vs.* ln (C_e) enables the determination of the isotherm constants K_T and b, from the intercept and slope, respectively.

2.4.1.4 Dubinin-Redushkevich isotherm

The Dubinin–Radushkevich isotherm **[164]** is an empirical model initially conceived for the adsorption of subcritical vapors onto micro porous solids following a pore- filling mechanism. This model is often successful for high and intermediate concentration ranges but deviates at lower concentration. This has been used to distinguish the physical and chemical adsorption of metal ions. The model is expressed by following Equation:

$$\ln q_e = \ln q_m - \beta\varepsilon^2 \quad \textbf{(2.13)}$$

$$\varepsilon = RT\ln(1+1/C_e) \quad \textbf{(2.14)}$$

$$E = \frac{1}{\sqrt{2\beta}} \quad \textbf{(2.15)}$$

Where β is the degree of heterogeneity ($0 < \beta < 1$) andε is the Polanyi potential.E is the mean free energy per molecule of adsorbate can be computed by the above equation.

2.4.1.5 Redlich-Peterson isotherm

Redlich–Peterson isotherm **[165]** is a hybrid isotherm of Langmuir and Freundlich isotherms incorporating three parameters into an empirical equation stated below.

$$\ln\left(\frac{K_F C_e}{q_e} - 1\right) = g \ln C_e + \ln a_R \quad \textbf{(2.16)}$$

This model incorporates a wide concentration range which can be applied to homogeneous and heterogeneous systems. In this isotherm model linear dependence on concentration in numerator and exponential dependence on concentration is there to incorporate Langmuir and Freundlich isotherm features.

2.4.1.6 Sips isotherm

Sips isotherm **[166]** is also a combined form of Langmuir and Freundlich isotherms for predicting heterogeneous sorption systems. At low concentration, the equation reduces to Freundlich isotherm where as at high concentration of the adsorbate the equation reduces to Langmuir, Isotherm predicting a mono layer adsorption capacity. The equation is written as

$$q_e = \frac{q_{max} K_{Lf} C_e^{1/n}}{1 + K C_e^{1/n}} \quad \textbf{(2.17)}$$

2.4.2 Sorption kinetics

Sorption kinetics gives an idea about the time-dependent evolution of the sorption process until equilibrium is reached. Such studies yield information about the possible mechanism of the sorption, effectiveness of adsorption and the different transition states involved on the way to the formation of the final sorbate-sorbent complex. The results of such study help to develop appropriate mathematical models, to describe the interactions. In this work, four different models have been used for predicting the adsorption kinetics on to the different adsorbent used. These are:

2.4.2.1 Pseudo first-order kinetic model

Lagergren equation **[167]** is probably the earliest known one, describing the rate of sorption in the liquid-phase systems. This equation is called the pseudo first-order equation, or the Lagergren's rate equation, and can be written as

$$\text{Log}\ (q_e - q_t) = \log q_e - ((k_1 * t)/2.303) \qquad \textbf{(2.18)}$$

Where q_t is the amount of sorbate sorbed at time t, and k_1 is the rate constant of the first order sorption. The values of k_1 and q_e can be determined from the slope and intercept, respectively, of the straight line plot of log (q_e - q_t) versus t.

2.4.2.2 Pseudo second-order kinetic model

The pseudo second-order kinetics **[168]** is usually associated with the situation, when the rate of direct sorption/desorption process controls the overall sorption kinetics. The pseudo second-order kinetic model is expressed as

$$\frac{t}{q_t} = \frac{1}{k_{2ads} \times q_e^2} + \frac{t}{q_e} \qquad \textbf{(2.19)}$$

k_{2ads} is the rate constant of the pseudo second-order sorption and the plot of t/q_tvs. t gives a straight line from where the slope and intercept of the values of q_e and h, respectively, can be determined.

2.4.2.3 Elovich model: Elovich equation **[169]** is used to describe second order kinetic assuming the actual solid surfaces are energetically heterogeneous but the equation does not propose any definite mechanism for adsorbate- adsorbent. The equation depicting the Elovich model is given as follows:

$$q_t=\ln (a_e b_e)/b_e+(1/b_e) \ln t \qquad \textbf{(2.20)}$$

Where, a_e is the initial adsorption rate (mg/g min) b_e is related to the extent of surface coverage and activation energy for chemisorptions (g/mg).

2.4.2.4 Intraparticle diffusion model

This model **[170]** is represented by the following equation:

$q_t=k_d t^{1/2}+C$ **(2.21)** Where k_d is the intraparticle diffusion rate parameter and C (mg/g) is a constant that gives an idea about the thickness of the boundary layer. The values of k_d and C can be determined from the slope and the intercept, respectively, of the plot of q_t *vs* $t^{1/2}$.

2.5 Error analysis: Linear regression is the most efficient tool for defining the best fitting relationship which quantifies the distribution of adsorbates, mathematically analyzing the adsorption systems and varying the consistency and theoretical assumptions of an isotherm model [**171].** For the simplicity of theoretical calculation, isotherm equations are linearized which results into different observations of dependent value i.e. maximum sorbed quantity for different linear form for a single isotherm model equations. These differences in outcomes for different linearizes form of a linearized non linear equation arise from the variation in the error structure related to this transformation of linearzing the non linear equation. On doing this, the basic assumption of linear regression analysis is violated which causes distortion of experimental error, different axial setting etc **[172]**. For all these reasons, Non linear regression analysis has been adopted to estimate the best fit isotherm for sorption studies. It has the advantage of not altering the error distribution as there is no involvement of linearization is there and the equation is used as it is without any transformation, thus no axial change. This method assumes a trial and error calculation in a computer operation followed by an iterative method for minimization of the error. For minimization of error, it follows some statistical functions. The minimum value of these statistical error functions will give the idea for best fit isotherm for the sorption process for a particular metal ion onto a sorbent. The statistical error functions used here are stated as below.

SAE=EABS =$\sum_{i=1}^{n} Mod \llbracket(q\rrbracket_{exp} - q_{calc})$um of Absolute Error (mg/g), with an increase in the errors will provide a better fit, leading to the bias towards high concentration range.

ARE= $\frac{\sum_{i=1}^{n} MOD\left(\frac{q_{calc}-q_{exp}}{q_{exp}}\right)}{n}$ age Relative Error, It indicates a tendency to underestimate or overestimate the experimental data, thus it will attempt to minimize the fractional error distribution across the entire studied concentration range.

MPSD=100*SQRT $((\Sigma(q\_exp - q\_calc)\hat{}2 / q\_exp)/(n-p))$, Marquardt’s Percent Standard Deviation, It is nearly a modified geometric error distribution

MPSED =SQRT$((\Sigma \llbracket((q_exp - q_calc) / q_exp)\rrbracket \hat{}2)/(n-p))$, it is the same as MPSD but it takes account for the squares value of experimental data.

SSE=$\Sigma(q_{calc} - q_{exp})^2$, Sum of the Squares of the Error, most widely used error function. At higher end of the liquid concentration range and squares of the errors tend to increase, and then SSE will be useful for error estimation.

ARED=$\frac{100}{\square}\sum_{\square=1}^{\square} \text{Mod}\left(\left(q_{exp} - q_{calc}\right)/q_{exp}\right)$, Average relative Error Deviation

ARS=$SQRT\left(\left(\Sigma\left(\left(\left(q\_exp - q\_calc\right)\right) / q\_exp\right)^{\wedge}2\right) / \left(n-1\right)\right)$, Average relative Standard Error

HYBRID=$\left(\Sigma\_(i=1)^{\wedge}n\ mod\left(\left(q\_exp - q\_calc\right) / q\_exp\right)\right)/(n-p)$, Hybrid Fractional error function introduced to include low concentration range error.

q (%) =100* ARS, Normalized Standard Deviation

Standard deviation of Relative Error (RE) =SQRT$\left(\frac{\sum_{\square=1}^{\square}\left[\left(q_{exp}-q_{calc}\right)-ARE\right]^{2}}{\square-1}\right)$

Chi Squared æ^{2}=$\sum_{\square=1}^{\square}\frac{\left(q_{calc}-q_{exp}\right)^{2}}{q_{exp}}$, chi squared Error, very powerful statistical tool for the best fit for an adsorption system. It is obtained by judging the sum squares differences between the experimental and the calculated value of data with each squared difference is divided by its corresponding value.

2.6 Conclusion: In conclusion this chapter gives detailed description of synthesis methodology characterization techniques and general idea about sorption study carried out in this work. The specific examples will be discussed in subsequent chapters.

CHAPTER 3

Sorption of uranyl and other metal ions using nanocrystalline manganese oxide (MnO_2) sorbent

---

The work reported in this chapter has been published as follows:

Sorption characteristics of nano manganese oxide: Efficient sorbent for removal of metal ions from aqueous streams
J. Mukherjee, J. Ramkumar S.Chandramouleeswaran, R.Shukla and A.K.Tyagi
Radioanal. Nucl. Chem. 297 (2013) 49-57

3.1 Introduction: Separation of metal ions for the selective sorption of an ion of interest from aqueous stream is of great importance in different fields like recovery of precious metal ions from the waste, hydrometallurgy, removal of toxic metals from the environment etc. Selective separation of uranium ions (uranyl ion) from a source containing the different metal ions at low concentration level has attracted the attention because of its importance in nuclear industry. There are a number of procedures including solvent extraction and membrane separation for the separation of metal ions. Although widely used in nuclear fuel reprocessing, traditional liquid–liquid extraction still has disadvantages such as the use of toxic or flammable solvents, the formation of emulsions, and the generation of large volumes of secondary hazardous organic wastes. In contrast, solid-phase extraction based on solid sorbents with large sorption capacity is preferred due to its simplicity, reliability, low consumption of solvent, and the ability to achieve a high separation factor **[173–179].** A great deal of research is carried out continuously to develop new sorbents which are cheap and easily available so that they need not be regenerated using expensive processes after their use for sorption. Hence the research in developing new sorbents can be focused on the development of simple and economic procedures for the synthesis of the sorbents or on the development of methods for the reusability of these sorbents. Nanocrystalline compounds appeared as a good alternative sorbent due to their improved sorption characteristics resulting from high surface area and surface active sites. Transition metal oxides constitute one of the most fascinating classes of the inorganic solids capable of exhibiting wide variety of structures and properties. Residual surface hydroxides can contribute to the rich surface chemistry exhibited by metal oxides and this chemistry is generally attributable to Lewis acid, Lewis base, and Bronsted acid sites of varying coordination. Different techniques like solid-state synthesis, sol-gel etc have been used for the preparation of transition metal oxides

[180-192]. One such important type of oxide is the manganese dioxide. The use of functionalized nanoparticles has been reported for sorption of uranium. However, in the present study, the aim was to use the nanooxide without any functionalization and thus avoid the additional step of surface modification and to see if there was a possibility of achieving removal for metal ions of interest. Therefore, in this work, the synthesis of nano-manganese oxide was carried out and its potential application as room temperature sorbent for uptake of different metal ions including uranium has been investigated. Various experimental conditions were optimized to get maximum uptake.

3.2 Synthesis and characterization of nano manganese oxide: The nanocrystalline MnO_2 was prepared by treating $KMnO_4$ with excess of ethanol **[146].** The synthesis and characterization procedure has been given in Chapter 2.

3.3 Sorption experiments: The uptake studies were carried at room temperature ($25^{O}C$) in batch mode using aqueous solutions containing metal ion or its mixture with other cations. 10 ml of aqueous metal ions of interest (or mixture) solution of known concentration at a particular pH was equilibrated with a weighed amount of oxide sample for a known period of time. The concentration of metal ion left behind in solution after equilibration was determined. The pH of the solution before and after equilibration was also measured. The solution after equilibration was analyzed completely for the presence of other cations using atomic emission spectroscopy. The oxides after equilibration were again characterized using XRD technique.

3.4 Results and discussions

3.4.1 Characterization of nano manganese oxide: The nano MnO_2 powder sample obtained was characterized using different techniques. The X-Ray diffraction pattern of the nano manganese oxide is shown in **Fig. 3.1(a)** and matches well with the reported data on MnO_2 [PC-PDF number # 440141]. However, the much higher background in this XRD pattern shows a poor crystallinity in this sample. The average crystallite size calculated from the Scherrer's formula was found to be ~ 8 nm. The TEM micrograph **(Fig.3.1b)** confirms the results obtained by XRD. The surface area of the synthesized nano oxide is 145 m^2/g and this when compared to the bulk MnO_2 obtained from Alpha AESAR was far superior. The comparisons of the data for the bulk and nano oxides are shown in **Table 3.1.**

Table 3.1: Physical characteristics of nano and commercially available MnO_2

Sample name	**Zeta potential(mV)**	**Surface area (m^2/g)**	**Pore volume(cm^3/g)**
MnO_2 (commercial)	-17.3+1.0	~16	0.049
Nano MnO_2 (present study)	-47.6+4.6	~145	0.729

The zeta potential values for the nano manganese oxide were measured as a function of pH and the results are shown in **Fig.3.2.**

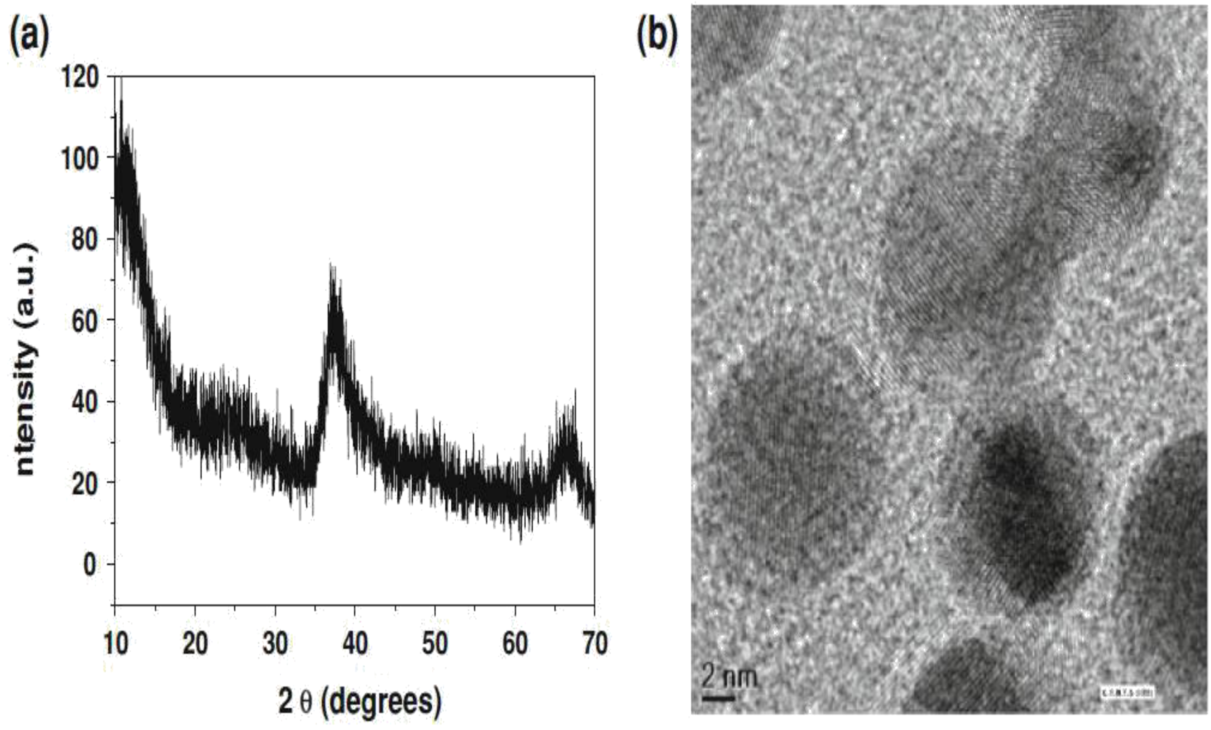

Fig. 3.1: (a): XRD pattern and (b): TEM micrograph of nano manganese dioxide

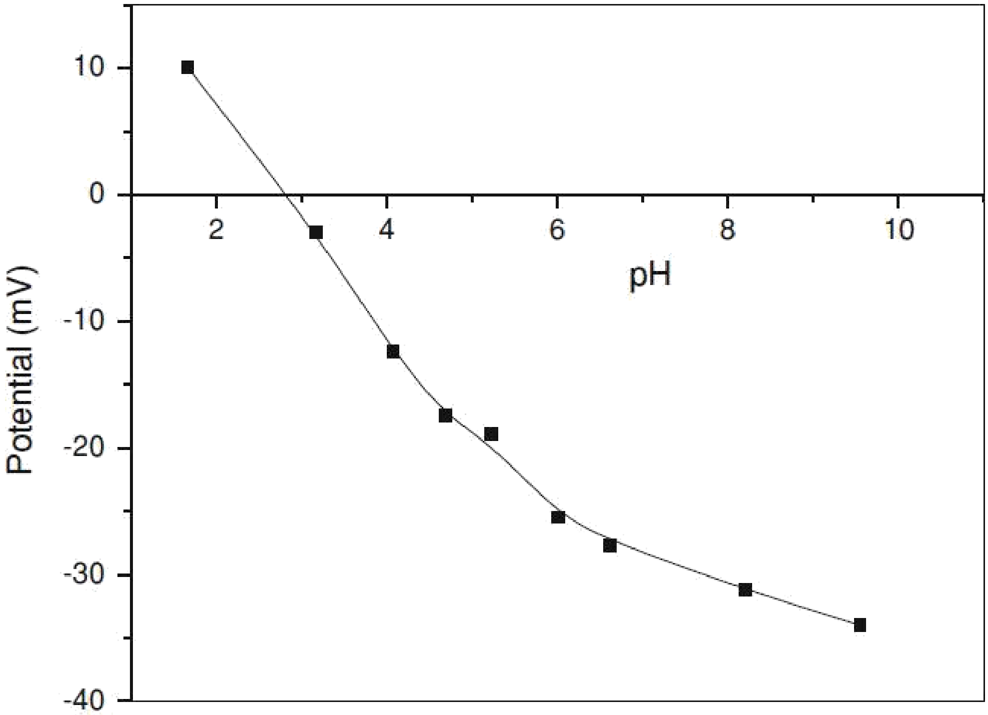

Fig 3.2: Variation of surface charge of Nano MnO_2 with pH

3.4.2 Sorption studies: Manganese oxide in bulk form is known to take up most metal ions. However, in the present study it was seen that the powder characteristics of the synthesized nano-manganese oxide are much superior to that of bulk and hence it was expected the uptake of metal ions would be much superior to that of commercially available MnO_2. Earlier studies on the use of the manganese oxide in both bulk and nano form showed that the sorption efficiency for metal ions of the manganese oxide was far superior to the bulk manganese oxide **[146]**. It is to be noted that the present work deals with the use of nano manganese oxide for the removal of different metal ions including uranyl ion. Reports reveal the sorption of uranium has been carried out using various solid phase materials **[193-199].** Further it is to be noted that the use of nano manganese oxides for the studies of sorption of uranyl and transition metal ions have not be covered to such an extent. Hence it was thought that the transition metal oxide with easy preparation procedure and relatively low cost could be used as possible alternative sorbent.

Hence the studies were carried out with an aim to evaluate whether the nano manganese oxide could have some sorption properties for transition and uranyl metal ions.

Various experimental parameters were studied to get the optimum conditions to achieve maximum uptake of metal ions. The sorption studies were not carried out as a function of different particle sizes. The nanoparticles synthesized in one single batch were used for the sorption with an aim of understanding the role of surface phenomena in sorption. It was also of interest to know whether nano manganese oxide could have a possible application to actual samples at room temperature. Manganese oxide in bulk form is known to take up most metal ions. The different parameters were optimized to obtain maximum uptake. In the present study, the sorption of single ions of copper, nickel, cobalt, zinc and uranyl ions was studied. From the results of the single ion studies, it was proposed to understand whether a selective uptake of the ions could be achieved.

The time of equilibration is an important parameter which affects the sorption phenomena. The studies were carried out by equilibrating 10 mL of metal ion solution ($Cu^{2+}/Ni^{2+}/Co^{2+}/Zn^{2+}/UO_2^{2+}$) maintained at pH of 5 with 0.1 g of the nanoxide. The results of the studies are given in **Table 3.2**.

Table 3.2: Experimental factors for various single ion studies to get maximum uptake

Metal Ions	Time of equilibration (h)	pH
Cu^{2+}	2	3
Ni^{2+}	3	5.5
Co^{2+}	8	3-5
Zn^{2+}	3	5
UO_2^{2+}	8	4.5

It is seen that the time of equilibration needed for the transition metal ions were 3 h whereas the period of equilibration for uranyl ion is 8h. The studies were carried out for cobalt (II) even for 8 h to reveal that even after 8h of equilibration, the uptake of cobalt is low. This gives an idea of difference in the kinetics of uptake of the metal ions by nano manganese oxide.

Since the nano manganese oxide carries a surface charge which varies with pH, it is expected that the initial pH of the solution will have an effect on the sorption behavior. In order to understand this effect, 10 mL of uranyl ion solution of 10 mg/L concentration was equilibrated with 0.1 g of sorbent for a period of 3h for transition metal ions and for 8h for uranyl ion and the results are shown in Table 3.2. It is seen that maximum uptake for the different metal ions was different thus providing a means for separating the metal ions from one another. It was observed that at lower pH values, the uptake is low and with increasing pH, it increases and reaches a maximum at the particular pH. With further increase in pH, there is a decrease in the amount of metal ion taken up. All these results can be explained as follows. At lower pH of 2, it is seen that the surface charge is positive due to the protonation of the surface active sites, resulting in lower up take of metal ions. In this pH, the metal ions are exchanged with the protons on the surface of manganese oxide and therefore there is some uptake despite the surface charge being positive. At pH greater than 3, the surface is negatively charged and the electrostatic attraction becomes responsible for the increased uptake of cations. With further increase in pH, the hydrolysis of metal ions becomes a dominant and results in the decrease in the uptake of metal ions [**200**]. The single ion studies of transition metal ions like Cu^{2+}, Ni^{2+}, Co^{2+} and Zn^{2+} were also studied as a function of pH. The results of all these studies are given in **Table 3.2.** At the optimized period of equilibration, the amount taken up was studied as a function of pH and the results are shown in **Fig 3.3.**

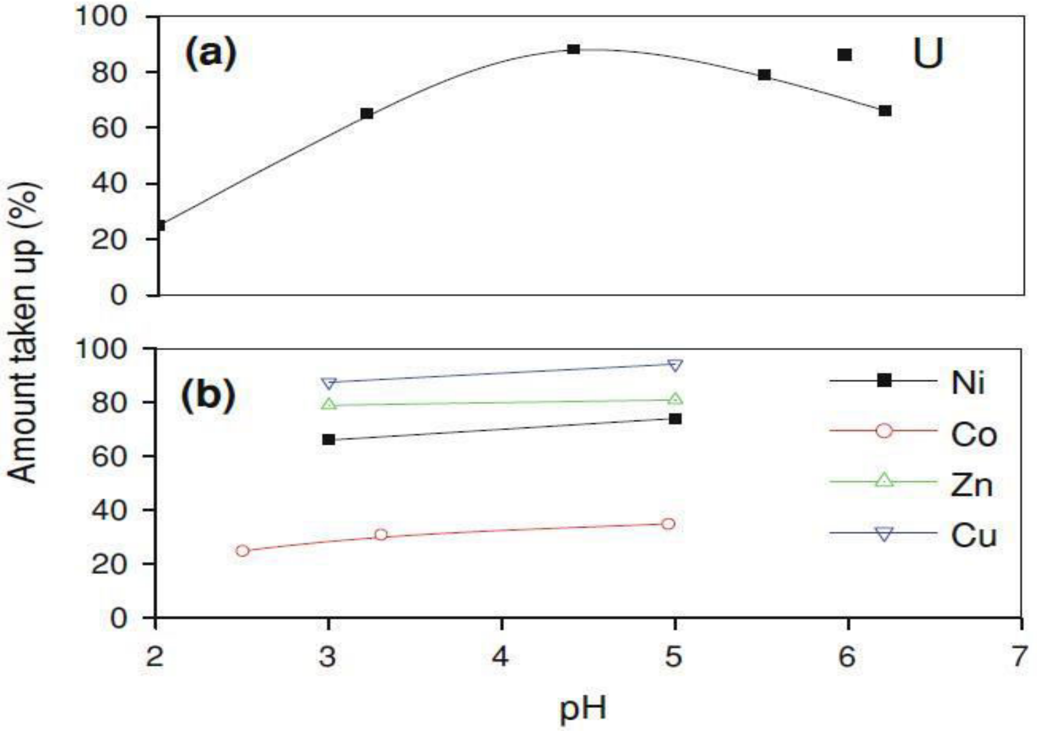

Fig. 3.3: Effect of pH on the amount of metal ions (UO_2^{2+}, Cu^{2+}, Ni^{2+}, Co^{2+}, Zn^{2+}) taken up at optimized time of equilibration

It is seen that the amount of cobalt taken up as a function of time and pH was less than 40%. Thus it is seen that for other ions, the optimized pH could be used for removal of the metal ions from one another.

The effect of initial concentration on the uptake studies was carried out by varying the initial metal ion concentration in the range 10-100 μg/mL at the conditions of pH optimized for each metal ion. The results are plotted in **Fig. 3.4.**

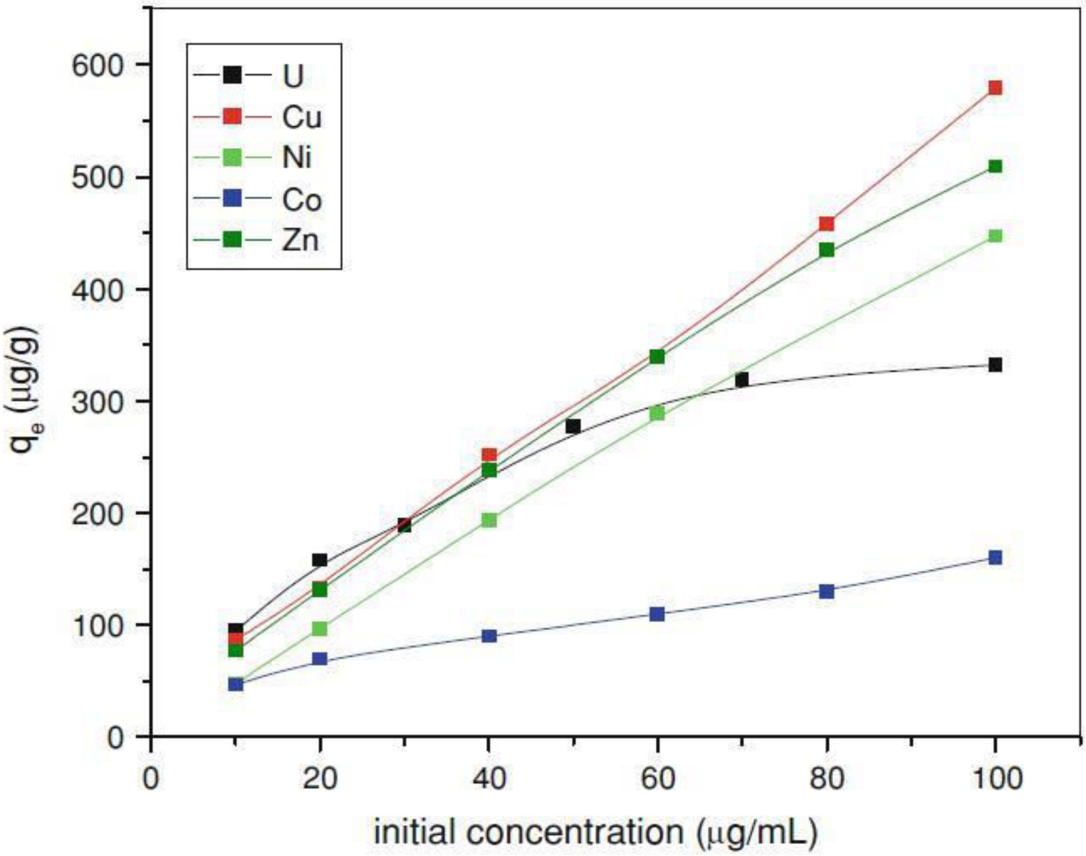

Fig.3.4: Effect of initial metal ions (UO_2^{2+}, Cu^{2+}, Ni^{2+}, Co^{2+}, Zn^{2+}) concentration on the amount taken up

From the studies, it is seen that in the concentration range studied, the amount taken up increases with the initial metal ion concentration and for Ni^{2+} and Zn^{2+}, it nearly reaches saturation.

However, for other two metal ions it does not reach saturation, indicating that the uptake capacity of nano manganese oxide is higher for these two metal ions.

The effect of interferences of these ions on one upon another becomes an important issue as it is seen that the all the ions show uptake by manganese oxide. In order to get some idea as to the interference studies, the effect of various ions on the uptake of uranyl ion was studied from binary mixtures with compositions given in **Table 3.3.**

Table 3.3: Uptake studies using binary mixtures containing uranyl ion and the various other ions in varying concentration levels

Interfering ions	**Initial concentration (ppm) in solution**		**Final concentration (ppm) in solution**	
	Uranyl ion	**Interfering ions**	**Uranyl ion**	**Interfering ions**
Na^+	1	1	0.2	1
	10	10	0.5	9.8
	10	100	0.5	98.1
K^+	1	1	0.5	0.75
	10	10	-	9.2
	10	100	1.2	97.1
Ba^{2+}	1	1	0.8	0.65
	10	10	-	8.9
	10	100	0.51	91.3

Cu^{2+}	1	1	0.29	0.54
	1	10	0.72	3.6
	10	10	0.1	3.1
	10	95.2	3.4	65
	10	952	3.6	794
Ni^{2+}	1	1	0.39	0.78
	1	10	0.85	4.8
	10	10	0.1	6.9
	10	100	1.1	82.3
Co^{2+}	1	1	0.4	0.95
	1	10	0.7	6.63
	10	10	0.11	6.87
	10	100	0.5	73.6
Zn^{2+}	1	1	0.35	0.25
	1	10	0.7	6.1
	10	10	0.01	7.8
	10	65.4	0.4	48.6
	10	100	1.1	88
	10	654	1.9	524

From the table, the value of uranium left behind in solution is given for each binary mixture. It is seen that the effect of interference of the other metal ions is severe for lower concentrations of uranium in the mixture. Based on the binary mixture studies, the system was applied to a mixture containing all these ions in different concentration ratios and the results are shown in **Table 3.4.**

Table 3.4: Uptake studies using mixtures containing uranyl ion and the various other ions in varying concentration levels

	Initial concentration (ppm) of		**Final concentration (ppm) of uranyl ion**
	Uranyl ion	**Other ions**	
Mixture 1	1	10 ppm each of Zn^{2+}, Co^{2+}, Cu^{2+}, Ni^{2+}	0.63
Mixture 2	10	All ions of 10 ppm except 95.2 ppm Cu^{2+} and 65.4 ppm Zn^{2+}	3.3

It is seen that in presence of all these ions, the reduction of the uptake is about 30% for higher concentration of uranium. Thus all these studies showed that interference is more severe for concentration of 1 ppm of uranyl ion.

The effect of sorption on the nature of oxide is evaluated to establish the stability of the nano manganese oxide after equilibration. This is an important aspect for the nano-manganese oxide to have potential application as sorbent for removal of metal ions. Therefore, the nano manganese oxide was again characterized using XRD after equilibration, to ascertain whether there are any structural changes due to equilibration. XRD patterns showed that the original oxide did not undergo any change or degradation due to sorption confirming that the metal ions ion is exchanged with the active sites present in the oxide and does not cause any structural degradation. Further, the analysis of the filtrate after equilibration did not reveal the presence of manganese indicating the stability of these oxides during equilibration.

3.4.3 Modeling of the data: In order to understand the sorption of the different ions on the surface of the nano-oxide, the data are fitted to various models for both equilibrium and kinetic modeling. An adsorption isotherm is a curve describing the phenomenon governing the retention of a substance from the aqueous media to a solid-phase at a constant temperature and pH. Adsorption equilibrium is established when an adsorbate containing phase has been contacted with the adsorbent for sufficient time, with its adsorbate concentration in the bulk solution is in a dynamic balance with the interface concentration and the ratio between the adsorbed amounts with the remaining in the solution is calculated. The mathematical correlation is an important aspect of modeling analysis and is depicted graphically and gives an understanding of the degree of affinity of the adsorbents. There are a number of equilibrium isotherm models which have been used for understanding the sorption process. However, an interesting trend in the isotherm modeling is the derivation in more than one approach, thus directing to the difference in the physical interpretation of the model parameters. The equilibrium modeling can be classified into two categories namely two and three parameter models based on the number of parameters associated in the model equation.

3.4.3.1 Two parameter isotherms: Langmuir isotherm is one of the best examples in this category and the Langmuir isotherm can be used to compare the sorption efficiency of various sorbents. The model makes some basic assumptions like monolayer adsorption (the adsorbed layer is one molecule in thickness), at a finite (fixed) number of definite localized sites, that are identical and equivalent, with no hindrance between the adsorbed molecules, even on adjacent sites **[161].** Thus Langmuir isotherm refers to homogeneous adsorption, which each molecule possess constant enthalpies and sorption activation energy (all sites possess equal affinity for the adsorbate) **[201],** with no transmigration of the adsorbate in the plane of the surface resulting in equilibrium saturation where once a molecule occupies a site, no further adsorption can take place. This is given by the plateau in the graph. It is also to be understood that there is a rapid decrease of the intermolecular attractive forces with increase in distance. The mathematical expression of Langmuir isotherm is given in equation 2.9. The main aspect of Langmuir isotherm can be expressed by R_L, a constant known as the constant separation factor or equilibrium parameter which can be used to predict if an adsorption system is "favorable" or "unfavorable". The separation factor, R_L is defined by Eq.2.10.

Another example of two parameter model is the Freundlich isotherm **[202]** which is the earliest known relationship that describes the non-ideal and reversible adsorption and can be applied to multilayer adsorption [**162**]. The linear form of the equation is given in Eq.2.11, the slope gives the value of n which is a measure of sorption intensity or surface heterogeneity and the sorption is termed chemisorptions when the value is between 0 and 1. The value of n if within the range of 1-10, indicates favorable sorption.

Another type of two parameter models is the Dubinin–Radushkevich isotherm **[203]** which is an empirical model initially conceived for the adsorption of subcritical vapors onto micro pore solids following a pore filling mechanism. This model is often successful for high and intermediate concentration ranges but deviates at lower concentration. This has been used to distinguish the physical and chemical adsorption of metal ions **[164].**The model equation and parameters has been given in Eq.2.13 and 2.14.

Temkin isotherm **[163],** expressed as inEq.**2.12** is another example of two parameters model which contains a factor that explicitly takes into the account of adsorbent–adsorbate interactions.

By ignoring the extremely low and large value of concentrations, the model assumes that heat of adsorption (function of temperature) of all molecules in the layer would decrease linearly rather than logarithmic with coverage **[204]**.

3.4.3.2 Three parameter isotherms: Redlich–Peterson isotherm model is a hybrid isotherm featuring both Langmuir and Freundlich isotherms, which incorporates three parameters into an empirical equation **[205],** expressed as Eq.2.16**.** It has a linear dependence on concentration in the numerator and an exponential function in the denominator **[206]** to represent adsorption equilibria over a wide concentration range, that can be applied either in homogeneous or heterogeneous systems due to its versatility **[207].** Under limiting conditions of very high and low concentrations, the model approaches Freundlich (as the exponent tends to zero) and Langmuir (as the values are all close to one) isotherm models, respectively.

Sips isotherm model is a combination of both Langmuir and Freundlich expressions and is used to predict sorption in **[208]; linear** form is expressed as in Eq.2.17. At low and high sorbate concentrations, it reduces to Freundlich and Langmuir isotherms respectively

The sorption data in the present study has been fitted to the various models given in Chapter 2 and the respective graphs are given in **Fig. (3.5-3.10).**

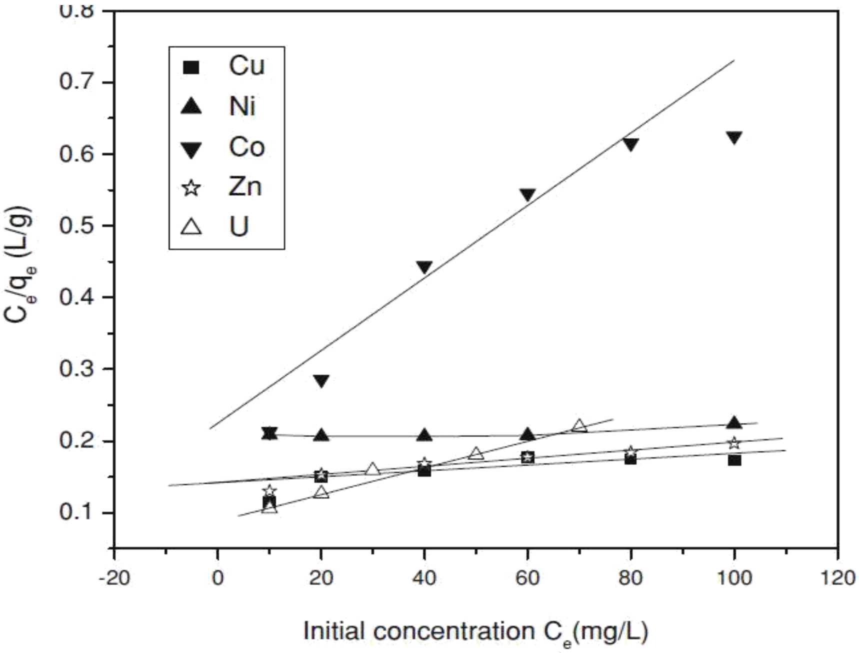

Fig.3.5: Langmuir isotherm model for sorption of Cu^{2+}, Ni^{2+}, Co^{2+}, Zn^{2+}, UO$_2^{2+}$ ions

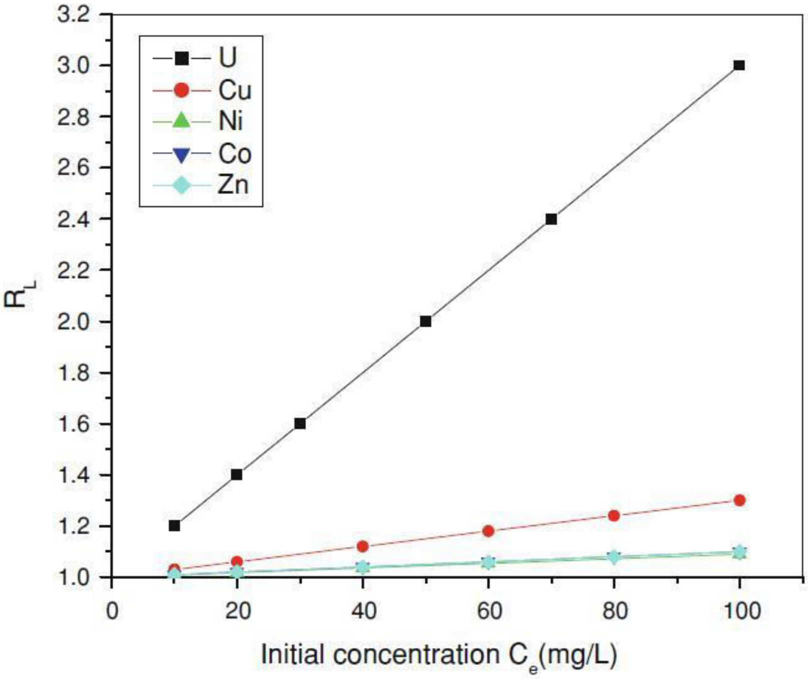

Fig.3.6: Effect of initial metal ion concentration on the Langmuir isotherm model parameter

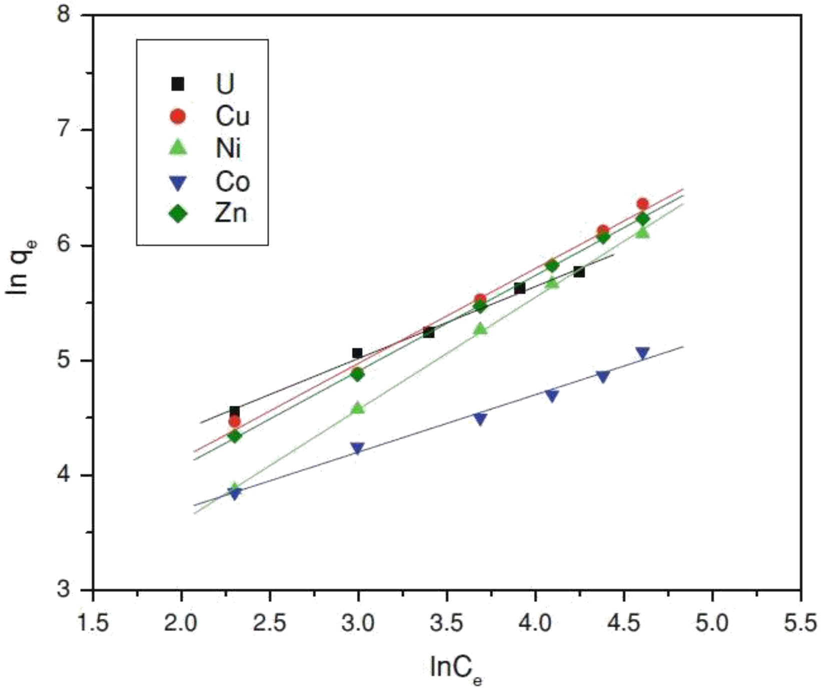

Fig.3.7: Freundlich isotherm model

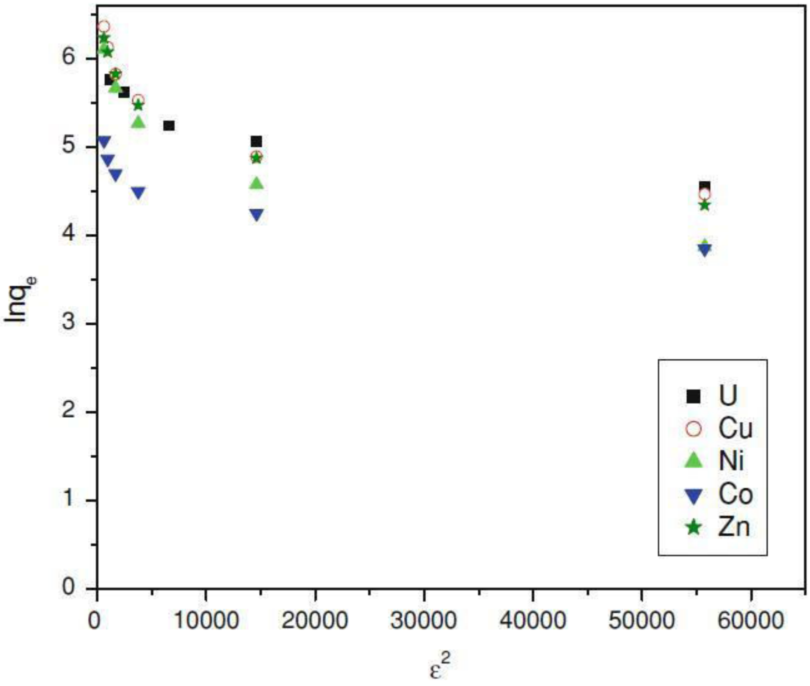

Fig.3.8: Dubinin–Radushkevich isotherm model

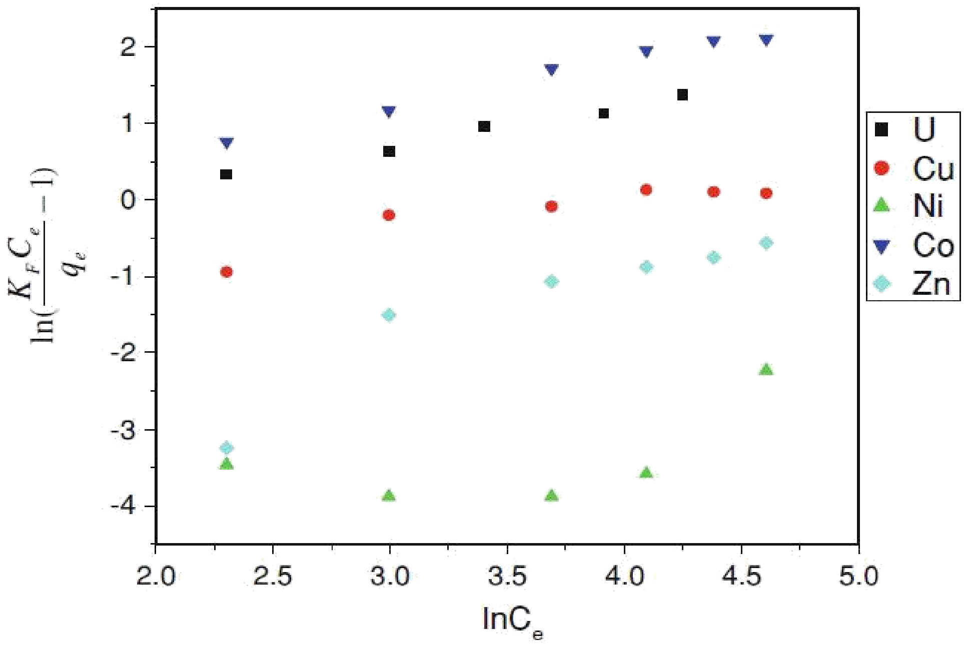

Fig. 3.9: Redlich–Peterson isotherm model

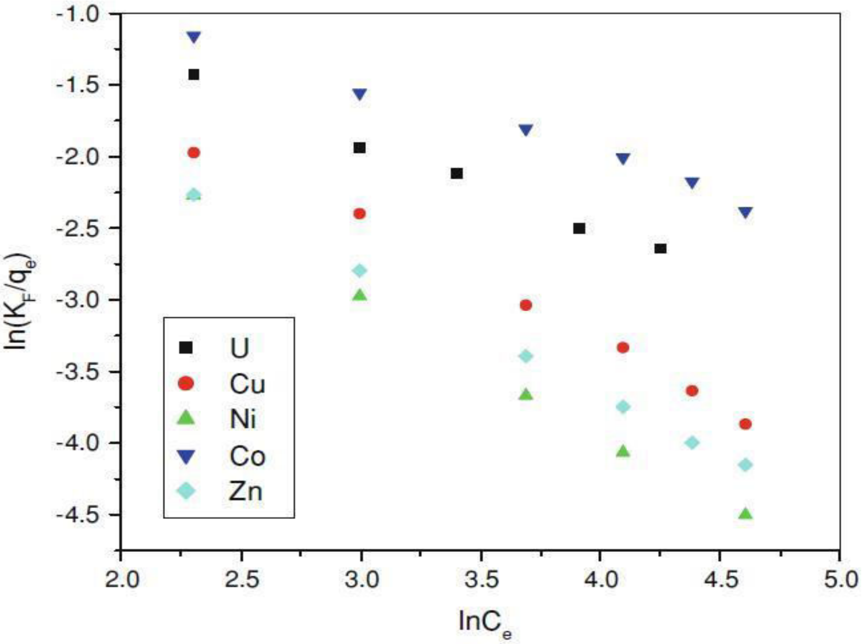

Fig.3.10: Sips isotherm model for various metal ions Cu^{2+}, Ni^{2+}, Co^{2+}, Zn^{2+}, UO_2^{2+}

The various parameters calculated from the different plots are given in **Table 3.5**.

Table 3.5: Parameters calculated from the different equilibrium models

Model	**Langmuir**		**Freundlich**		**Dubinin–Radushkevich**		**Redlich–Peterson**		**Sips**	
	Q^0 (µg/g)	**B**	**K_f**	**n**	**Q**	**β**	**A**	**g**	**a**	**B/g**
UO_2^{2+}	526	0.022	22.8	1.56	259	2E-5	0.4	0.54	0.99	1.9
Cu^{2+}	2439	0.003	12	1.2	3650	3E-5	0.18	0.42	1.02	2.3
Ni^{2+}	5555	9E-4	5	1.02	2731	3E-5	0.01	0.43	0.96	2.6
Co^{2+}	200	0.023	15	2	121	2E-5	0.57	0.62	0.99	1.6
Zn^{2+}	6250	0.001	8	3.05	3474	3E-5	0.05	1.05	0.73	2.3

3.4.4 Sorption mechanism: Based on all the different studies, a mechanism was proposed for the possible uptake of metal ions. The pH variation showed that the uptake followed an ion exchange or an ion interaction mechanism. This was confirmed by the decrease in the pH of the solution after equilibration. This showed that on uptake of metal ions, there was a release of proton resulting in the decrease in the pH of the solution after equilibration. However, the change in pH even for a very high concentration of metal ions is very marginal showing the potential application of the oxide for sorption applications. A possible explanation of the uptake is as follows. Metal oxides will have units like $M\text{-}O^{\delta+}$ and $M\text{-}O^{\delta-}$ based on the pH of the solution with which they are in contact. It is these units, which help in sorption of metal ions. At lower pH, the cationic species will predominate but at higher pH, it is the anionic unit, which predominates. The cationic species will take up metal ions ion resulting in release in protons. However this mechanism of uptake is not very favored and so at lower pH, the uptake of metal ions is less.

With increase in pH, the metal ions ion will interact with the anionic species and get sorbed on the surface. Zeta potential measurements give an idea of the surface charge. When the surface is negatively charged, it will take up cations, including the protons in solution. Hence when the metal ions are taken up, there is a release of proton in solution thus leading to decrease in the pH of the solution. This phenomenon is quite clear at pH less than that of point of zero charge. At pH values above the point of zero charge, the surface is negatively charged and hence there is a direct uptake of the metal ions. However, at higher pH, the hydrolysis of metal ions become more predominant and thus results in the reduction of sorption.

3.5 Conclusions

Nanocrystalline manganese oxide was prepared by the hydrolysis of $KMnO_4$ and it was found to have a size of 8 nm and surface area of 145 m^2g^{-1}. Due to the high surface area, the sorption of the metal ions of interest on the nano manganese oxide was high. It was found that the sorption was achieved at different pH values and with varying time of equilibration. Thus it is seen that the kinetics was an important aspect for the separation of metal ions. However, it was seen that the interferences was appreciable when metal ions were in low trace levels. Thus nano manganese oxide was found to be a good room temperature sorbent. The present study showed that the kinetics of sorption for different metal ions are different and hence there is a possibility of separating the transition metal ions from a solution mixture containing these ions along with uranium, thus leaving behind a nearly pure uranyl ion solution. Thus the favored sorption properties of the nano manganese oxide with respect to the transition metal ions can be used for the purification of mixture of ions. It is to be noted that the manganese oxide used in the present study has been used as such without any modification. The maximum capacity obtained in the present study is comparable to mesoporous silica sorbents but is less compared to polyacrylic ester resins. However, the main aspect of these results showed that there is a possibility of using the nano manganese oxide as room temperature sorbent for engineering scale separation. Another advantage of MnO_2 is that it is amenable to glassification.

Chapter 4

Sorption of radioactive cesium and strontium on nanocrystalline magnetite based sorbents

---

The work reported in this chapter has been published as follows:

Uptake of Cs and Sr radionuclides within oleic acid coated nanomagnetite-haematite composite
Joyeeta Mukhopadhyay, Pranesh Sengupta, D. Sen, S. Mazumdar and A.K. Tyagi J. Nucl. Mater. 467 (2015) 512-518

4.1 Introduction

The concept of deep geological disposal of high level nuclear waste for its isolation from biosphere for nearly one million years is widely accepted among the countries which are pursuing nuclear energy generation program **[209-214].** Over the last two decades significant progress has been made in the (i) development of new inert matrices for immobilization of high level liquid wastes **[215-223]** and (ii) management of radioactive metallic wastes **[224-229]**. Parallel to this, initiatives have also been taken to develop 'environmental clean-up methodology' in case of unforeseen release of radionuclide's within 'near-field' domain of geological repository due to unlikely pre-mature breach in 'engineered barrier system' components, especially canisters and over packs which are made-up of iron (Fe) based alloys i.e. stainless steels (SS 304, SS 316 etc). This exercise becomes all the more important after the recent reports on (i) leakage in high level nuclear waste from storage tank at Hanford, USA **[230]** and (ii) environmental contamination due to Fukushima accident **[231-232].** In such situations of release of radioactivity, major threats come from ^{137}Cs and ^{90}Sr radio nuclides as they get very easily mobilized within geochemical environment and can get accumulated within biological systems, including human beings, through elemental substitution routes **[216, 230-232].** The concerns associated with ^{137}Cs and ^{90}Sr radio nuclides are their short half-lives (~30 years) and heat generation plus emission of γ-rays and β–particles during decay. To address this issue it is therefore important to identify a novel material which not only can absorb ^{137}Cs(I) and ^{90}Sr(II) radio-nuclides in high quantity but also should be compatible with natural rocks, especially soil. Additionally structure of the material should be resistant to radiation damage over long time scale.

Towards this objective natural analogues were studied as part of present thesis, particularly from uranium ore horizons associated with shear zones, as along such zones 'crustal fluid – host rock' interactions are reported to be significant **[233-234].** In many such cases it was noted that magnetite is a common accessory mineral which remains associated with radioactive uraninite (UO_2) over long time scale (hundreds of millions year) without showing any structural changes due to associated radiation source. An example of such a coexistence of uraninite and magnetite over 1800 million years has been documented by Krishna Rao et al. **[234]**. The sample was collected from Narwapahar uranium ore mine of 'Singhbhum shear zone', India. Like uranium, association of cesium (Cs) and strontium (Sr) with iron-oxides have also been reported in nature. In fact radioactivity release in nature, often lead to dissolution of certain soil minerals and the iron content of the same are generally found to precipitate as iron oxide with which radioactive ^{137}Cs and ^{90}Sr get associated **[230].** Because of the importance of iron in controlling mobility of radio-nuclides within deep geological repository, France carried out detail geochemical investigation in Bure Callovian-Oxfordian formation where they propose to build 'underground repository laboratory (URL)' **[235].**

No wonder, earlier researchers have also noted these advantageous geochemical and radiochemical feature of magnetite **[236]** and carried out some experimental sorption studies with radio-nuclides e.g. uranium, technetium, cesium, strontium etc **[237-242].** Most of these experiments offered better results with nanomagnetite particles. Such nanoparticles, in the form of iron oxides and hydroxides, are quite common in nature especially within weathered rocks (physical erosion of minerals or chemical alteration) and direct precipitates from ground water **[243].** Over the last few years considerable efforts have been made to synthesize iron oxide nanoparticles using different routes e.g. co-precipitation, thermal decomposition, hydrothermal-, micro emulsion, sonochemical, electrochemical, laser pyrolysis and bacterial methods etc. **[244].** However, the major difficulty faced with these procedures was to obtain monodispersed, biocompatible nanomagnetite with optimum shape and size synthesis etc. Further, nanomagnetite being hydrophilic in nature makes its applications all the more difficult in specific cases e.g. nuclear waste management. It is understood that nanomagnetite can exhibit its beneficial novel physical and chemical properties the best only when it is of particular shape, size and structure. To circumvent such shortcomings, composite nanoparticles with functionalized surface have been proposed in literature **[245-247].** Keeping this in mind, in the present investigation an attempt has been made to synthesize nanomagnetite with hydrophobic oleic acid shell ($CH_3(CH_2)_7CH.CH(CH_2)_7COOH$) and silica coated shell to examined their Cs and Sr sorption capacity over wide pH range. The effect of experimental parameters such as pH, initial concentration, and contact time for cesium and strontium removal were studied for these materials. However, considering the geological repository environment where partial oxidation of magnetite to hematite cannot be ruled out, a composite of nanomagnetite – nanohematite has also been synthesized rather than nanomagnetite alone. Again, the bare metal oxides are not target selective, so unsuitable for complicated matrix samples. Thus the modification with a suitable coating with silica and oleic acid makes them efficient sorbent for target specific caesium or strontium removal.

4.2 Synthesis and characterisation of magnetites: The synthesis and characterisation procedure for magnetite, oleic acid coated and silica coated magnetite has been discussed in details in **chapter 2.**

4.3 Sorption experiments: The uptake studies were carried at room temperature ($25^{O}C$) in batch mode using aqueous solutions containing metal ion. 10 ml of aqueous metal ion [cesium (I)

/strontium (II)] of interest solution of known concentration at a particular pH was equilibrated with a weighed amount (0.1 mg) of magnetite sample for a known period of time. The concentration of metal ion left behind in solution after equilibration was determined. The oxides after equilibration were again characterized using XRD technique.

4.4 Results and discussion

4.4.1 Structural and micro-structural studies

Crystallographic studies of nanocomposite samples were done using X-ray powder diffraction method and Transmission Electron Microscopy (TEM).

X-ray diffraction pattern [PC-PDF number # 190629] of the as-prepared nanocomposite is shown in **Fig. 4.1 (a), (b) and (c).** High resolution electron microscopic images of these three materials are shown in **Fig. 4.2(a-c).** Grain sizes of the as prepared samples are found to be 10 nm on an average and for oleic acid coated magnetite it is 8 nm on an average and for silica coated magnetite it is 15 nm. A careful observation of the images reveals that grain-clustering effect is much less in oleic acid coated and silica coated sample compared to the as prepared sample. This is essentially due to development of greater ‘weak repulsive potential’ within the later two samples as evidenced from zeta potential study of all the three materials.

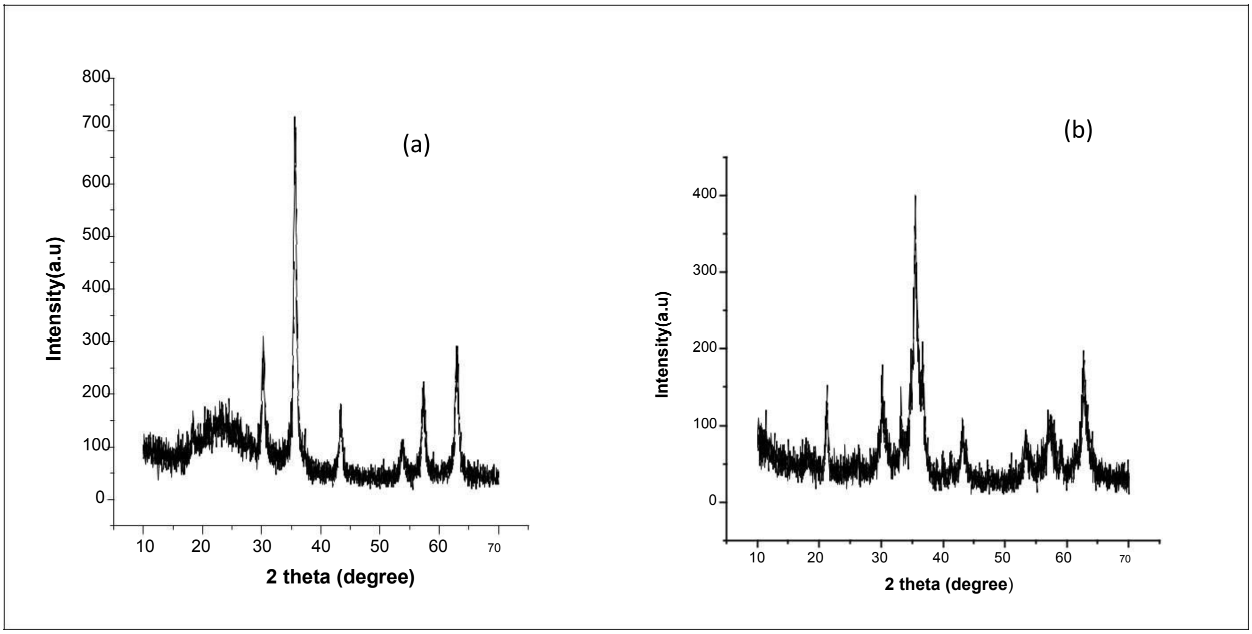

Fig. 4.1: XRD pattern of (a) bare magnetite (b) oleic acid coated haematite - magnetite composite material (OHMC)

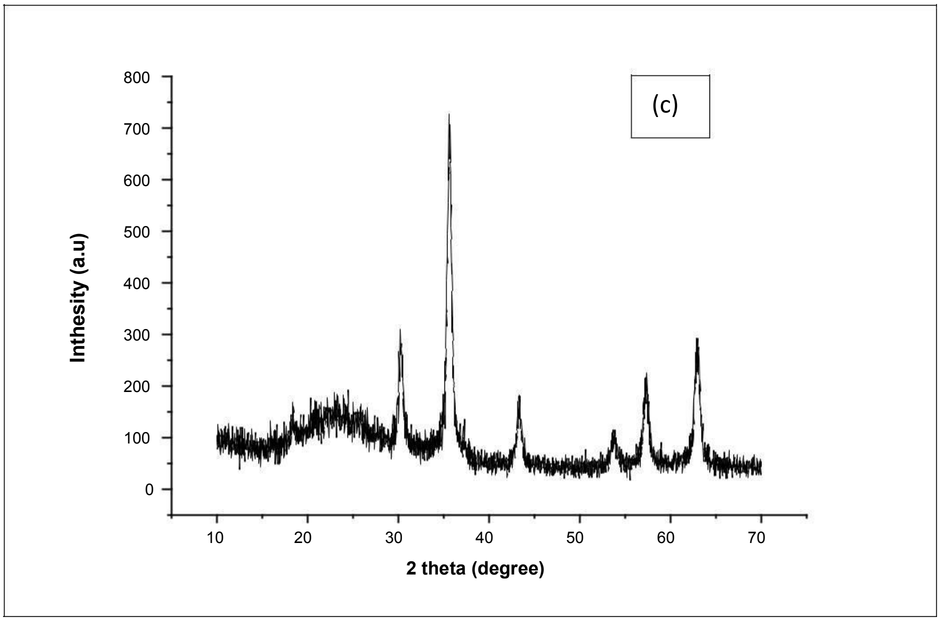

Fig.4.1 (c): XRD pattern of silica coated magnetite

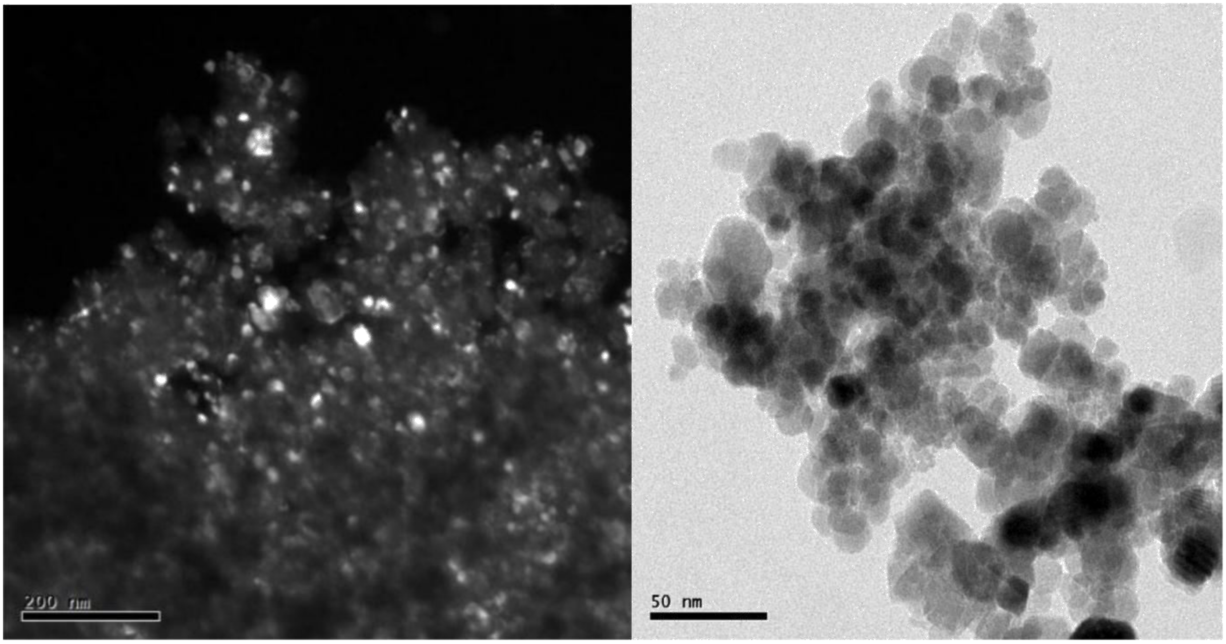

Fig. 4.2 (a): TEM images of bare magnetite

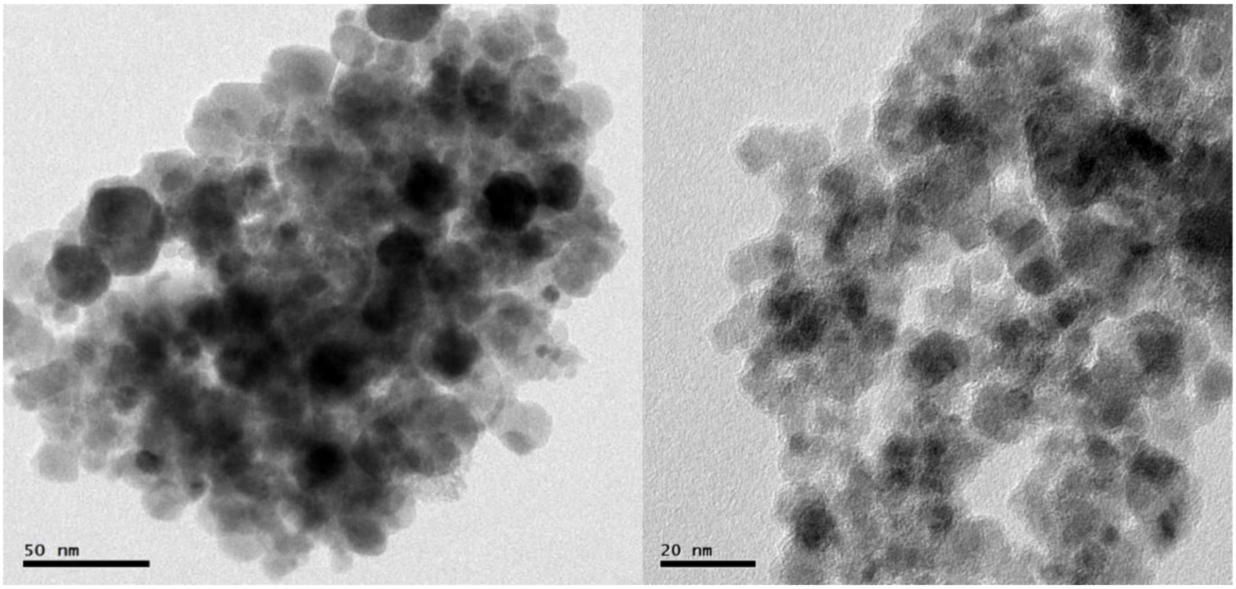

Fig. 4.2(b) TEM image of oleic acid coated haematite-magnetite composite material (OHMC)

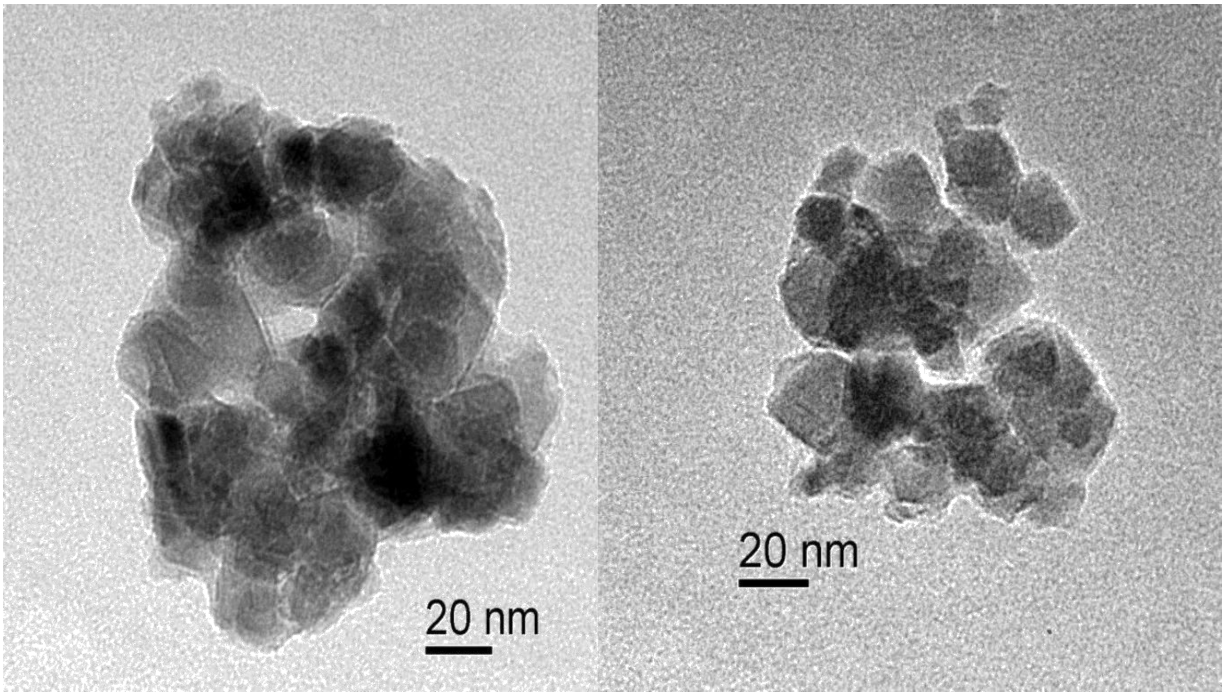

Fig.4.2 (c): TEM images of silica coated magnetite

4.4.2 Small Angle X-ray scattering studies

X-ray scattering experiments were performed using a laboratory based small-angle X-ray scattering (SAXS) instrument. The sample to detector distance was ~1070 mm and the wavelength (λ) of X-ray was ~1.54 Å. The scattering intensity was recorded as a function of wave vector transfer q (= $\frac{4\pi\sin\theta}{\lambda}$, where 2θ is the scattering angle). The scattered intensity I (q) at small angle region corresponding to spherical poly disperse particles, under local mono disperse approximation, may be expressed as

$$I(q)=C\left(\int_0^\infty D(R)\,R^6 P(q,R)\,S(q,R)\,dR\right) \tag{4.1}$$

where, D(R) represents the size distribution of the basic constituents of the fractal, *i.e.* D(R)dR represents the probability of finding a particle with radius R to R + dR. A standard log-normal distribution of the form is given as

$$D(R) = \frac{1}{\sqrt{2\pi\sigma^2 R^2}} \exp\left[- \frac{[\ln(R/R_0)^2]}{2\sigma^2} \right] \tag{4.2}$$

Here, R_0 and σ represent the median radius and the polydispersity index, respectively. P(q, R) is the form factor of a particle of radius r. In present case, a spherical form factor is assumed for the data analysis,

$$P(qR) = 9\left(\frac{\left(\sin(qR) - qR\cos(qR)\right)^2}{(qR)} \right) \tag{4.3}$$

C is the scale factor which is independent of q but depends on the number density of the particles and the scattering contrasts (q, R) are the inter-particle structure factor. Due to the slightly agglomerated nature of the particles, a mass fractal type structure **[248]** factor with fractal dimension d_m was found necessary to explain the functionality of the scattering profile in the whole accessible q range. The above model was fit to the experimental SAXS data. The fit of the model to the data is depicted in Fig. 4.2 along with the SAXS data. It is found that the model is indeed capable of explaining the scattering data in the whole accessible q range. The parameters from the fit are tabulated in **Table 4.1**. It is seen that the median size of the uncoated sample is almost double in comparison to that of coated samples.

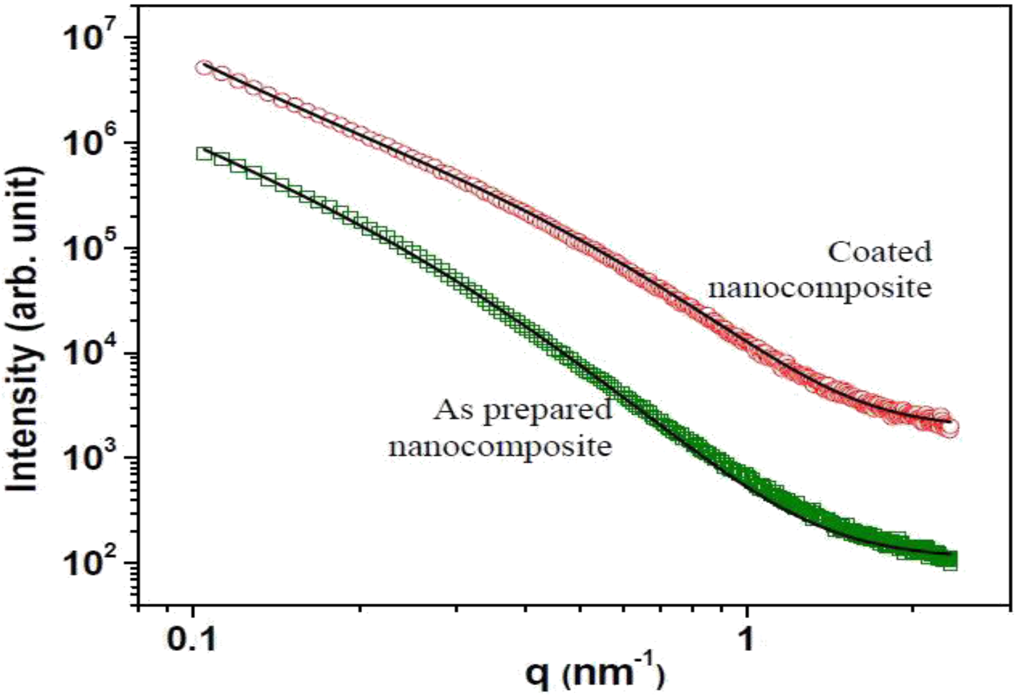

Fig. 4. SAXS scattering data obtained for as prepared and coated nanocomposites. Model fitting is indicated by black line.

Fig.4.3: SAXS scattering data obtained for as prepared and coated nanocomposites. Model fitting is indicated by black line.

Table 4.1: SAXS data for as prepared and coated nanocomposites

Sample	**R_o(nm)**	**Σ**	**d_m**
Coated nanocomposites	1.2	0.60	2.57
As prepared nanocomposite	2.2	0.64	2.57

4.4.3 Zeta potential study for surface charge

Surface charge property of all the samples in the form of zeta potential measurement has been carried out. The uncoated nanocomposite has a zeta potential of around -22 mV, whereas oleic acid coated nanocomposite shows value close to -28mV and silica coated sample shows -52mV. In oleic acid and silica encapsulated magnetite samples the weak repulsive potential shifts to more negative value which gives information that the nanocomposite is more stable while dispersed in the solution. Zeta potential study on freshly prepared nanocomposite and oleic acid as well a silica coated nanocomposite samples were carried out and the results are tabulated in **Table 4.3.** The leaching of iron and the low negative potential of uncoated nanocomposite drives the surface modification of nanocomposite with a long chain fatty acid like oleic acid which can modify nanocomposite surface by its COO^- and OH^- group or in silica surface the surface containing SiOH (silanol) group. Thus, in coated nanocomposites the negative potential has changed from -22mV to-28mV. The point of zero charge (pzc) for uncoated nanocomposite was found to be 7.2 pH. This material shows two point of zero charge due to its designed biphasic nature as shown from the XRD image of **Fig.4.3 (b).**The pzc for silica coated and oleic acid coated magnetite were found to be at pH 2.7 and pH 6.9, respectively.

Shifting in weak repulsive potential facilitates enhanced sorption for a longer period of time in stable condition in comparison of uncoated nanocomposite which forms larger aggregates. These results will be discussed in subsequent sections.

Table 4.2: Zeta potential measurement for three different magnetites at different pH

Sample	**ξ(mV) at pH 2**	**ξ(mV) at pH 5**	**ξ(mV) at pH 7**
Magnetite	8.86	-30.35	-23.64
oleic acid coated magnetite-haematite composite material	3.24	-27.28	-28.68
Silica coated magnetite (SM)	6.74	-51.23	-47.83

4.4.4 Magnetic properties study

Magnetic properties were analyzed by VSM (Vibrating Sample Magnetometer). The magnetization curve shows the room temperature magnetization curves of the bare magnetite, silica coated magnetite and oleic acid coated magnetite powder (**Fig. 4.4**). All the curves show no hysteresis or remnant magnetization and thus show super paramagnetism. These particular types of super paramagnetic materials are very effective in environmental concern as because the separation of material is very quick through an external magnet. As they do not have any remnant magnetization, the separation of cesium or strontium is easy when the field is on and easily separable in the filtration system. The saturation magnetization of the silica coated magnetite was found to be 25 emu /g and that of oleic acid coated magnetite was 30 emu/g. These values are about half of the saturation magnetization of the bare magnetite which is 64emu/g. This is nearly equivalent to having 60 percent of silica or oleic acid in the respective coated nano materials. It may be noted that when only oleic acid or silica materials were used as sorbent then they could not be easily separated from the solution by applying a strong external field, while the encapsulation of these material on bare magnetite can be separated by applying a simple magnetic field. This is another advantage of surface modification by oleic acid or silica.

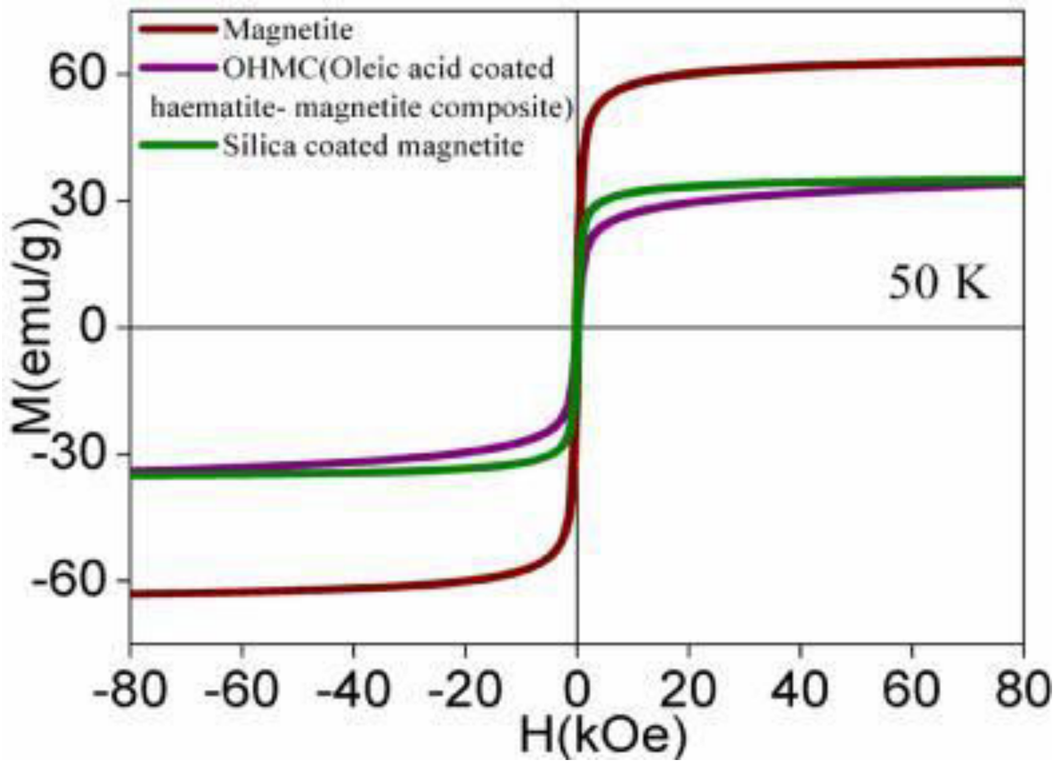

Fig. 4.4: Magnetization curve of all the three magnetite at 50 K

4.4.5 Iron-leaching studies

The iron leaching after sorption was studied by ICP-AES. Bare nanomagnetite due to its weak repulsive potential shows iron leaching in the solution while uptake of cesium or strontium was carried out. This showed the highest leaching of iron almost as 25-30 percent, whereas oleic acid coated nanocomposite and silica coated magnetite showed less than 1 percent iron leaching from the parent solution after sorption, which is a remarkable improvement achieved by surface modification.

4.4.6 BET sorption isotherm study

The Brunauer–Emmett–Teller (BET) surface area was determined by nitrogen sorption using a Bel Japan Inc., Belsorp II surface area analyzer. Before the nitrogen adsorption, the samples were degassed under flowing argon at 100°C for 10h.

Table 4.3: Summary of specific surface area, pore volume and pore size distribution of magnetite and oleic acid magnetite

Sample	S_{BET} (m^2g^{-1})	Pore volume (cm^3g^{-1})	Pore size distribution (nm)
Magnetite	47.9	0.17	19.3
Oleic acid coated haematite-magnetite composite	78.7	0.22	13.4
Silica coated magnetite	10.9	0.13	45.7

4.5 Sorption studies

4.5.1 Effect of pH on cesium (I) and strontium (II) ions uptake

Sorption behaviour of cesium and strontium on to all these three magnetites at different pH has been shown in **Fig. 4.5 (a) and (b)**, respectively. It shows at pH 5 maximum value (99%) of sorption efficiency for Cs(I) ion takes place by magnetite, after that uptake slightly decreases (90%) in alkaline medium of pH range 6-10, nearly remaining a constant because in all pH range the cesium remains as Cs(I) ion in solution. For silica and oleic acid coated magnetite the removal remains above 95% in entire pH range which prove the effectiveness of surface modification by silica and long chain fatty acid like oleic acid. The high negative zeta potential value in this pH ranges show that the solution becomes more stable in these pH ranges. It implies that over the extensive range of acidic to basic medium uptake of cesium on magnetite could be achieved. Though in slightly acidic condition (pH 5), removal of waste containing cesium is at its best with magnetite but maximum radioactive waste water has a wide range of basic medium, so has a limited applicability for use of bare magnetite.

In strontium uptake study among these materials, bare magnetite shows similar trend like the other two surface modified materials as opposed to in cesium sorption study and in a wide range of pH 5-10 the uptake is nearly constant.The low sorption of Sr(II) in strongly acidic medium (pH2-4) was observed which is attributed to the competition between two ions (H^+ and Sr^{2+}) for the same active site of magnetite surface. Due to small size, H^+ ions suppressed the Sr^{2+} ions towards sorption at pH 2. However, with gradual increase in sportive solution pH gradually decreases the H^+ ions concentration in solution and thus increased the percent removal of Sr(II).

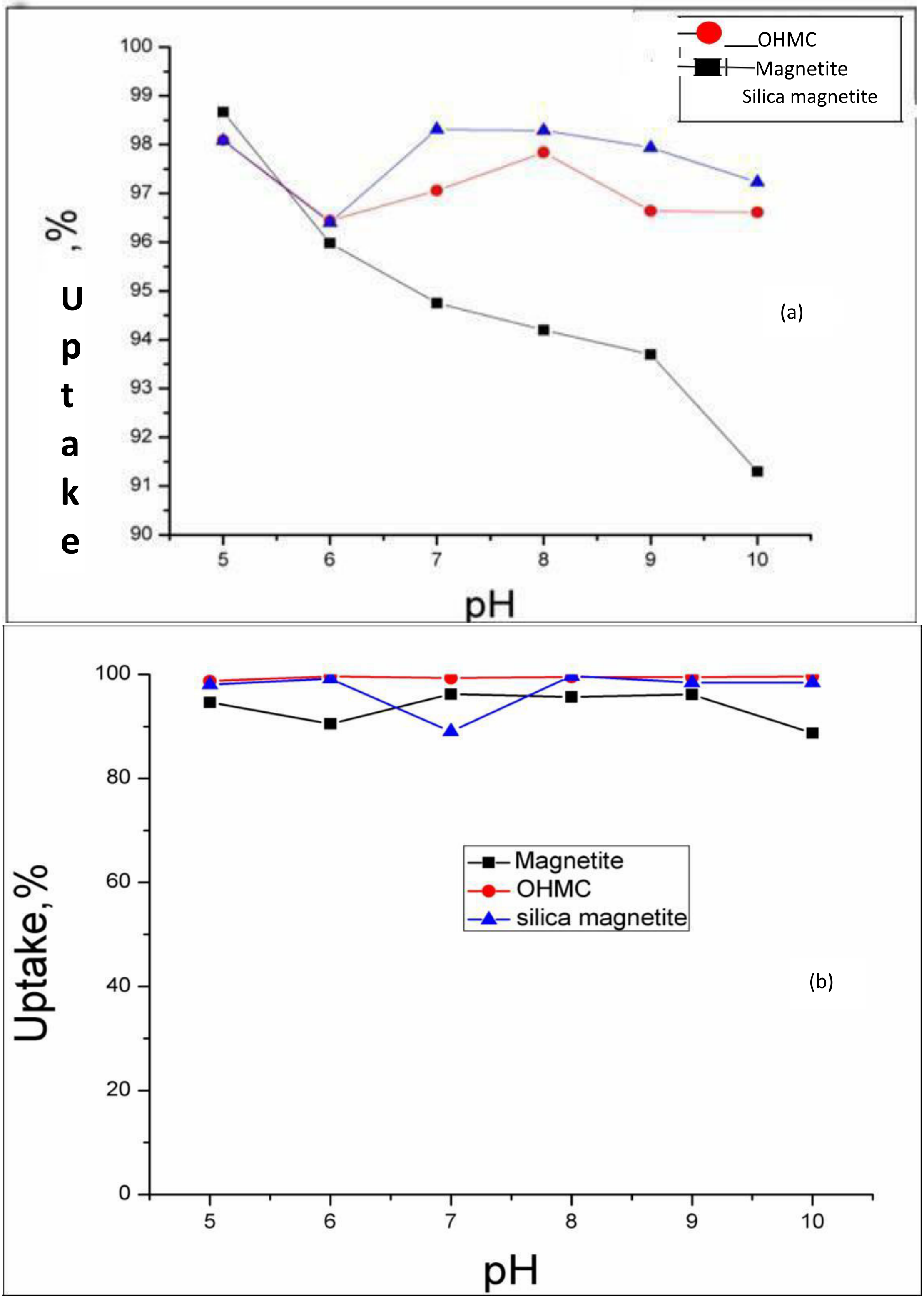

Fig.4.5: Effect of pH on percentage removal of (a) Cs (I) & (b) Sr (II)

4.5.2 Effect of initial concentration on cesium (I) and strontium (II) ions uptake

The effect of Cs and Sr concentration on sorption was investigated and the comparative results are shown in **Fig. 4.6(a) and (b).** The sorption capacity of the three magnetite based nanomaterials for cesium ions was determined, by studying the sorption as a function of cesium ion concentration, at 300 K, in a batch mode experiment. The concentration of inactive cesium ions in the aqueous solution was increased from 10 mg/L to 100 mg/L, and the q_e, maximum sorption capacity was determined as discussed earlier in Chapter 2. It was observed that, q_e increases gradually with increase in cesium ion or strontium ion concentration, and reaches a saturation value. The initial concentration provides an important driving force, to overcome all the mass transfer resistances to the Cs(I) ions or strontium ions between the aqueous and the solid phases. Therefore, a higher initial metal ion concentration will enhance the sorption process. The observed results can be explained by the fact that, with increase in concentration, the incremental increase in cesium ion uptake by sorbent will be more initially, as a large number of active sites are available, but, with further increase in concentration it decreases, as the number of the available active sites decreases. The qe value, maximum quantity sorbed per gram of sorbent taken was 11.82mg/g for silica coated magnetite and for bare magnetite and oleic acid coated magnetite they are 5.91mg/g and 11.33 mg/g, respectively. These values are near the experimental adsorbed amounts and correspond closely to the adsorption isotherm plateau, which are acceptable. Though it is seen from these results, magnetite gives high value over oleic acid coated magnetite but the other factors like leaching of iron from the solution also play a key role in selecting the most suitable iron oxide based sorbent. Magnetite, in its aggregated state leaches iron in the solution, making the determination process by AAS bit difficult. The maximum sorption of Cs (I) occurs at 80 mg/L (nearly 100 %) on freshly prepared magnetite and the uptake also varies between 75% to above 90 % for bare magnetite. However, strontium sorption studies revealed that the maximum amount sorbed for magnetite was above 3mg/g at a maximum concentration of 100 mg/L. The strontium uptake remained more than double as like 10 mg/g for the other two magnetite nano composite materials as shown in **Fig.4.6 (b).** With increase in strontium ion concentration, the entire three materials show increased uptake as the initial concentration gives the momentum to resist the mass transfer of ions between solution and sorbent.

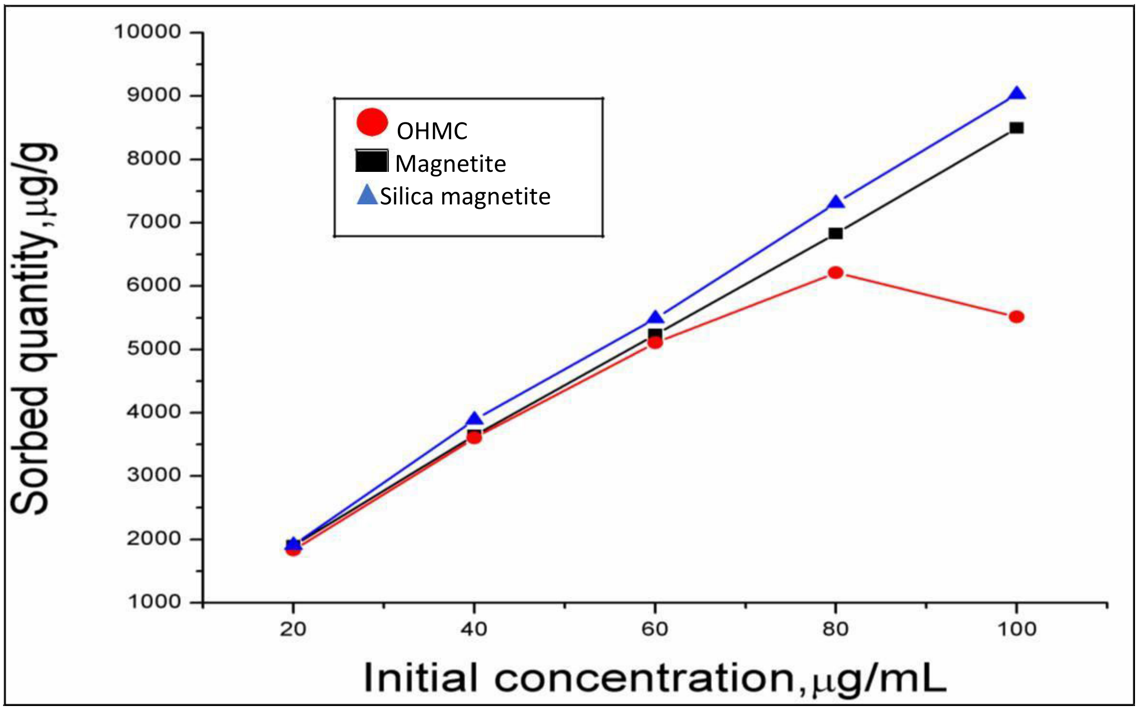

Fig. 4.6(a): Effect of initial concentration on sorbed Cs (I) quantity

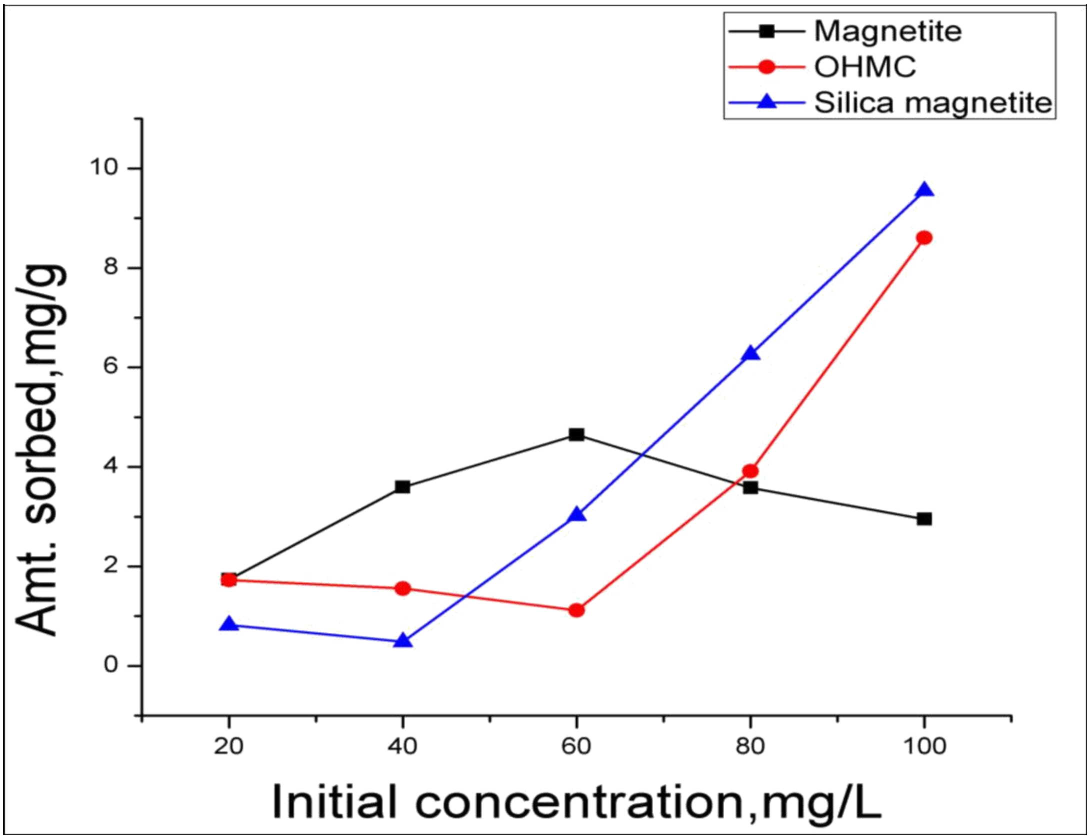

Fig. 4.6(b): Effect of initial concentration on sorbed Sr (II) quantity

4.5.3 Theoretical modelling of sorption data for cesium (I) and strontium (II) ion uptake

The distribution of adsorbing elements between the liquid phase and the solid phase when the adsorption process reaches equilibrium is indicated by adsorption isotherm. The analysis of the isotherm data by fitting them to different adsorption isotherm models is an important step to find the suitable model that can be used for predicting adsorption parameters and quantitative comparison of adsorbent behaviour and adsorption performance. There are several common isotherm models such as Langmuir, Freundlich, Temkin, Redlich- Peterson, Dubinin–Radushkevich and Sips models which are used to analyze experimental adsorption equilibrium data and to simulate the sorption isotherms. Langmuir model is homogeneous adsorption which assumes monolayer adsorption, fixed number of definite identical and equivalent localized sites, with no hindrance between the adsorbed molecules; even on adjacent sites. The monolayer coverage is obtained from a plot of C_e/q_eversus Ce. The slope and the intercept of the linear graph **[Fig. 4.7(a) and 4.7(b)]** for the three materials obtained from this plot give the value of $q_m$and b. The favourability of the Langmuir isotherm is expressed by R_L. The R_L value indicates the adsorption nature; it can be unfavourable (R_L<1), linear (R_L = 1), favourable (0\R_L\1) or irreversible (R_L = 0). The plot of R_L with the variation of initial concentration for all the three materials have been shown in **Fig.4.8**, which indicates the favourability of the sorption reaction

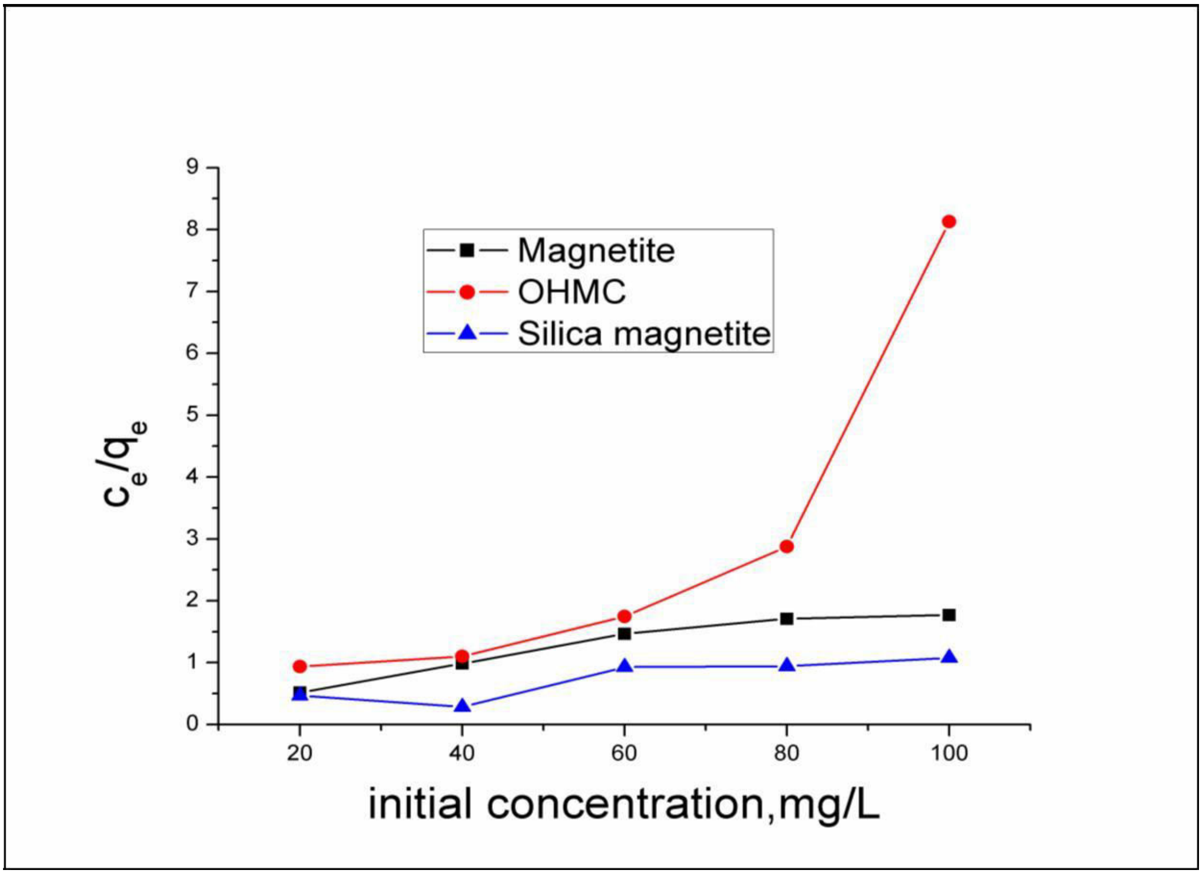

Fig. 4.7(a): Langmuir isotherm plot for Cs (I) sorption

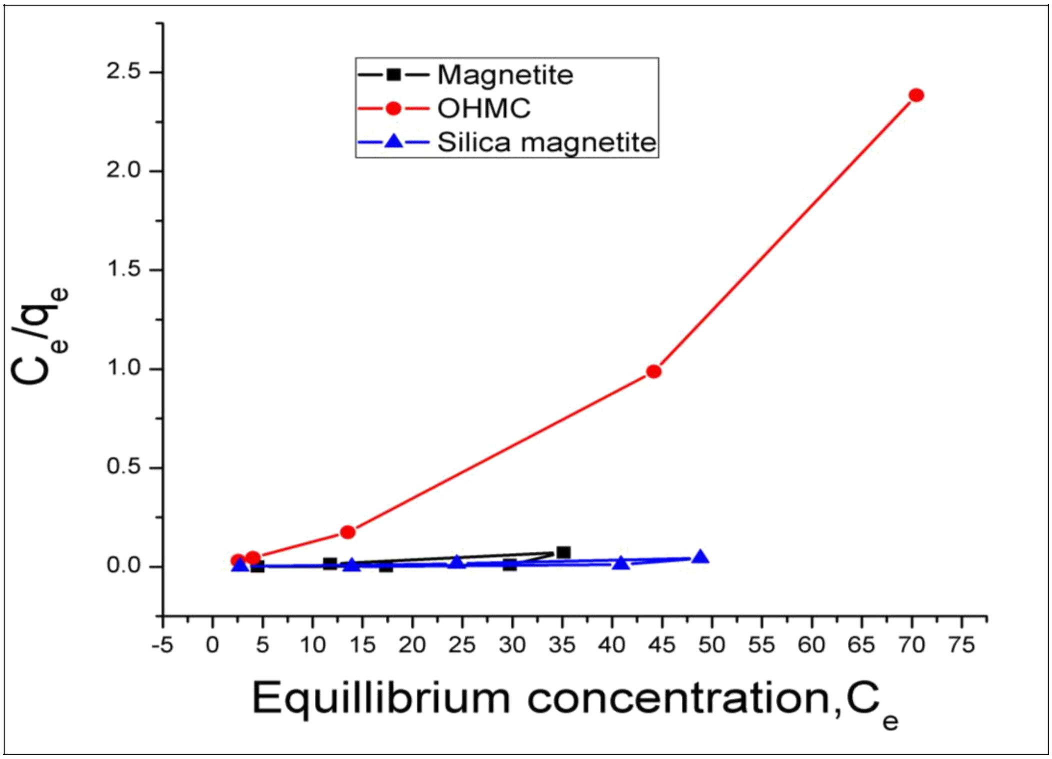

Fig. 4.7(b): Langmuir isotherm plot for Sr (II) sorption

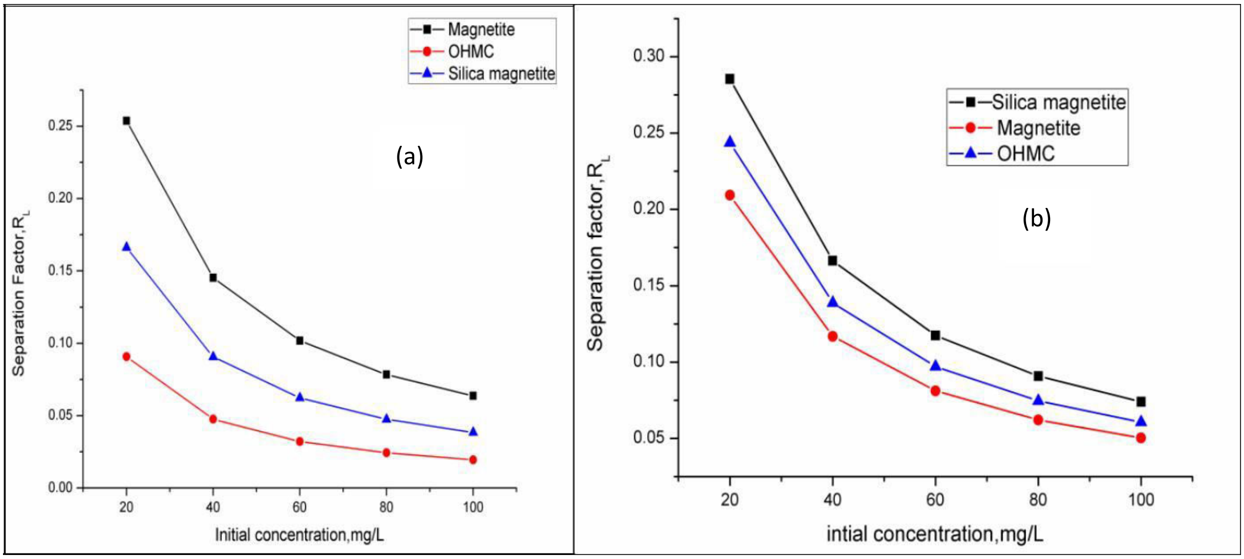

Fig. 4.8(a) and (b): Effect of initial metal ion concentration on the Langmuir isotherm model parameter of (a) Cs (I) & (b) Sr (II)

Table 4.4: Langmuir effect of initial metal ion concentration on the Langmuir isotherm model parameter for Cs (R_L stands for separation factor)

Initial concentration (mg/L)	Separation Factor (R_L)		
	R_L (magnetite)	R_L(oleic acid coated haematite - magnetite composite)	R_L(silica magnetite)
20	0.26	0.09	0.17
40	0.15	0.05	0.09
60	0.10	0.03	0.06
80	0.08	0.02	0.05
100	0.06	0.02	0.04

Freundlich isotherm, an empirical equation describes the non-ideal and reversible adsorption and can be applied to multilayer adsorption. The Freundlich coefficients n and Kf are obtained from the plots of Inq_e versus InC_e. The comparative plots for Cesium sorption are given in **Fig4.9.** For Sr (II), the data was mostly fitted to Langmuir isotherm; therefore other graphs have not been shown.

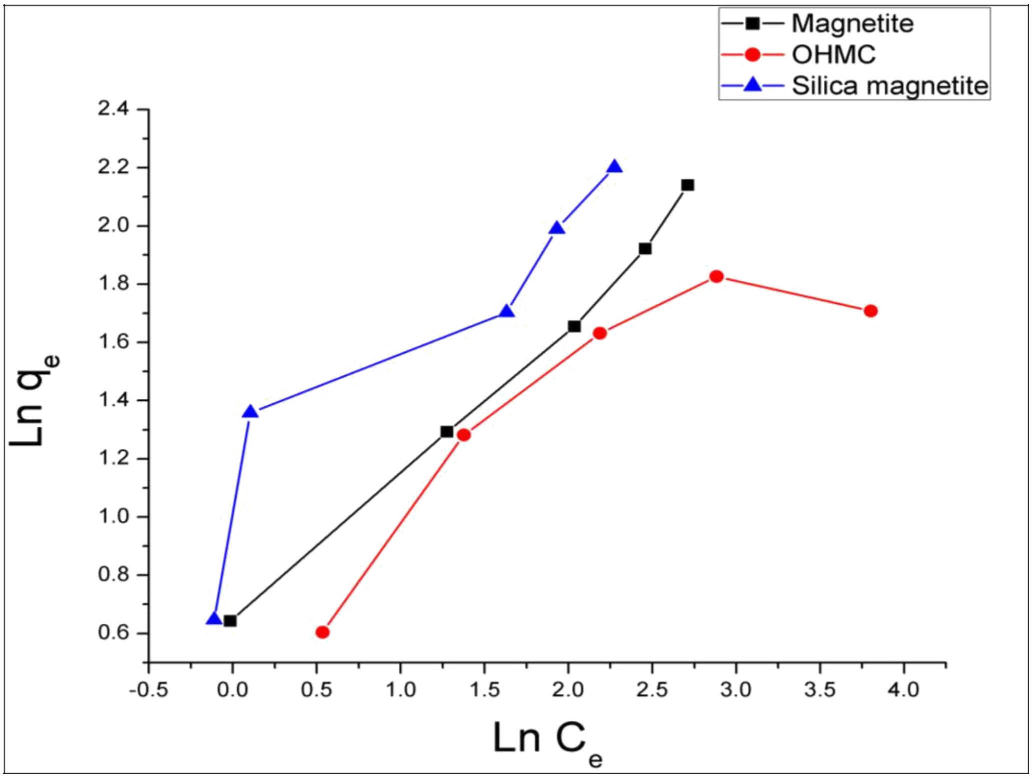

Fig.4.9 (a) Freundlich isotherm model of cesium (I) sorption

The value of n gives the information about sorption intensity or surface heterogeneity. The sorption is termed as chemisorptions when the value is between 0 and 1 and if its value is in between 1-10, that means the reaction is favourable.

Dubinin–Radaushkevich isotherm model **[164]** has been used to distinguish the physical and chemical adsorptions of metal ions on sorbent surfaces.They have reported that the characteristic sorption curve is related to the porous structure of the sorbent. Comparison of sorption isotherms of cesium onto three different magnetite nano materials according to the model has been shown in **Fig.4.10 (a) and (b).** The D-R model gives the characteristic sorption curve which is related to the porous structure of the sorbent. From the BET isotherm study (**Table 4.4);** it is clear that oleic acid coated magnetite haematite nanocomposite has the highest specific surface area among these materials. The constant β is related to the mean free energy of sorption per mole of the sorbate and q_m, value of theoretical monolayer saturation capacity has been shown in **Table 4.6.** Only Oleic acid coated magnetite haematite nanocomposite shows best fitted isotherm parameter value to support D-R model than the other two materials which shows poor relevance.

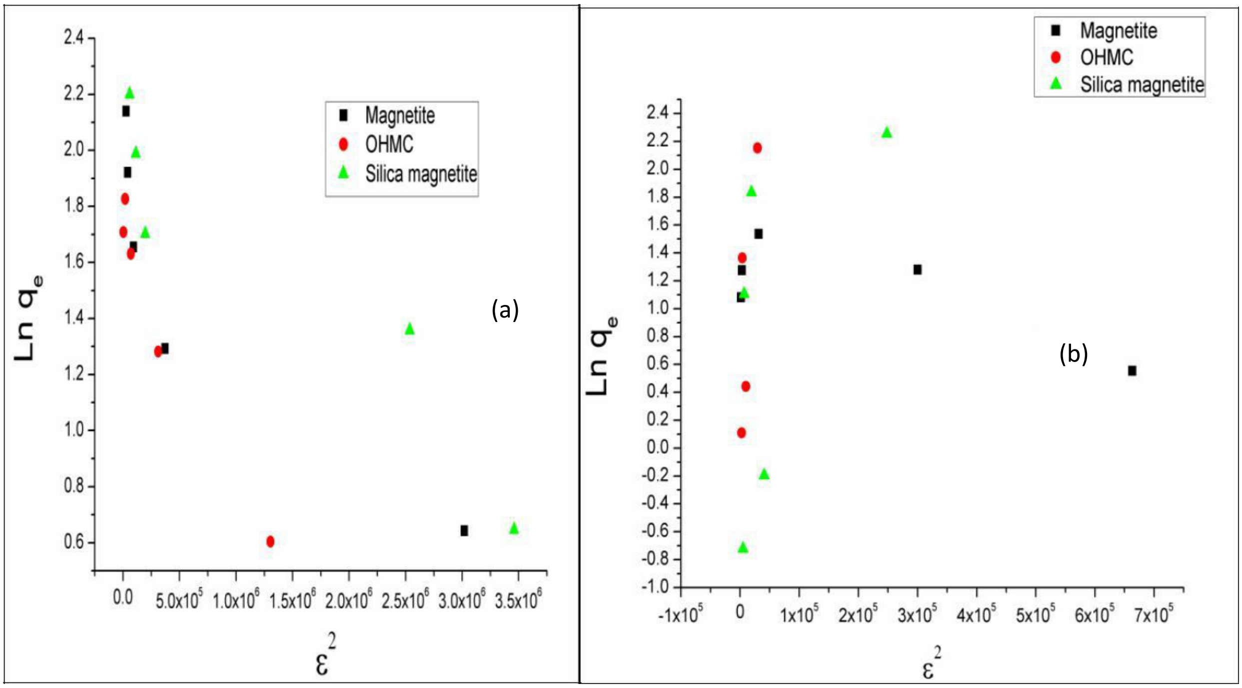

Fig. 4.10: D-R Isotherm model for (a) Cs (I) and (b) Sr (II)

Temkin isotherm: Another two parameter isotherm equation assumes that the heat of adsorption of all the molecules in layer decreases linearly with coverage due to adsorbent-adsorbate interactions, and that the adsorption is characterized by a uniform distribution of the bonding energies, up to some maximum binding energy. A plot of $q_e$versus ln C_e gives the idea of the determination of the isotherm constants b and q_m for the three materials as depicted in **Fig. 4.11**

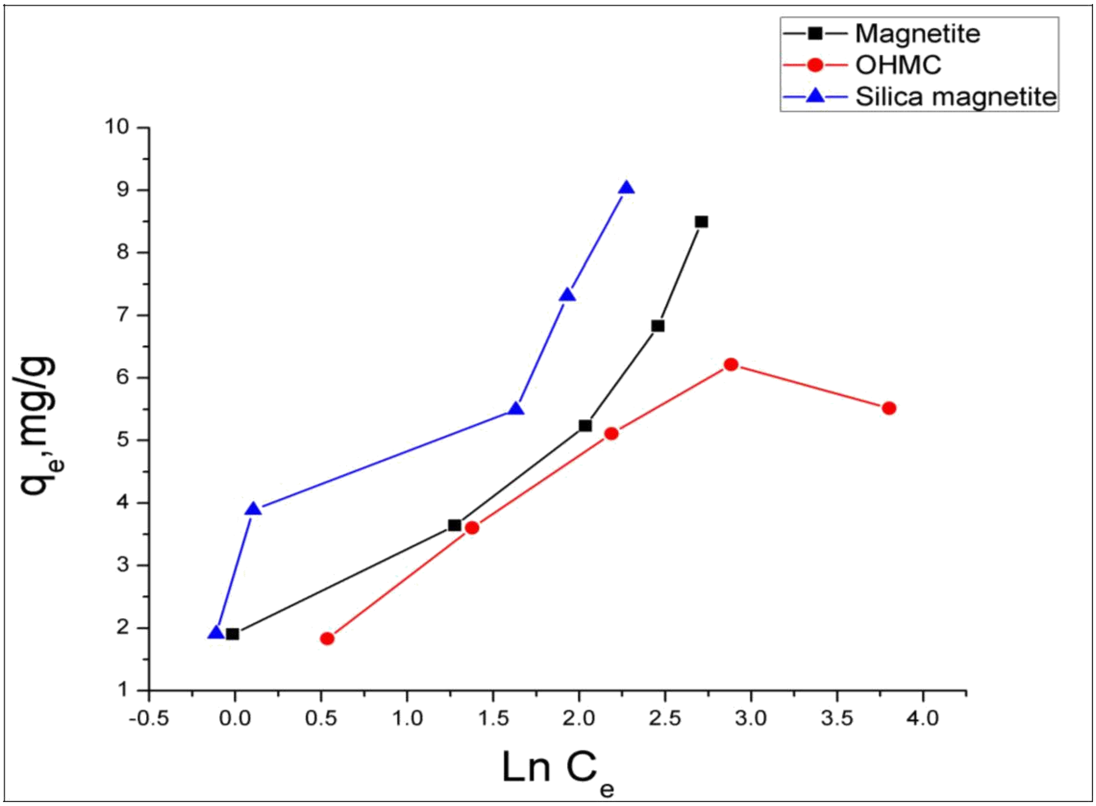

Fig. 4.11: Temkin isotherm model for cesium(I) sorption

In the Temkin model, information about the heat of adsorption and the adsorbent–adsorbate interaction on surfaces has been considered. The variation of adsorption energy, b, is positive for all three materials and has been tabulated (**Table no.4.6**) which indicate the sorption reaction is exothermic. From the data it is inferred that the Temkin isotherm cannot describe the sorption isotherms of cesium onto oleic acid coated and silica coated magnetite acceptably except for the bare magnetite.

Redlich–Peterson isotherm model, a three parameter isotherm model is a hybrid isotherm featuring both Langmuir and Freundlich isotherms shown in **Fig. 4.12.** The Redlich‑Peterson isotherm and Sips model is the three parameters model which combines the Langmuir and Freundlich isotherm. Again, examination of the plot shows that the Redlich‑Peterson isotherm accurately describes the sorption behaviours of cesium sorption onto silica coated magnetite or than the other two nano materials over the concentration ranges studied though all the three materials show good R^2 values for cesium(I) sorption. As all parameters are maximized the linear coefficient of determination all materials sharply shows, extremely high R^2 values which indicates, a considerably better fit compared to the earlier used two-parameter isotherms.

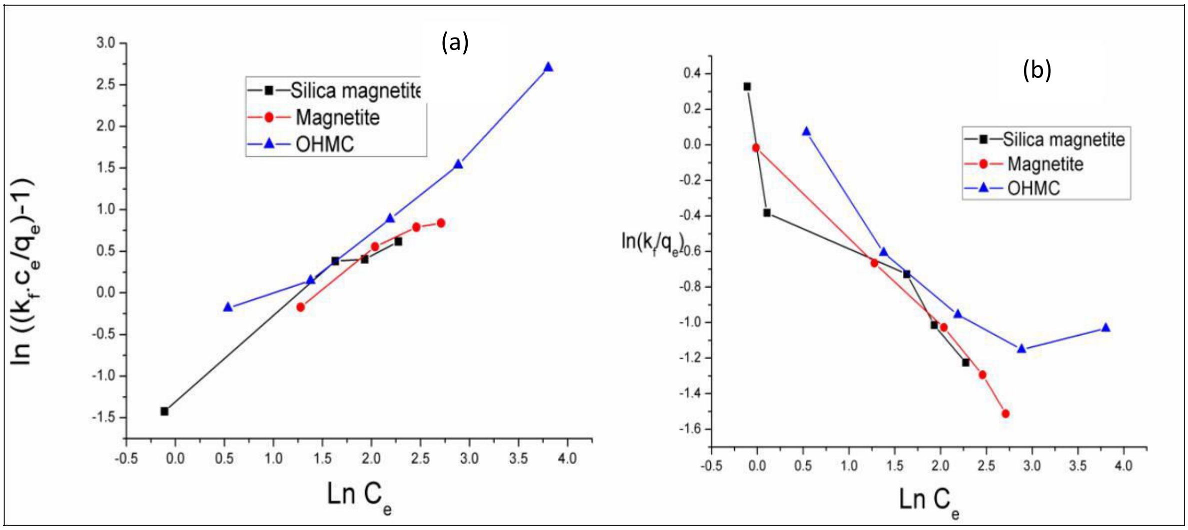

Fig. 4.12: (a) R-P model and (b) Sips model for cesium (I) ion sorption

Comparison of the pseudo linearized form of the equation for all the materials gives the isotherm constants, A, B and g, value for all the these isotherms were found to be linear over the entire concentration range studied with extremely high R^2 values. The R^2 values suggest that the Langmuir isotherm provides a good model of the sorption constant; b and the saturated monolayer sorption capacity, q_m for silica magnetite were higher than those magnetite, which is further higher than oleic acid coated magnetite. **Table 4.6** shows the linear Freundlich sorption isotherm constants, K_f and 1/n, and the coefficients of determination, R^2. Based on the R^2 values, the linear form of the Freundlich isotherm appears to produce a reasonable model for sorption in all three systems, with the cesium sorption onto nano magnetite sorption showing better fit of the experimental data than the other two isotherms.

Table 4.5. Isotherm parameters for adsorption of Cs (I) on magnetite, oleic acid magnetite-haematite composite and silica magnetite at 25^{0}C

Sample	Langmuir isotherm			Freundlich isotherm			D-R isotherm				Temkin isotherm			Redlich Piterson isotherm			Sips isotherm	
	q_{max} (mg/g)	b (L/mg)	R^2	K_f (mg/g)(mg/L)^n	N	R^2	Q_m (mol/g)	E (KJ/mol)	β (mol^2/J^2)	R^2	A(L/g)	B	R^2	a	g	R^2	a	B/g
Magnetite	11.33	0.15	0.88	1.87	1.9	0.99	6.2	4E-7	1.1	0.72	1.86	2.25	0.89	2.82	0.73	0.94	1	0.53
OHMC	5.91	0.50	0.99	1.97	2.9	0.69	5.5	8.75E-7	7.5	0.95	4.32	1.23	0.73	2.47	0.89	0.95	1	0.34
Silica magnetite	11.82	0.25	0.84	2.67	1.9	0.82	7.6	3.55E-7	1.2	0.84	3.06	2.42	0.86	3.57	0.88	0.96	1	0.52

All the above equilibrium isotherms parameters for cesium sorption onto the three magnetite materials have been shown in **Table 4.6** and/or strontium sorption study, the equilibrium isotherm data for Langmuir isotherm plots have been shown in **Table 4.7.**

Table 4.6: Parameters describing the Langmuir equilibrium isotherm model for Sr

Nano composite	**Parameter**		**R^2**
	q_0 (mg/g)	**b (L/mg)**	
Magnetite	29.90	0.19	0.95
OHMC	1.35	0.16	0.53
Silica coated Magnetite	0.59	0.13	0.36

Table 4.7: Langmuir effect of initial metal ion concentration on the Langmuir isotherm model parameter for Sr

Initial concentration (mg/L)	**Separation Factor (R_L)**		
	$R_{L\ (magnetite)}$	**$R_{L(OHMC)}$**	**$R_{L(silica\ magnetite)}$**
20	0.21	0.24	0.28
40	0.12	0.14	0.17
60	0.08	0.09	0.12
80	0.06	0.07	0.09
100	0.05	0.06	0.07

4.5.4 Non Linear Regression analysis of equilibrium isotherm models for cesium sorption on magnetites

The detailed description for non linear regression analysis has been discussed in Chapter 2.The error functions used here is sum squared error (SSE), hybrid fractional error function, average relative error (ARE), sum of the absolute error (SAE), Marquardt's percent standard deviation (MPSD and MPSED), coefficient of determination, Spearman's correlation coefficient, standard deviation of relative error, non linear chi squared test etc. In case of non linear regression models, the best fit of the models to the experimental data mandatorily has nearly zero chi squared value and the lower values have been used to further validate the applicability of the isotherms. Here all the above six isotherms have been attempted which include four two parameters model and two three parameters model isotherm. It was observed that the highest R^2 value and the lowest ARED, ARE, SAE, ARS, MPSD, MPSED, Δq SSE and hybrid values were suitable and meaningful to predict the best fitting equation models.

4.5.4.1 Calculation of error function

All the values of the error functions of the two-parameters and three parameters isotherm models are given in T**able 4.9 to 4.11.**With the help of iteration techniques, aiming for a minimum value of these special functions, the isotherm equations has been iterated by a trial and error method.

Table 4.8: Error deviation data for different equilibrium isotherm models related to the cesium sorption onto silica capped nano magnetite using most commonly used error functions

Error functions	**Isotherm Models**					
	Langmuir	**Freundlich**	**Temkin**	**Dubinin- Radushkevich**	**Redlich Peterson**	**Sips**
R^2	0.886	0.930	0.898	0.910	0.970	0.929
SSE	3.536	2.170	3.167	550.117	1.804	2.196
SAE/EABS	3.621	1.560	3.503	38.734	0.472	2.818
ARE	0.162	0.154	0.165	2.730	0.155	0.100
ARED	16.209	4.403	16.514	233.022	15.580	15.467
ARS	0.421	0.222	0.215	10.251	0.249	0.221
MPSD	84.352	44.742	47.894	872.867	55.817	54.886
MPSED	0.247	0.256	0.249	5.918	0.353	0.313
HYBRID	0.129	0.256	0.275	4.746	0.389	0.386
q(%)	42.177	22.202	21.564	1025.175	24.974	22.170
Spearman coefficient	0.943	0.964	0.947	0.915	0.970	0.964
S Dev of RE	0.943	0.752	0.908	14.132	1.382	0.745
æ^2	0.754	0.600	0.688	228.569	0.623	0.602

Table 4.9: Error deviation data for different equilibrium isotherm models related to the cesium sorption onto nano magnetite using most commonly used error functions

Error functions	**Isotherm Models**					
	Langmuir	**Freundlich**	**Temkin**	**Dubinin-Radushkevich**	**Redlich Peterson**	**Sips**
R^2	0.978	0.990	0.916	0.942	0.996	0.959
SSE	1.177	0.299	2.252	3.124	0.094	74.691
SAE/EABS	2.240	1.159	3.033	3.506	0.645	7.444
ARE	0.127	0.054	0.147	0.197	0.029	0.586
ARED	12.780	5.450	14.707	19.779	2.928	31.459
ARS	0.204	0.072	0.190	0.315	0.036	0.670
MPSD	35.909	14.815	40.397	56.393	10.046	234.334
MPSED	0.236	0.083	0.219	0.363	0.051	0.948
HYBRID	0.213	0.090	0.245	0.253	0.073	1.466
q(%)	20.448	7.216	19.044	31.521	3.635	67.090
Spearman coefficient	0.983	0.994	0.957	0.949	0.998	0.969
S Dev of RE	0.472	0.274	0.768	0.873	0.157	3.767
æ^{2}	0.386	0.065	0.489	0.954	0.020	10.982

Table 4.10: Error deviation data for different equilibrium isotherm models related to the cesium sorption onto oleic acid capped nano magnetite using most commonly used error functions

Error functions	**Isotherm Models**					
	Langmuir	**Freundlich**	**Temkin**	**Dubinin-Radushkevich**	**Redlich Peterson**	**Sips**
R^2	0.912	0.695	0.798	0.610	0.988	0.963
SSE	1.073	3.729	2.466	4.771	0.142	0.453
SAE/EABS	1.991	3.838	3.184	4.299	0.679	1.215
ARE	0.079	0.217	0.161	0.232	0.047	0.046
ARED	10.199	21.795	16.185	23.208	5.094	5.236
ARS	0.143	0.332	0.214	0.303	0.089	0.064
MPSD	29.164	60.701	44.098	62.843	17.995	20.309
MPSED	0.165	0.383	0.247	0.350	0.127	0.091
HYBRID	0.169	0.363	0.269	0.386	0.127	0.130
q(%)	14.325	33.213	21.443	30.346	8.980	6.467
Spearman coefficient	0.957	0.836	0.893	0.958	0.995	0.981
S Dev of RE	0.453	1.003	0.805	0.872	0.205	0.339
$æ^2$	0.255	1.105	0.583	1.184	0.064	0.082

4.6 Sorption Kinetics

4.6.1 Effect of time on uptake of cesium (I) and strontium (II) ion on magnetites

The effect of time on Cs and Sr sorption was also investigated and the comparative uptake of cesium and strontium results are shown **in Fig. 4.12(a)** for cesium and **Fig 4.12(b)** for strontium. It was observed that with variation of time, the cesium percentage uptake remains maximum nearly 100% but for strontium the trend is reversed in case of freshly prepared nano magnetite. With oleic acid coated and silica coated material the strontium uptake gets a major change in uptake efficiency (80-85%) and cesium sorption also steeply increases after 40 min.

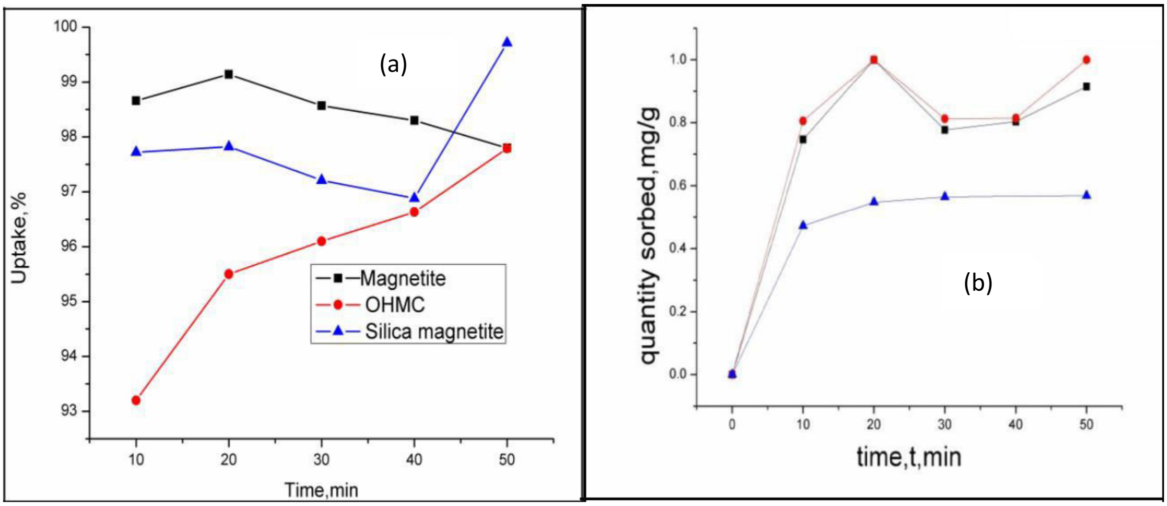

Fig. 4.13: Effect of time on uptake (a) cesium & (b) strontium

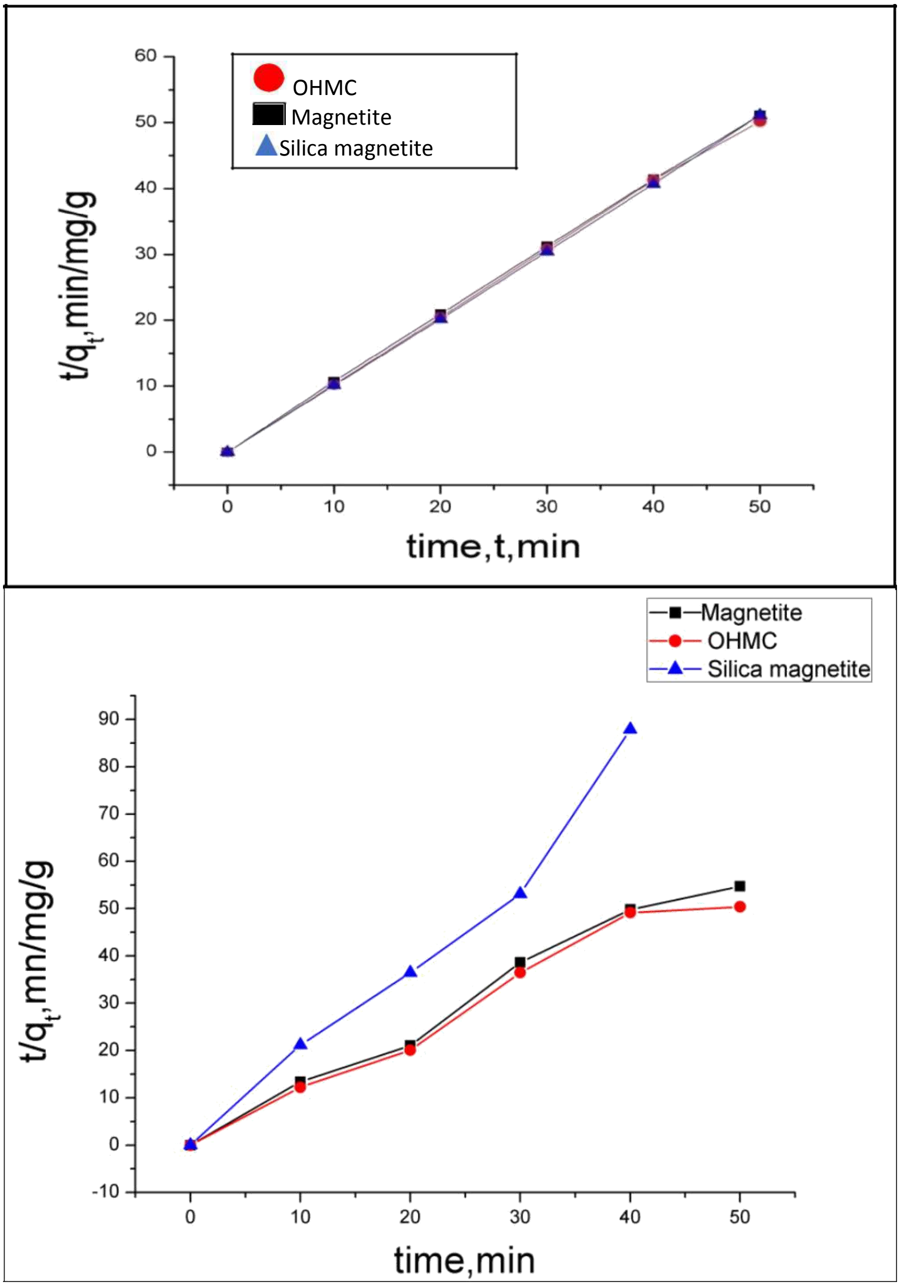

Fig.4.14: Pseudo second order kinetic model for (a) cesium(I) and (b) strontium(II) uptake

Table 4.12: Fitted parameters of Sr (II) adsorption kinetics and diffusion on magnetite, oleic acid magnetite and silica magnetite at 25°C

Sample	Pseudo second order				Elovich			Intra particle pore diffusion model	
	h (mg/m/min)	q_e(exp)	K_{ads} (g/mg min)	R^2	a_e(mg/g min)	b_e(g/mg)	R^2	K_i(mg/g min$^{1/2}$)	R^2
magnetite	1.004	0.874	1.314	0.97	0.78	4.41	0.79	0.117	0.79
OHMC	1.026	0.923	1.203	0.96	0.78	4.20	0.81	0.124	0.77
Silica magnetite	0.586	0.578	1.750	0.99	0.78	6.47	0.92	0.082	0.76

Table 4.13: Fitted parameters of Cs (I) adsorption kinetics and diffusion on magnetite, oleic acid magnetite-haematite composite and silica magnetite at 25^{o}C

Sample	Langmuir isotherm			Freundlich isotherm			D-R isotherm				Temkin isotherm			Redlich Piterson isotherm			Sips isotherm	
	q_{max} (mg/g)	b (L/mg)	R^2	K_f (mg/g)(mg/L)^n	n	R^2	Q_m (mol/g)	E (KJ/mol)	β (mol^2/J^2)	R^2	A(L/g)	B	R^2	a	g	R^2	a	B/g
Magnetite	11.33	0.146	0.88	1.872	1.9	0.99	6.2	4E-7	1.1	0.73	1.86	2.25	0.89	2.82	0.73	0.93851	1	0.53
OHMC	5.91	0.500	0.98	1.97	2.9	0.69	5.5	8.75E-7	7.5	0.94	4.32	1.23	0.73	2.47	0.89	0.95468	1	0.34
Silica magnetite	11.820.250		0.83	2.67	1.9	0.82	7.6	3.55E-7	1.2	0.84	3.06	2.42	0.86	3.57	0.88	0.9649	1	0.52

4.7 Conclusions

Nano magnetite and nano magnetite-nano hematite composite samples have been prepared for cesium(I) and strontium(II) uptake studies. Low concentration of up to 100 ppm of cesium and strontium ions solution and 0.1 g of nano-composite material for a maximum contact time of 1 h ensures nearly 100 percent removal of cesium(I) and strontium(II) ions. To prevent nano-aggregate and to minimize iron leaching in the filtrate, these nanosorbants were coated by a long chain fatty acid like oleic acid. The magnetic property shows super-paramagnetism in these samples which is very effective in environmental concern as because the separation of material is very quick through an external magnet. The point of zero charge for magnetite was at pH 7.2 and for the nano- composite magnetite- hematite was at pH 2.7 and at pH 6.9. This biphasic condition helps the sorption efficiency in the alkaline condition. It appears that RP, Sips model and Freundlich isotherm models dominate, for all the error function selection methods. The comparison table shows that for cesium sorption onto magnetite is better explained by RP model than Freundlich model which was best fit by linear regression method. For oleic acid coated magnetite, RP and Sips model dominates the better suitability, where as DR model has been best fit by linear regression. This change is also seen in silica coated magnetite case, where both RP and Freundlich model favours more than the other model. Thus linear regression and the non-linear regression analytical results give two different models as the best-fitting isotherm for the given set of data. This indicates a surprising difference between the analytical methods. For the simplicity of linear regression sometimes chemical analysis leads to inaccurate results which are not good for design and development of sorption system.

Chapter 5

Sorption of cesium(I), strontium(II) and chromium(VI) ions on nano MnO_2

5.1 Introduction: The ever increasing need of nuclear energy and related radioactive waste released from various nuclear power plants is being managed by following various protocols. The main constituents of radioactive waste are Cs^{137}, Cs^{135}, Cs^{133}, Sr^{90} and Sr^{89}.The separation of radioactive cesium and strontium is thus necessary from the waste stream for radioactive waste management due to their several health hazards **[249].** The different sources of contamination from this radionuclide have already been discussed earlier in Chapter 1. Among the different types of removal processes, sorption by using inorganic metal oxides is gaining much attention due to their high porosity and surface area, easy amenability for scale up and stable chemical properties in the entire sorption process **[250,251].** Natural sorbents like bentonite **[252],** various clay minerals like zeolite, activated sericite, smectite clay **[56,253,254,255,256]** have been used by earlier workers. The main criteria for an effective sorbent to be used in situ application are that it should be steady and stable within the wide pH ranges along with its quick response and cost effectiveness features. Recently Jamal Al Abdullah et al. **[257]** have shown that synthetic nano manganese oxide has potential for cesium, cobalt and lead removal from aqueous solutions. Some workers have synthesized nanocomposites for cesium(I) and strontium(II) removal [**255,258,105,259**]. Again, in actual radioactive waste samples coming from nuclear power plants, broad range of liquid waste starting from acidic to basic environment are found. Thus, sorbent which can take up metal ions in acidic and basic both medium equally has the better advantage. Some workers have used composite materials for this purpose of selective removals of radionuclides **[260]**. In the present work, sorption of Cs (I), Sr (II) by nano MnO_2 has been attempted for a convenient application of practical purposes. This material has also been used for Cr(VI) sorption from a synthetic aqueous solution. In the effluent treatment plant and wastewater disposal containing chromium, contamination has been reported as a serious environmental concern due to the fast growing chemical and leather industry **[137].** Chromium is present in two common stable oxidation states Cr(III) and Cr(VI). Out of these two states hexavalent chromium is mostly present in industrial wastewater and is highly mobile and toxic ions **[261].** In fact, hexavalent chromium is 500-times more toxic than chromium (III) **[262]**, and is a proven carcinogenic. It can modify the deoxyribonucleic acid (DNA) transcription process causing important chromosomal aberration **[263**]. The toxicity of chromates is due to the rapid diffusion of ions across cell membranes and high oxidative potential of Cr(VI). Due to its high mobility these discharges might mix with drinking water sources and cause health hazards and are hence a serious environmental problem. EPA has given maximum contamination level in drinking water standard as 1 mg/L **[264],** whereas World Health Organization (WHO) has recommended for maximum allowable concentration as 0.05 mg/L. According to Indian Standard 1993, the limit for hexavalent chromium in drinking water is 0.05 mg/L and the tolerance limit for discharge of wastewater containing chromium in land surface water, public sewers and marine/coastal areas is 2.0 mg/L **[265].** Hence, removal of this toxic species from industrial effluents is essential.

In this chapter, simple and quick application of nano oxides of manganese (IV) has been shown for sorption of cesium (I), strontium (II) and chromium (VI). It was seen that within a broad range of pH 3-8, the Cs (I) and Sr (II) sorption nearly remains maximum within one hour interval and hexavalent chromium shows an appreciable sorption within one hour at pH 3.

Nano MnO_2 has been prepared by co-precipitation method discussed in Chapter 2. The synthesis is simple and rapid, particle size and composition has been confirmed by using various characterization techniques.

5.2 Synthesis and characterization of nano manganese dioxide: The nanocrystalline MnO_2 was prepared by treating $KMnO_4$ with excess of ethanol **[146].** The synthesis and characterization procedure has been given in **Chapter 2**

5.3 Results and discussion

5.3.1 Characterization results have been discussed **in Chapter 3**

5.3.2 Sorption studies

5.3.2.1 Effect of pH on cesium (I) and strontium (II) ion uptake

The solution pH is the most determining factor for a sorption process of metal ions. By varying pH the surface charge of the oxide nano material changes which influences the speciation of the sorbed metal ions (Cs(I)/Sr(II)/Cr(VI) in the present case). The surface properties of nanomaterials heavily depend on their zero point charge (PZC), which is a deciding factor for a surface to act as a positive or negative surface either side. At the pH of PZC the surface is neutral, but above this PZC, the sorbent surface behaves as negatively charged and below this PZC the surface behaves as positively charged. In this case nano MnO_2 has a PZC of 2.7 which means above the pH 2.7, the MnO_2 surface is expected to take up cationic species. This is evident from the pH variation study of Cs(I) and Sr(II) **(Fig.5.1).** It was seen that from pH 3, cesium sorption starts and it becomes maximum at pH 6. After that the sorption remains same upto pH 8. For strontium the sorption starts at pH 4, and it remains nearly constant in the pH range of 4-8 (above 95%). In case of Cs solution, Cs(I) is the only species in solution whereas for Sr, the dominant species is Sr^{2+} in the entire pH range of 2-14, after pH 14, $Sr(OH)^+$ remains in the solution. In the range of 4-8, that cover acidic to basic range, the uptake is above 98% for both the ions, which is an encouraging result as it favors the applicability of MnO_2 in practical situation of radionuclide separation from aqueous radioactive waste solution. However, in case of Cr (VI) sorption, the pH speciation shows that at different pH the equilibrium that exists between different ionic species of chromium as **[141].** At pH=3 sorption on nano manganese oxide is favored as its surface carries positive charge and a series of mono/divalent chromate ions like $HCrO_4^-$, CrO_4^-, $Cr_2O_7^-$ and $Cr_3O_{10}^{-2}$ co-exist of which $HCrO_4^-$ ions predominate and are again attracted by the positively charged surface of nano oxide, hence maximum sorption capacity of 87% is observed at pH 3. As pH is increased, dominance of sorption of chromate ions is reduced due to the presence of OH^- due to its smaller size and better solvation, which drastically reduces the sorption. This is evident from the following equations.

$$H_2CrO_4 \leftrightarrow H^+ + HCrO_4^- \text{ (pH 2-4)}$$

$$HCrO^-_4 \leftrightarrow H^+ + CrO_4^{-2} \text{(pH4-8)}$$

$$2\ HCrO^-_4 \leftrightarrow Cr_2O_7^{-2} + H_2O \text{ (beyond pH 8)}$$

Owing to the presence of different species of Cr at different pH leads to somewhat irregular trend for Cr (VI) uptake study **(Fig.5.2).**

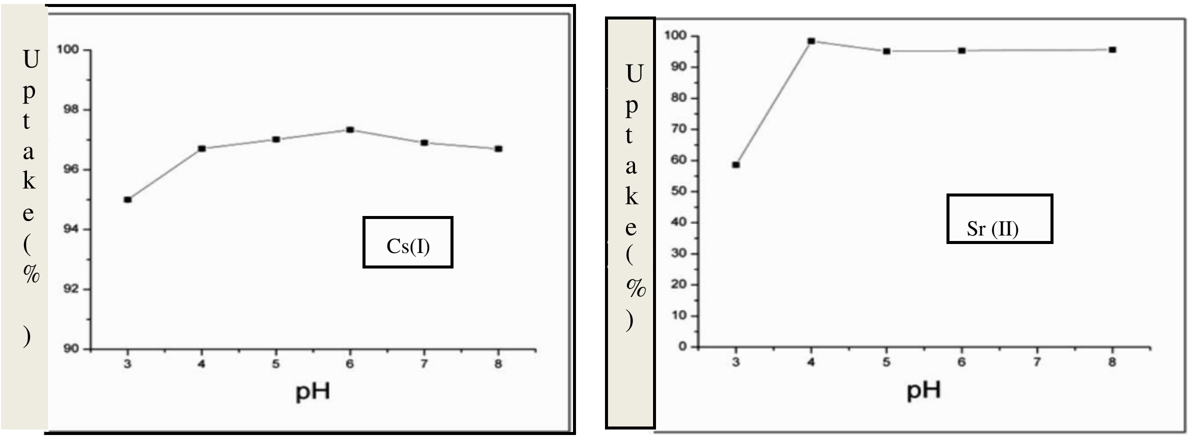

Fig. 5.1: Effect of pH on the amount taken up for Cs (I) and Sr (II), respectively

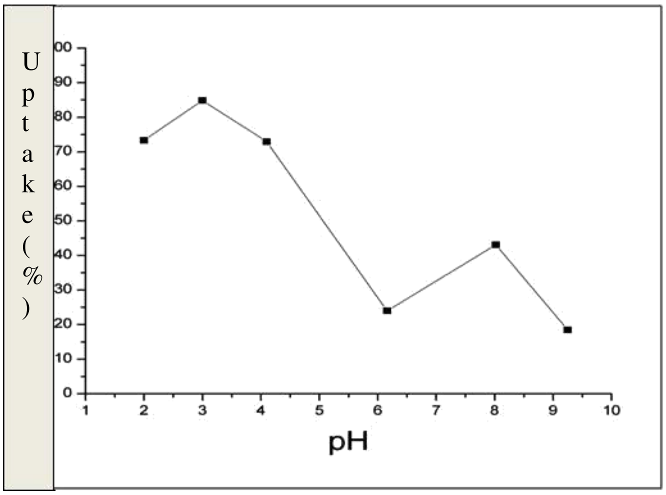

Fig. 5.2: Effect of pH on Cr (VI) uptake by nano MnO_2

5.3.2.2 Effect of initial concentration on cesium (I) and strontium (II) ion uptake

The gradual uptake study with increasing initial concentration of metal ion (Cs/Sr) was carried out with optimum pH 6 and pH 4 for Cs and Sr solutions, respectively. Initially, the sorbent concentration drives the uptake by overcoming the mass transfer barrier between the solid and liquid interface which reflects in both the cases by sudden rise in percentage uptake from 20 mg/L to 40 mg/L. The increase in the sorption efficiency with the increase in sorbent amount might be due to increase in the active sites available on the sorbent. The concentration range was taken from 20mg/L to 100 mg/L. After 40 mg/L, cesium and strontium uptake gradually decreases. To be very precise, the percentage removal drops from 82% to 20% for a range of 20mg/L to 80 mg/L for cesium ion concentration at 25^{o} C and for strontium ion concentration of 20 mg/L to 100 mg/L the percentage removal is decreased from 90 % to 20 %. This result shows that even at very low concentration of metal ions (Cs/Sr) the nano manganese dioxide is able to remove maximum Cs(I) and Sr(II) ions. This promptly suggests the potential effectiveness of this material for use in a very low level radioactive contamination environmental sample. The graphical representation of the process is given in **Fig. 5.3**.

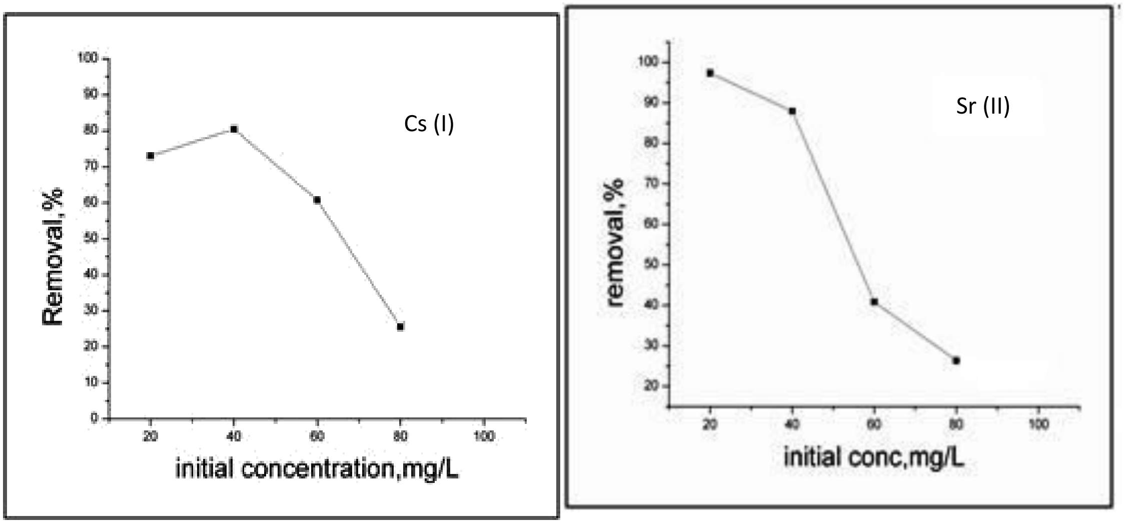

Fig. 5.3: Effect of initial concentration on the amount taken up

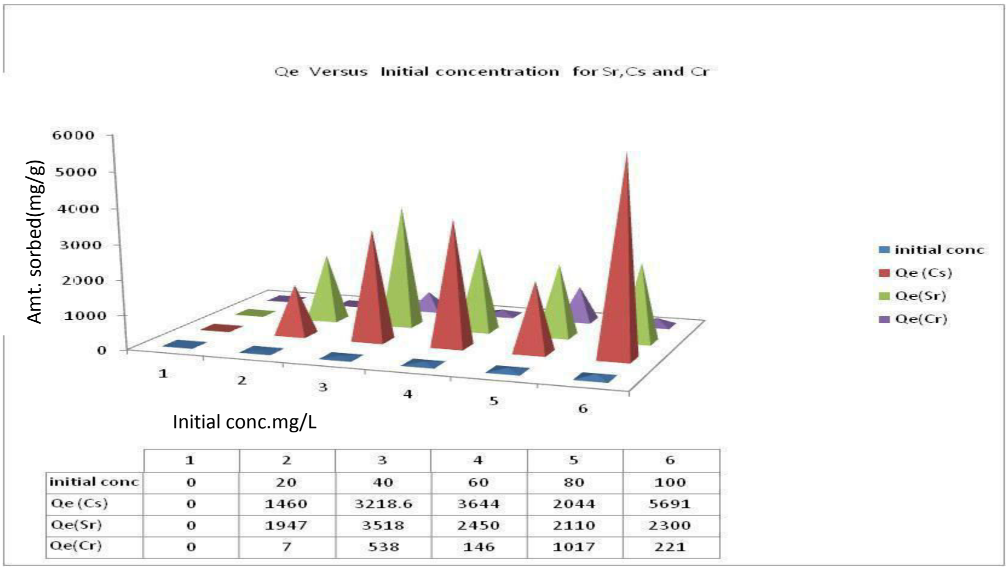

	1	2	3	4	5	6
initial conc	0	20	40	60	80	100
Qe (Cs)	0	1460	3218.6	3644	2044	5691
Qe(Sr)	0	1947	3518	2450	2110	2300
Qe(Cr)	0	7	538	146	1017	221

Fig. 5.4: Comparative uptake study with varying initial concentration of three metal ions (Cs(I)/Sr(II)/Cr(VI)) on nano MnO_2

5.3.2.3 Theoretical modeling of sorption data for cesium (I) and strontium (II) ion uptake

5.3.2.3.1 Sorption isotherms

The equilibrium isotherm models have been applied to the sorption data at different concentration levels for theoretical study. Freundlich, Langmuir and DR isotherm were used in their linearized form. The details of these isotherm parameters have been already discussed in Chapter 2. The graphical representation of these models applied in Cs(I),Sr(II) and Cr(VI) has been depicted in **Fig. 5.5 and 5.6.** Different isotherm parameters have been calculated from the graphs which are tabulated in **Table 5.1**. From the regression coefficient (R^2) values calculated, it was seen that Langmuir isotherm is best fitted than the Freundlich and DR isotherm within the experimental concentration range (20mg/L to 100mg/L). Careful observation of Freundlich parameter of comparatively high n values indicates the heterogeneity of the manganese oxide surface which favors that there must have exponential active sorption sites.

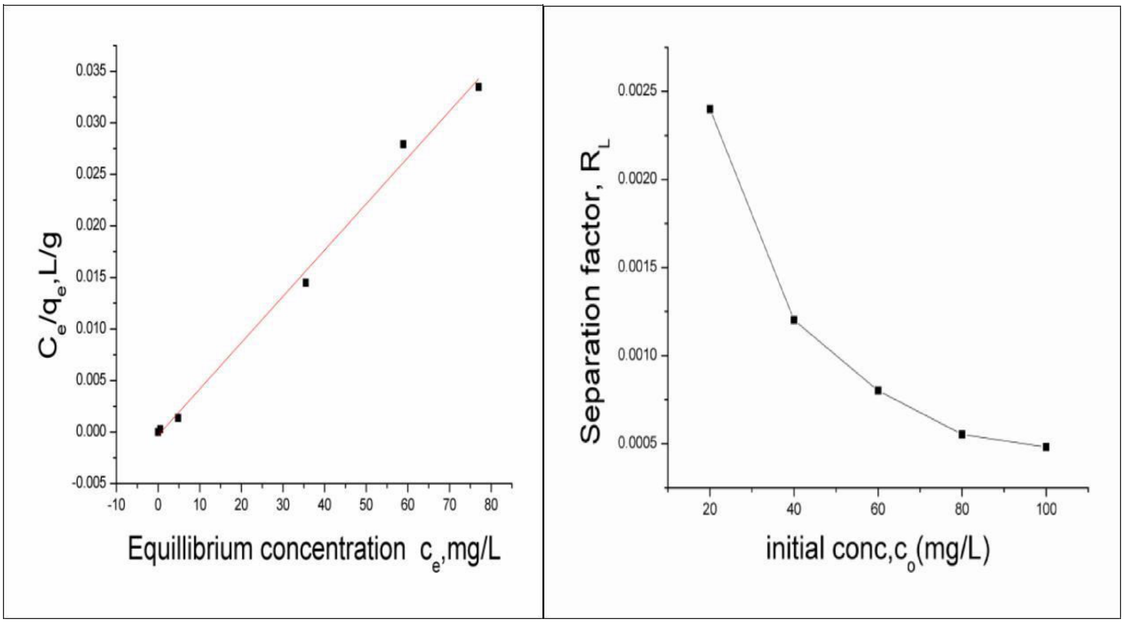

Fig.5.5 (a) & (b): Langmuir isotherm plot for Sr (II) sorption &Variation of separation factor (RL) as a function of initial concentration of Sr (II)

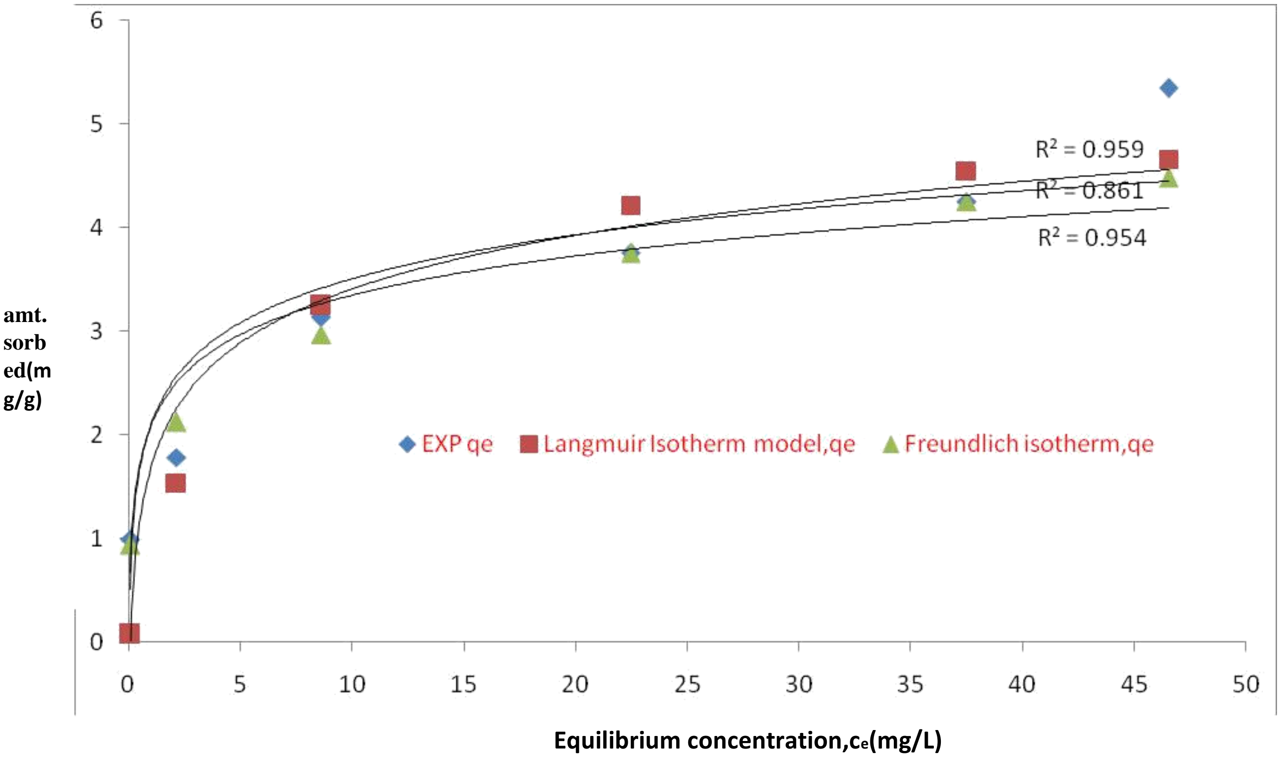

Fig. 5.6: Sorption isotherms for Cr (VI) sorption studies

Table 5.1: Different isotherm parameters for adsorption of strontium (II), cesium (I) and chromium (VI) on manganese oxide at 25^{o}C

Ions	**Langmuir isotherm**			**Freundlich isotherm**		**D-R isotherm**		
	q_{max}(mg/g)	**b(L/mg)**	**R^2**	**K_f(mg/g) (mg/L)^n**	**n**	**Q_m (mol/g)**	**E(J/mol)**	**β(mol^2/J^2)**
Strontium(II)	2.2	0.97	0.99	2.4	4.42	2.5	3.7E+03	3.7E-08
Cesium(I)	2.5	0.27	0.95	1.5	4.51	3.7	3.3E+02	4.5E-06
Chromium(VI)	2.4	0.18	0.96	1.9	0.48	1.640	4.2E+01	2.8E-04

5.3.2.3.2 Sorption kinetics

The amounts of metal ions sorbed on nano MnO_2 with time variation has been carried out and it was seen that an increase in sorption percentage occurred and within one hour the uptake levels off to reach equilibrium. Pseudo first order, pseudo second order, Elovich models have been studied for these sorption processes, the results of which has been shown in **Table 5.2**. Graphs for the same have been plotted for the pseudo second order kinetic model for sorption of three metal ions (**Fig. 5.7** and **Fig. 5.8)**. From the regression coefficient values, it was seen that pseudo second order kinetic model fits well than the other model to establish the sorption kinetics, so the pseudo second order graph has only been shown. It can be predicted that the sorption of metal ions may have occurred through chemical sorption from the better suitability of pseudo second order kinetic model. Y S Ho **[168]** has given the chemical sorption as a probable mechanism for sorption to occur in this kinetic model where valence forces through sharing or exchange of electrons between the sorbate/sorbent systems takes place as a sorption mechanism. Again, from the calculated kinetic parameters it is seen that the initial sorption rate, h is 0.52 mg/m/min for Sr (II) ions. This value is nearly double than that of Cs (I) (0.27 mg/m/min) and more than 4 times that of Cr (VI) (0.12 mg/m/min) which indicates that with Sr (II) ions the sorption is initially fast than the other ions and Cs(I) and Cr(VI) ions in single system faces greater inhibitory effect. The rate constant obtained for pseudo- second order sorption for Sr(II) ions also show good value (2.10 g/mg min)than the Cs(I)/or Cr(VI) metal ions. In fact, Cr (VI) kinetics is comparatively slower than Cs/Sr kinetics as can be seen from **Table 5.2**

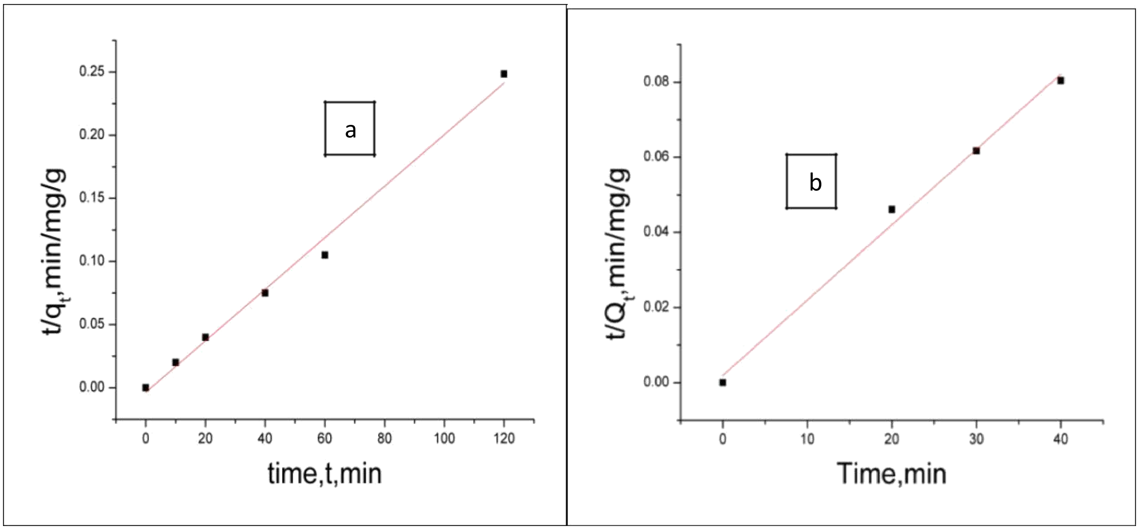

Fig. 5.7: Pseudo second order kinetic models for (a) Cs(I) and (b) Sr(II) sorption on MnO_2

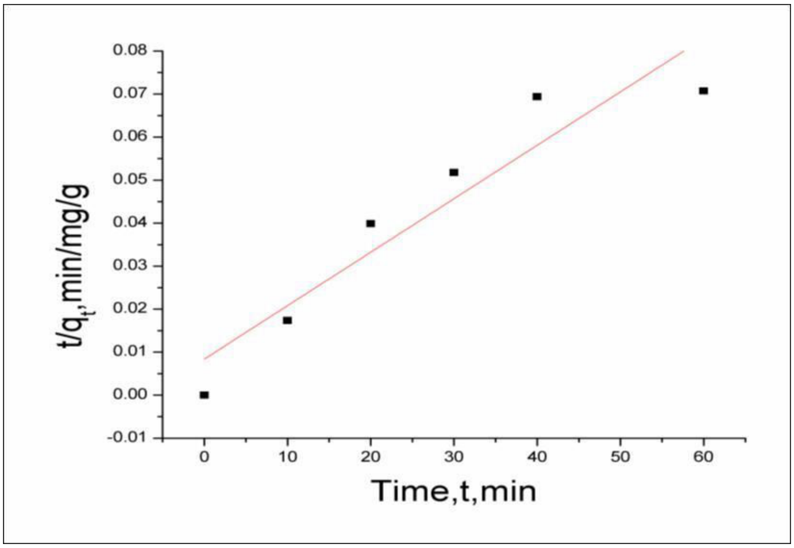

Fig. 5.8: Pseudo second order kinetic model of Cr (VI) sorption by nano MnO_2

In order to investigate the involvement of kinetically controlled diffusion, intra particle diffusion model **[170]** has been studied for the Sr(II)/Cs(I)/Cr(VI) metal ions separately and the same has been plotted for Cs/Sr sorption study in **Fig.5.9**. As the regression coefficient for Cr (VI) is very poor, the graph for the same has not been shown here.

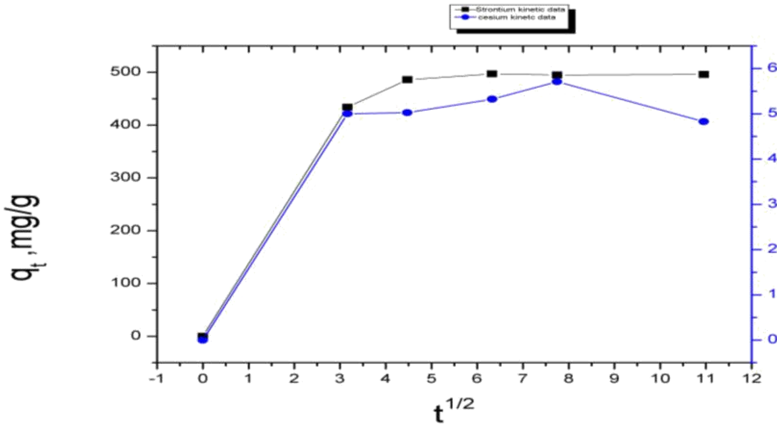

Fig. 5.9: Comparative intraparticle model for sorption of Cs(I) and Sr(II) onto nano MnO_2

Linear correlation was observed only in strontium (II) sorption mechanism as observed from the graph, and in case of cesium (I) or chromium (VI) sorption it does not point towards the intraparticle diffusion. From a closer look at the **Fig.5.9**, it can be inferred that the intra particle diffusion of strontium(II) ions within the nano MnO_2 may be governed by two steps. The first step is the boundary layer diffusion which can be seen as initial straight portion in the graph and the second step is the intra particle diffusion denoted by linear curve which states that the Sr (II) diffuses very fast into the MnO_2 surface initially which is again confirmed by high pseudo second order rate constant and h value discussed earlier, for the sorption process to occur and then slowed down to stable form. The multi linearity curve indicates that intra particle diffusion is not a fully operative mechanism in the sorption of strontium(II) by MnO_2 **[17]**. From these observations, it can be concluded that intra particle diffusion along with pseudo second order kinetics governs the sorption process in case of strontium (II) sorption whereas for cesium (I) or chromium (VI) only the pseudo second order mechanism may decide the entire sorption process.

Table 5.2: Different fitted parameters of strontium (II), cesium (I) and chromium (VI) adsorption kinetics and diffusion on manganese oxide at 25 ^{0}C

Sample	Pseudo second order				Elovich			Intra particle pore diffusion model	
	h (mg/m/min)	q_e(exp)	K_{ads} (g/mg min)	R^2	a_e (mg/gmin)	b_e (g/mg)	R^2	K_i(mg/gmin$^{1/2}$)	R^2
Strontium(II)	0.52	0.49	2.10	0.99	8.3E-07	7.18	0.99	0.06	0.87
Cesium(I)	0.27	0.49	1.14	0.99	1.3E-05	9.19	0.68	0.04	0.35
Chromium(VI)	0.12	0.80	0.18	0.86	1.4E-05	5.66	0.85	0.06	0.74

5.4 Conclusions: The potential of as prepared nano manganese oxide has been established for uptake of Cs(I),Sr(II) and Cr(VI) ions from simulated waste water. The sorption isotherm mainly follows Langmuir isotherm and the kinetics follows pseudo second order model for all the metal ion sorption. Intraparticle diffusion model may have a role in Sr(II) sorption also. Although the temperature effect has not been studied but it can be inferred from isotherm studies that the sorption may occurs via chemisorption process. In a very low metal ion concentration this nano MnO_2 can be used for effective removal of specific contaminants (Cs/Sr) from Low level environmental radioactive solutions and Cr (VI) solution from industrial effluent.

Chapter 6

Nanocrystalline molybdates and tungstates Potential sorbents for removal of radio-nuclides, toxic metal ions and other species

---

The work reported in this chapter has been published as follows:

A comprehensive Study on the Uptake of Dyes, Cu (II) and Radioactive ^{137}Cs(I) by sonochemically synthesized strontium / yttrium tungstate and molybdate nanoparticles

Joyeeta Mukherjee, Dimple P. Dutta, J. Ramakumar and A.K.

Tyagi J. Environ. Chem. Eng. 4 (2016) 3050-3064

6.1 Introduction: Environmental pollution is the biggest bane of rapid urbanization and industrialization in recent years **[266]**. The detrimental effects are generally manifested in the form of increased air and water pollution. Untreated sewage and effluents from various industries contaminate the water bodies creating a huge pressure in effectively managing this life saving resource **[267].** Wastewater containing dye residues and toxic heavy metal ions are common in effluents from textile, leather, food, cosmetics, battery manufacturing units as well as electronics industries. Various methods have been evaluated through the passage of time to remove such pollutants from wastewater and adsorption is a forerunner amongst them **[268-272].** In this technique, preferential partitioning of pollutants occurs from the gaseous or liquid phase onto the surface of a solid substrate **[273].** It is a simple, efficient and fast technique with comparatively low cost in terms of system design, initial investment and land requirement **[274].** One of the most widely investigated adsorbent in water treatment process is activated carbon but the commercially available form is expensive with poor regeneration efficiency **[275].** Consequently, there has been an upsurge in developing low cost adsorbents from industrial as well as agricultural wastes such fly ash, bentonite, peat, red mud, rice husk, etc. **[276,277].** However, the sorption capacities of these materials vary considerably depending on their method of production and origin which acts as a deterrent for deployment in large scale wastewater treatment **[280]**. The sorption properties of various synthetic adsorbents like activated alumina; zeolites, silica gel, etc have also been studied thoroughly. However, the poor sorption kinetics of these materials due to slow intraparticle diffusion of the solute, prove to be a hindrance **[281].** Recently, nanomaterials are being explored as new generation sorbents for wastewater treatment due to their small size and high surface areas **[282].** Consequently, ZnO, TiO_2, Al_2O_3, SnO_2, ZnS, Fe_3O_4, CuO, metallic iron nanoparticles and their composites with activated carbon have been synthesized and their applicability in wastewater treatment has been documented **[283-287].** However, the quest for novel adsorbents continues unabated since it is difficult to find a single adsorbent that can be equally effective for different types of pollutants.Contributing to this search of novel adsorbents, many researchers recently reported the superior sorption properties of sonochemically synthesized barium/ manganese/ copper tungstate and molybdate nanoparticles **[288-290].** The metal tungstates and molybdates are two important classes of inorganic materials finding application in optoelectronics, luminescence, magnetic materials, scintillating materials, catalysis, etc **[291-295].** However, the sorption properties of this series of materials have been explored recently **[288-290].** The efficiency of the sorption process is dependent on the surface charge as well as inherent crystal structure of the various metal tungstates and molybdates. The metal atoms attached to the tungstate/molybdate tetrahedra via the oxygen atoms play a crucial role in the resultant crystal structure and can affect the sorption properties. Recently, the photocatalytic activity for degradation of various pollutants has been studied for $SrWO_4$ and $SrMoO_4$ which belongs to this class of materials **[291, 296]**. However, there are no reports on their sorption properties. Hence it was of interest to study the sorption properties of tungstates and molybdates with divalent strontium ions and compare it with tungstates and molybdates of trivalent yttrium ions. In this work, sorption properties of sonochemically synthesized strontium and yttrium tungstates/ molybdates has been studied for various pollutants like dyes, heavy metal ions and radioactive wastes. Rhodamine B (RhB) and methylene blue (MB) were chosen as model pollutants for the dye sorption studies. The choice was since both find extensive application as colorants in textile and food industry and are known to be carcinogenic, neurotoxic and cause irritation in the eyes, skin and respiratory tract of animals and human **[297,298].** Their slow kinetics makes them unsuitable for biological remediation and hence remediation by adsorption on nanoparticles appears to be a suitable alternative technique. Copper was chosen for the heavy metal sorption studies since copper toxicity is prevalent nowadays due to widespread use of copper in utensils, fungicides, hot water pipes etc. **[299].** Excess copper in the digestive tract causes gastrointestinal distress and its presence in water bodies is toxic to fish and algae **[288].** The applicability of these sonochemically synthesized strontium and yttrium tungstates/ molybdates in treating radioactive wastes was tested via ^{137}Cs sorption. This is one of the biotoxic radioactive fission product generated from the nuclear fuels in the reactors and have a long half life of 30 years. Hence, the safe removal of ^{137}Cs from aquatic environment attracts special attention, particularly after the Fukushima Daiichi accident **[289].**

6.2 Synthesis and characterization: The detailed synthesis procedure for these four materials has been discussed in **Chapter 2**. Among the characterization techniques, powder XRD analysis on the samples were done on PANalytical X -Pert Pro instrument using CuK (k = 1.5406 and 1.5444Å) radiation. Conventional TEM were done using a JEOL 2000 FX microscope. The Brunauer–Emmett–Teller (BET) surface area was determined by nitrogen sorption using a Bel Japan Inc., Belsorp II surface area analyzer. Before the nitrogen adsorption, the samples were degassed under flowing argon at 100°C for 10h. The UV-visible spectra were recorded using a Shimadzu UV-1650PC UV-visible spectrophotometer. The zeta-potential measurements were done on a Zetasizer nano series from Malvern Instruments.

6.3 Sorption studies

6.3.1 Copper uptake experiments

The uptake studies were carried at room temperature (25°C) in batch mode using aqueous solutions containing copper ion. 10ml of aqueous copper ion solution of known concentration (50ppm, 100ppm, 200ppm) at a particular pH (2 and 7) was equilibrated with 10mg of

$SrWO_4/SrMoO_4/Y_2WO_6/Y_2(MoO_4)_3$ sample. The concentration of metal ion left behind in solution after equilibration was determined by appropriate techniques. The solution after equilibration was analyzed for the presence of copper ions by complexation with PAR (2-pyridyl-azo-resorcinol) ligand using UV-visible spectroscopy and measuring the absorption at 545nm **[288].**

6.3.2 ^{137}Cs uptake experiments

For studying the uptake of the gamma ray emitting ^{137}Cs radionuclide, 20ppm of ^{137}Cs solution was equilibrated with 10/100mg of the sonochemically synthesized $Y_2Mo_3O_{12}$ / Y_2WO_6 samples in a plastic container of standard geometry. The activity at fixed time intervals was measured by gamma spectrometry using NaI (Tl) detector. The analytical techniques and instrumentation used for the radiochemical assay was based on standard procedures as described in “USEPA. Multi-Agency Radiological Laboratory Analytical Protocols Manual,” Volume II: Chapter 10 - 17 and Appendix F, EPA/402/B-04/001B/(NUREG-1576), 2004.

6.3.3 Dye sorption studies

The sorption studies were carried out in the batch mode using nano tungstate and molybdate sorbents namely yttrium molybdate (YM), yttrium tungstate (YW), strontium molybdate (SrM) and strontium tungstate (SrW) and the sorption efficiency with respect to uptake of different organic dyes like Rhodamine B (RhB) and Methylene blue (MB) was evaluated.

6.4 Results and discussion

6.4.1 Characterization results: The powder XRD patterns obtained for the as synthesized strontium tungstate and strontium molybdate are shown in **Fig. 6.1a and 6.1b**, respectively. Both the as synthesized samples display good crystallinity. All the diffraction peaks in Figure 6.1a could be indexed to tetragonal $SrWO_4$ having lattice constants of a = 5.415Å and c =

11.935Å which matches well with earlier reports (JCPDS card number 080490) **[300].** In case of **Fig. 6.1b,** the diffraction peaks confirm the formation of tetragonal $SrMoO_4$ with space group I41/a. The lattice parameters obtained were a = 5.391Å, c = 12.04Å which matched well with that reported for JCPDS card number 080482. No other impurity peaks could be seen in the powder XRD data. The powder XRD analyses of the as synthesized yttrium tungstate and molybdate confirmed their amorphous nature. **Fig. 6.2a** shows the powder XRD pattern obtained for yttrium tungstate which was furnace heated at 300°C for 1h. The diffraction peaks are well formed suggesting development of crystallinity in the sample and they matched with that reported for monoclinic Y_2WO_6 with space group P2/c. The lattice parameters of a = 7.590Å, b = 5.334Å, c = 11.35Å, concurred with that reported for JCPDS card 73-0118. In case of yttrium molybdate, the as prepared sample was furnace heated at $750^{\circ}C$ for 1h. The powder XRD pattern obtained is in good agreement with the standard pattern of $Y_2Mo_3O_{12}$ reported in JCPDS No 28-1451.

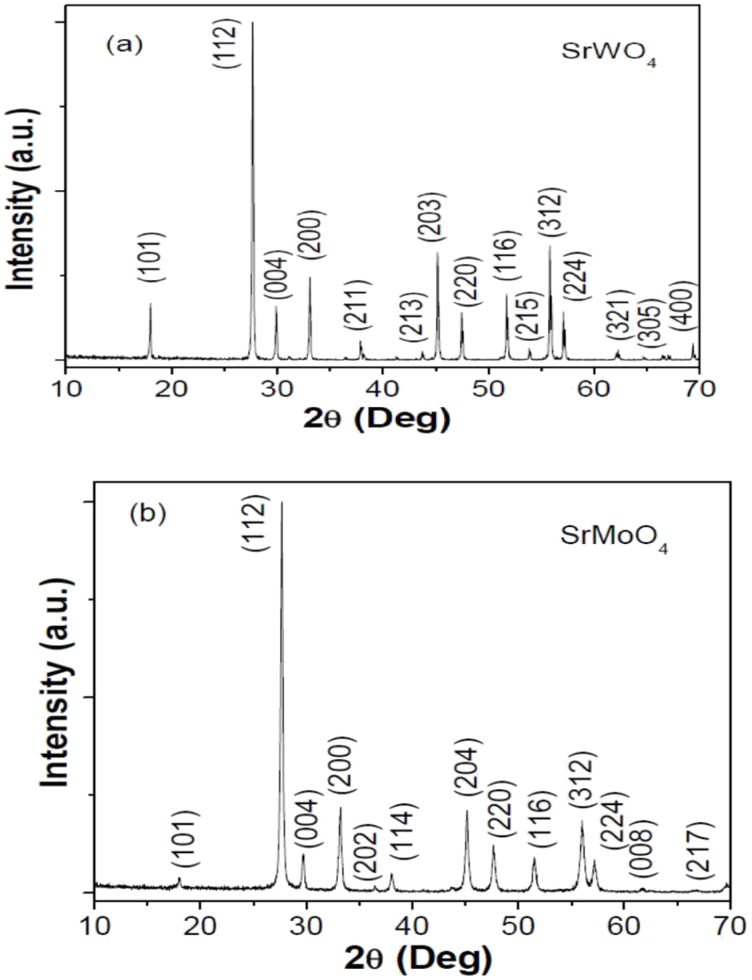

Fig. 6.1(a-b):Powder XRD patterns of SrWO4,SrMoO4, respectively

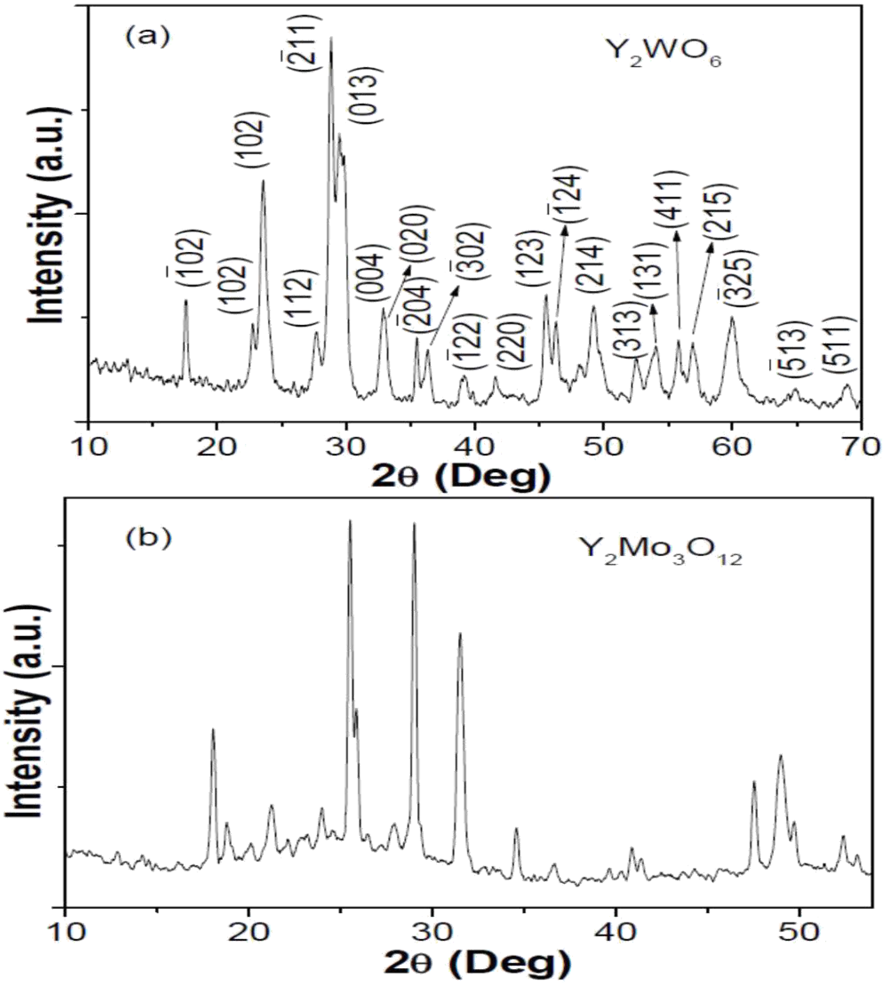

Fig. 6.2(a-b):Powder XRD patterns of Y_2WO_6 and $Y_2(MoO_4)_3$ heated for 1h at 300^{O}C and 750^{O}C, respectively

TEM of all the four samples were recorded to get an insight into their size, morphology and composition (**Fig. 6.3**). Both $SrWO_4$ and $SrMoO_4$ exhibits spindle shaped nanostructures as shown in **Fig. 6.3a and 6.3b**, respectively. In case of $SrWO_4$, the spindles varied in size with the smallest ones having centre diameters of25-50nm and lengths of100-150nm and the larger ones have diameters of 100-150nm and lengths of 250-300nm **(Fig. 6.3a)**.

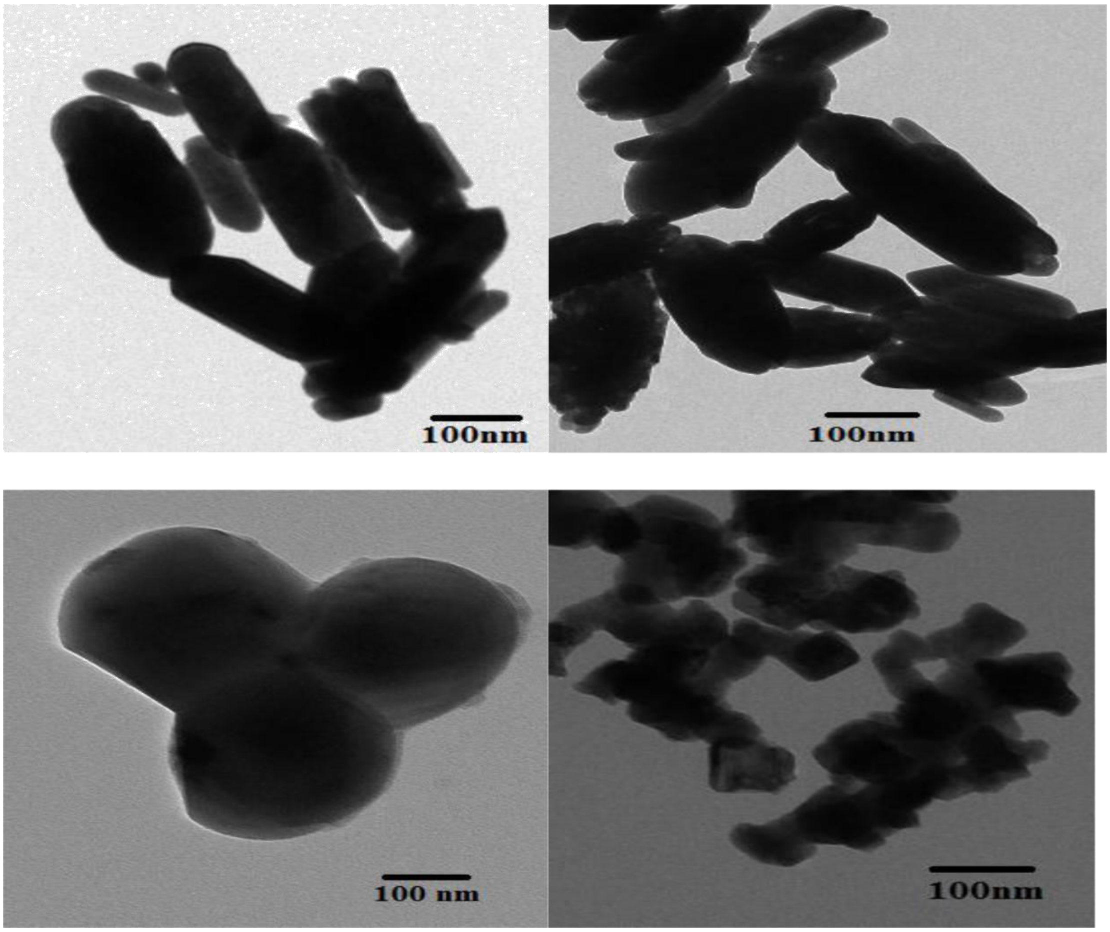

Fig. 6.3: TEM of (a) $SrWO_4$, (b) $SrMoO_4$, (c) Y_2WO_6 and (d) $Y_2Mo_3O_{12}$

Recent report on sonochemical synthesis of $SrWO_4$ in acidic pH led to the formation of products with hierarchical structures **[301].** However, in present case the synthesis has been done at neutral pH which might hinder the oriented growth of various crystallographic faces that leads to the formation of such superstructures. Similar variation in the size of the nanospindles was observed in case of $SrMoO_4$. The smaller spindles have center diameter 10nm and length 100nm while the larger ones have diameters of 100-120nm and lengths of 300-500nm. Formation of spindle shaped $SrMoO_4$ via sonochemical synthesis done at neutral pH has been reported earlier **[302].** Predominantly spherical particles with diameters of 250nm were obtained in present case of sonochemically synthesized and subsequently thermally treated Y_2WO_6 (**Fig.6.3c**). Hydrothermal synthesis of Y_2WO_6 microstructures under acidic pH has been reported in literature **[303,304].** The formation of microstructures has been aided by the presence of various surfactants and chelating agents used in the process of synthesis. In case of present sonochemically synthesized samples, the heat treatment and the absence of surfactants led to the formation of slightly aggregated spherical nanoparticles. Figure 6.3d shows the morphology of our thermally treated $Y_2Mo_3O_{12}$ sample obtained via sonochemical synthesis. The nanoparticles are of irregular shape with sizes in the range of 40-50nm. Formation of irregular shaped nanoparticles has also been reported in case $Y_2Mo_3O_{12}$ synthesized using sol gel method **[305].** The specific surface areas of all the samples have been calculated by the BET method using the nitrogen adsorption desorption isotherm data (**Fig. 6.4a-6.4d**).

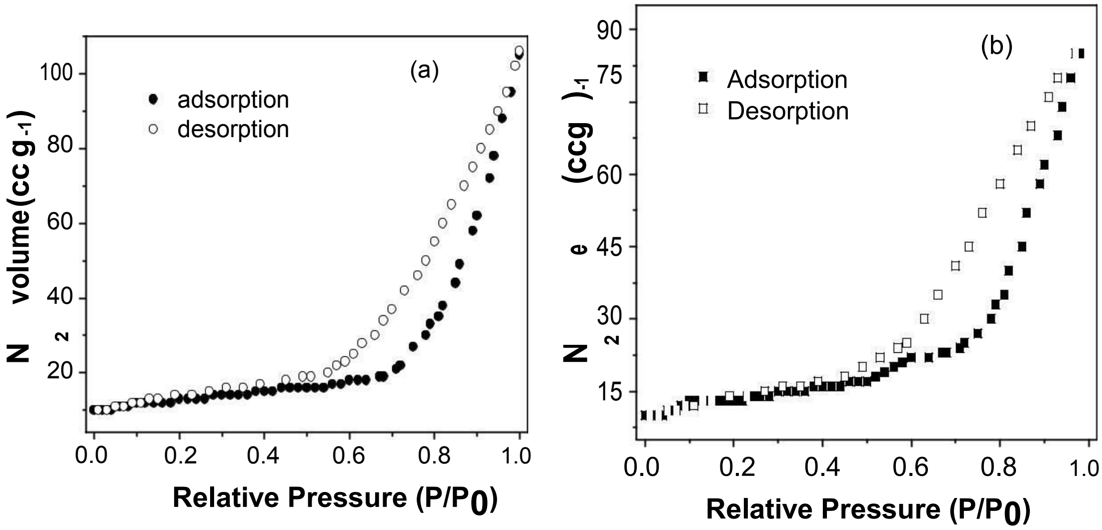

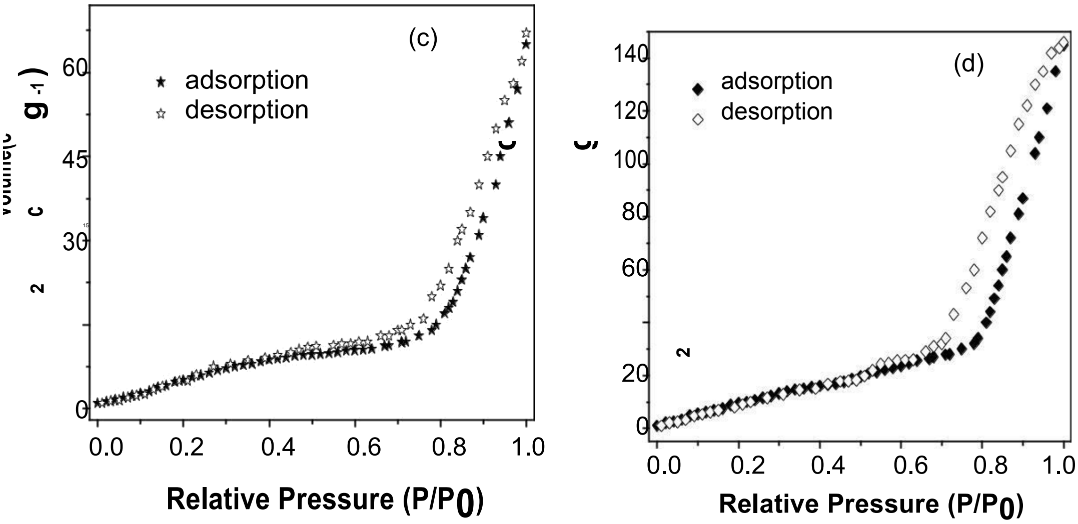

Fig. 6.4: BET N_2 adsorption-desorption isotherm of (a) $SrWO_4$, (b) $SrMoO_4$ (c) Y_2WO_6 and (d)$Y_2Mo_3O_{12}$

In all the cases a Type IV isotherm with stepwise adsorption has been obtained indicating a mesoporous structure. Pronounced desorption hysteresis suggests the existence of large mesopores in the $SrWO_4$ and $SrMoO_4$ samples. A broad increase in N_2 uptake in the P/P_0 range from 0.52 to 0.95 in case of $SrWO_4$ and $SrMoO_4$ clearly indicates that there is a wide range of mesopores within the samples. From the TEM images it can be inferred that the particles do not have a porous structure. Hence the mesoporous nature of the isotherms is most likely due to interparticle porosity. The specific surface area has been calculated to be 37.4 ± 2.3m^2g^{-1}, 33.6 ± 1.1 m^2g^{-1}, 24.8 ± 1.1 m^2g^{-1} and 77.2 ± 1.5 m^2g^{-1} for our sonochemically synthesized $SrWO_4$, $SrMoO_4$, Y_2WO_6 and $Y_2Mo_3O_{12}$ samples, respectively. The higher surface area obtained in case of $Y_2Mo_3O_{12}$ can be attributed to the smaller size of the particles. Pore size distributions of these samples have been estimated by employing the Barret-Joyner-Halenda (BJH) method and the corresponding values have been given in **Table 6.1.**

Table 6.1: Summary of specific surface area, pore volume and pore size distribution of $SrWO_4$, $SrMoO_4$, Y_2WO_6 and $Y_2(MoO_4)_3$

Sample	$S_{BET}(m^2g^{-1})$	Pore volume (cm^3g^{-1})	Pore size distribution (nm)
$SrWO_4$	37.4 ± 2.3	0.19	38.03
$SrMoO_4$	33.6 ± 1.1	0.24	42.16
Y_2WO_6	24.8 ± 1.1	0.12	27.56
$Y_2(MoO_4)_3$	77.2 ± 1.5	0.16	4.56

6.4.2 Sorption of Cu (II) ions

The comparative effect of pH on the time of equilibration depicting the sorption efficiency of 10mg SrW, SrM, YW and YM nanosorbents for 100ppm of Cu(II) ions has been explored. For all the sorbents, the uptake of Cu(II) was better at a lower pH of 3 compared to pH 7. A representative plot of the effect of pH on Cu(II) uptake by YM is shown in **Fig. 6.5a**.

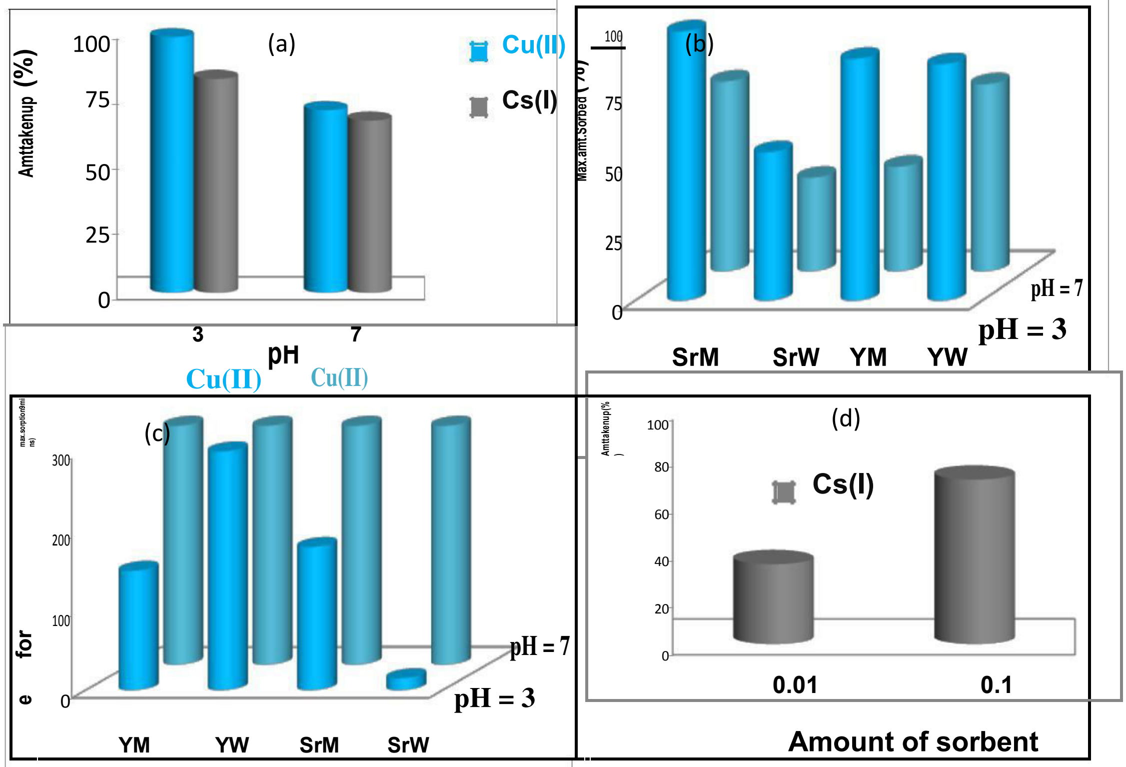

Fig. 6.5:(a) Amount of Cu(II) and Cs(I) taken up by $Y_2Mo_3O_{12}$, (b) maximum Cu(II) sorption exhibited by all four sorbents, (c) time taken for maximum sorption by all four sorbents and (d)effect of weight of $Y_2Mo_3O_{12}$ on Cs(I) uptake.

As in case of the dye sorption, the presence of negative surface charge on the sorbent at lower pH attracts the Cu(II) ions. The highest uptake is seen for YM with 98% removal of 100ppm Cu (II) ions within 150 min (**Fig. 6.5b**). The fastest uptake occurred for SrW with 90% removal of 100 ppm within a short time span of 15 min (**Fig. 6.5c**). SrW has got a reasonably high surface area and from the zeta potential value it can be concluded that the colloid in solution is also reasonably stable. This is crucial as it facilitates the equilibration process. Though the kinetics is fast, the maximum uptake was 90%. This could be due to its relatively low surface area as compared to YM. YM has highest surface area but the zeta potential value shows that the colloid is less stable and hence longer time is taken by the metal ion to reach the active sites. The above observations indicate that uptake of metal ions by sonochemically synthesized yttrium/strontium tungstates/molybdates is a combination of both surface charge and colloidal stability.

6.4.3 Sorption of ^{137}Cs ions

^{137}Cs has a relatively long half life of 30.2 years and forms a primary component in case of unlikely nuclear fallout. ^{137}Cs is highly soluble in water, follows the biological behavior profile of sodium/ potassium and is known to be carcinogenic. For sorption and consequent removal of cesium from nuclear waste, ammonium molybdophosphate (AMP) has been found to be highly effective. However, AMP becomes soluble in solutions with pH >4, and therefore, is only applicable to acidic solutions. Cesium can be eluted from AMP with concentrated ammonium salt solutions (NH_4NO_3, NH_4Cl, etc.) or the cesium and ammonium molybdophosphate complexes can be dissolved in caustic to separate the active exchanger material from an inert binder material, such as PAN**.** As mentioned earlier, nanosized sorbents are quite attractive due to their larger effective surface are and they can be used over a wide range of pH. The regeneration of the nanosorbents is quite simple as compared to the number of steps involved using AMP. These sonochemically synthesized YM/YW samples have been evaluated for ^{137}Cs uptake. It is seen that the uptake is pH sensitive and at lower pH of 3, the extent of sorption is more. The representative diagram for ^{137}Cs uptake by YM at different pH in 1h is shown in **Fig. 6.10a.** It indicates that the surface charge is the crucial factor that decides the uptake of Cs(I). The effect of sorbent dosage (**Fig. 6.5d**) showed that with increase in the amount of the YM nano sorbent from 10 to 100mg, the extent of ^{137}Cs sorption increases. This indicates that increasing the amount of sorbent effectively increases the number of sites available for sorption which facilitates the process.

The recycling of the sorbents in the removal of Cu(II)/Cs(I) have been also investigated. After adsorption, desorption was done by washing out the sorbent bound Cu(II)/Cs(I) with NaOH (pH ~9) and then rinsing the resultant sorbent repeatedly with nanopure water. The sorbent was then dried at 105°C and reused. It was observed that there is less than 2% decrease in the overall Cu(II)/Cs(I) sorption capacity after three recycles which indicates that the sorbents have good reusability.

6.4.4. Sorption of dyes: This work has been extended for effective application of dye removal study also. The detailed study has been carried out by batch sorption experiments.

6.4.4.1. Influence of pH

The pH of the external solution is an important factor that is expected to affect the sorption. These studies were carried out by equilibrating 10 mg of each of the sorbents with single dye (RhB or MB) solutions of 20 ppm concentration maintained for a period of half an hour at pH in the range of 2-9 (using hydrochloric acid or sodium hydroxide). The pH was measured by using a portable pH meter (Mettler Toledo, FG2- FiveGo pH). The results are shown in **Fig. 6.6**. From the figure, it is seen that at neutral pH, all the sorbents exhibited poor uptake of both RhB and MB. The quantitative uptake of the dye by each material at different pH is given in **Table 6.2**

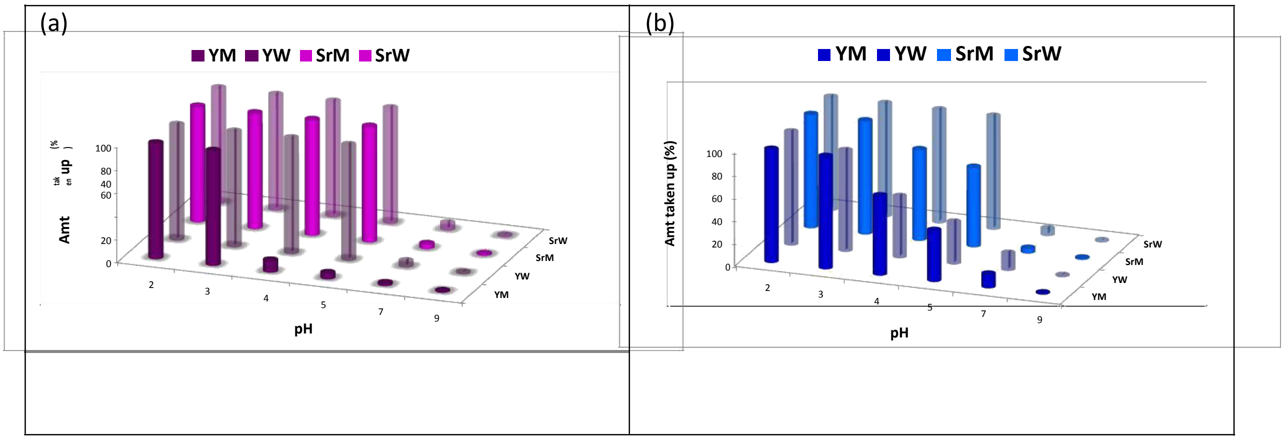

Fig.6.6: Effect of pH on the sorption of 20ppm solution of (a) RhB and (b) MB dye.

Table 6.2: Comparison of Dye sorption property of (a) $SrWO_4$, (b) $SrMoO_4$, (c) Y_2WO_6 and (d) $Y_2Mo_3O_{12}$nano particles with commercial activated carbon (CAC)

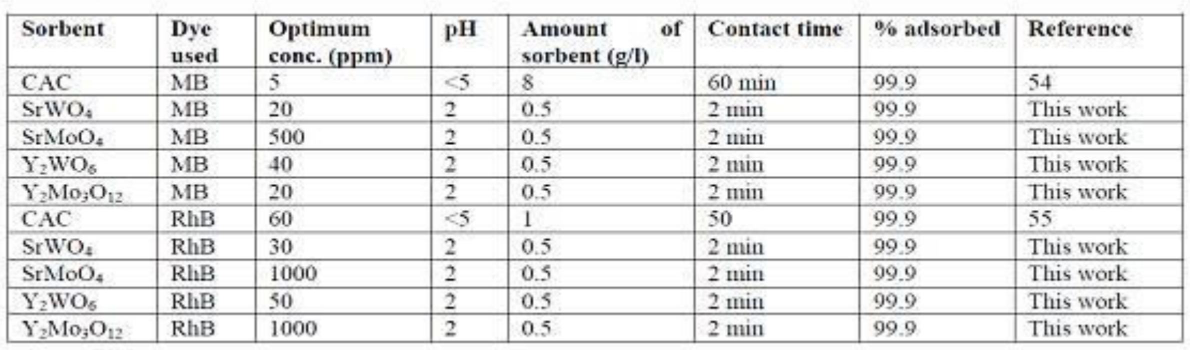

Sorbent	Dye used	Optimum conc. (ppm)	pH	Amount of sorbent (g/l)	Contact time	% adsorbed	Reference
CAC	MB	5	<5	8	60 min	99.9	54
$SrWO_4$	MB	20	2	0.5	2 min	99.9	This work
$SrMoO_4$	MB	500	2	0.5	2 min	99.9	This work
Y_2WO_6	MB	40	2	0.5	2 min	99.9	This work
$Y_2Mo_3O_{12}$	MB	20	2	0.5	2 min	99.9	This work
CAC	RhB	60	<5	1	50	99.9	55
$SrWO_4$	RhB	30	2	0.5	2 min	99.9	This work
$SrMoO_4$	RhB	1000	2	0.5	2 min	99.9	This work
Y_2WO_6	RhB	50	2	0.5	2 min	99.9	This work
$Y_2Mo_3O_{12}$	RhB	1000	2	0.5	2 min	99.9	This work

The sorption of both the dyes at pH 5 was considerably reduced in case of YM and YW. The effect of pH on sorption could be attributed to different controlling parameters. The nature of the adsorbate in solution as well as the surface charge on the adsorbent decides the efficiency of the sorption process. With change in pH the dyes have different ionic forms and RhB (pKa = 3.7) exists in the protonated form at pH < 3.7 **[306].** At higher pH, the zwitterionic RhB forms dimers due to attraction between the carboxyl and xanthenes groups resulting in its decreased sorption on the surface of the sorbent. The surface charge on the sorbent could be understood from the zeta potential measurements of the different nanomaterials. The results of these studies are given in **Table 6.3.**

Table 6.3: Zeta potential measurements for sonochemically synthesized $SrWO_4$, $SrMoO_4$, Y_2WO_6 and $Y_2(MoO_4)_3$ samples with RhB and MB dyes at various pH

Sample	ξ(mV) at pH 2	ξ(mV) at pH 5	ξ(mV) at pH 7
$SrWO_4$	-15.34	-11.11	-9.31
$SrWO_4$ + RhB	-10.74	-7.64	-4.25
$SrWO_4$ + MB	-10.56	-7.37	-4.53
$SrMoO_4$	-23.51	-22.03	-15.26
$SrMoO_4$ + RhB	-14.32	-13.45	-10.76
$SrMoO_4$ + MB	-15.92	-16.31	-11.87
Y_2WO_6	-7.35	0	6.38
Y_2WO_6+ RhB	-2.75	3.67	10.43
Y_2WO_6+ MB	-4.86	8.75	14.56
$Y_2(MoO_4)_3$	-3.25	5.02	2.45
$Y_2(MoO_4)_3$+ RhB	-0.65	12.01	10.25
$Y_2(MoO_4)_3$+ MB	-0.37	9.87	8.67

The zeta potential obtained in case of YW is negative in the pH range of 2-5 ($pH_{ZPC} = 0$). RhB and MB are basic dyes which exist in their cationic forms in aqueous solutions and thus have a natural attraction to adhere to the negatively charged surface and hence the sorption of RhB and MB dye is higher at pH5.

It can be seen from **Fig. 6.4** that the sorption of RhB on YW is better at acidic pH range of 2-5 compared to that of MB. This might be due to the tendency of the carboxylic group in cationic RhB to stay protonated at low pH which prevents the formation of zwitterions **[305-307]**. This protonated form has a higher affinity for the negatively charged YW surface. The zeta potential of YM is positive at pH 3 ($pH_{ZPC} = 2.9$) (**Table 6.3**). Hence the highest adsorption of both RhB and MB occurs on the negatively charged YM surface at pH 2 -3. The high sorption of RhB and MB on SrW and SrM in the acidic pH range of 2 to 5 can be explained on the basis of attraction of the cationic dyes to the negatively charged surface as shown by the obtained zeta potential values.

6.4.4.2 Influence of initial concentration of dye

The optimum pH for effective and fast sorption was 2 and hence all the further sorption studies were carried out at this pH. The pH dependence of the sorption gives an idea that the process follows an ion exchange mechanism. The time needed for complete removal of the dye was dependent on the nature and initial concentration of the dye and on the sorbent material and the amount of sorbent taken. The data obtained for these various sorption experiments using 10mg of the sorbent are shown in **Fig. 6.7a and 6.7b.**

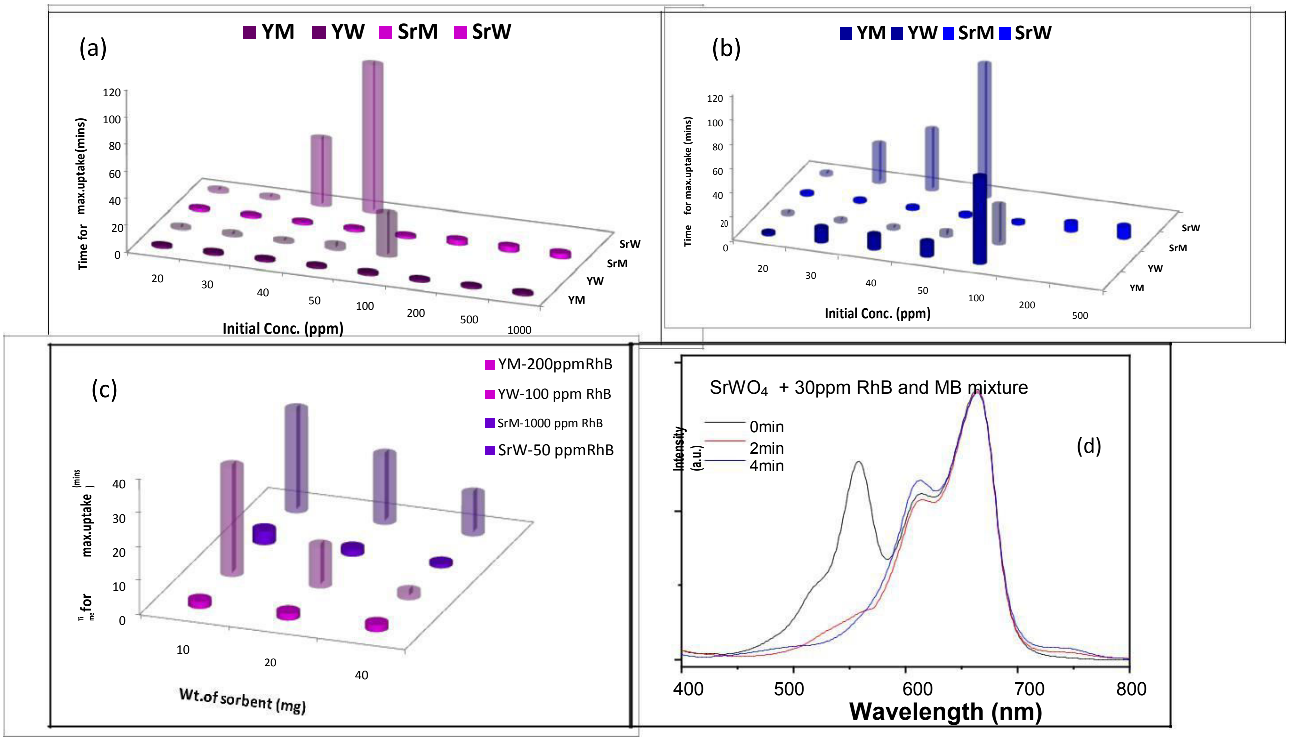

Fig. 6.7: Effect of initial concentration of (a) RhB and (b) MB dye on the time taken for sorption, (c) Effect of weight of sorbent on time taken for maximum uptake and (d) selective sorption of RhB dye by sonochemically synthesized $SrWO_4$ nanoparticles.

The results are quite interesting. It is seen that both the nano molybdates (YM and SrM) show very high uptake of RhB upto a concentration of as high as 1000 ppm within 2 minutes of equilibration. However the corresponding tungstates show less efficiency with YW scoring over SrW marginally. It is seen that the maximum concentration of RhB that can be almost completely removed using YW and SrW within 2 minutes is 50 and 30 ppm respectively. Further increase in the RhB concentration considerably enhances the time taken for complete dye sorption by the tungstates. The uptake of MB shows that SrM has the highest affinity for MB upto a concentration of 100 ppm. YM and SrW show fast kinetics for only 20 ppm of MB while YW can result in a nearly complete sorption within 2 minutes of upto 50 ppm concentration of dye. From BET surface area analysis, it can be seen that YM has the highest surface area (77.2 ± 1.5 m^2g^{-1}) among all four sorbents. However, even though the uptake of RhB on YM is fast and efficient, the uptake of MB is quite poor and slow. Hence it can be concluded that the different rates of sorption exhibited by these sorbents is not dependent solely on their surface area. Other parameters like surface charge on sorbent and functional groups attached on the dye molecules also affect the sorption efficiency.

6.4.4.3 Influence of weight of sorbent

The effect of sorbent weight on the uptake efficiency of RhB dye is given in **Fig. 6.7c**. In the figure, it is worthwhile to notice that the legends containing the names of the sorbent also indicate the concentration of RhB used for the study. This gives an indication of the maximum concentration of the dye that can be taken up by the sorbent completely. It is seen that with SrM and YM the maximum concentration is 1000 ppm while with YW the maximum concentration that can be taken up is 100 ppm.

6.4.4.4 Selective sorption of RhB by $SrWO_4$

Comparing **Fig. 6.7b** and **6.7c**, it is seen that though the uptake capacity of SrW with respect to RhB is the least among all four sorbents, it is still much higher than the uptake of MB. Thus the results obtained from **Fig. 6.7a-c** indicate that strontium tungstate could be used for the selective removal of RhB from a mixture of RhB and MB. The selectivity of our sonochemically synthesized $SrWO_4$ has been demonstrated by adding 10 mg of it to a 30ppm mixture of RhB and MB dye at pH 2. **Fig. 6.7d** shows the change in the absorbance values of the dye solution with the passage of time. The sorption of RhB is complete within 4 min while the absorbance peak pertaining to MB persists. This could lead to a possible application of $SrWO_4$ in the selective removal of RhB dye in waste water treatment. Size of the sorbent material affects the sorption process since smaller sized particles have larger surface area [**308,309**]. Here, synthesize of yttrium tungstate/molybdate in the absence of sonication has been done. On reacting yttrium nitrate with sodium salts of tungstate/molybdate, an amorphous mass was obtained which on being subjected to furnace heating at 300°C/1h and 750°C/1h yielded micron sized powders of Y_2WO_6 and $Y_2Mo_3O_{12}$, respectively. The TEM micrographs of the furnace heated powders are shown in **Fig. 6.8**.

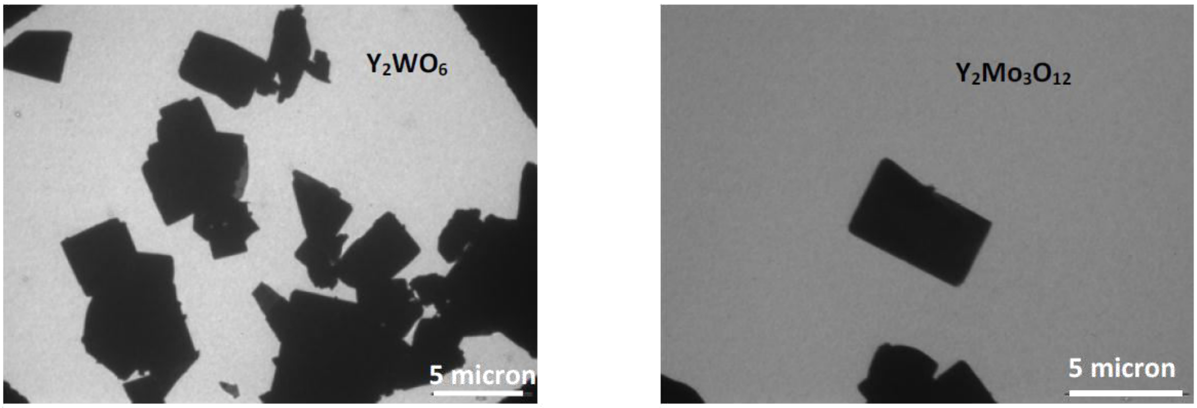

Fig. 6.8: TEM Micrograph of non-sonicated Y_2WO_6 and $Y_2Mo_3O_{12}$

Dye sorption studies of these materials were done at pH 2 with 20ppm RhB. It was seen that the 50% RhB was sorbed by 10mg Y_2WO_6 in 5h. In case of $Y_2Mo_3O_{12}$, 20% of the dye was sorbed in 5h. Hence, it can be inferred that the nanosized Y_2WO_6 and $Y_2Mo_3O_{12}$obtained from sonochemical synthesis followed by furnace heating shows much better sorption properties compared to the nonsonicated product.

6.4.5 Isotherm studies

To get an overall idea of the sorption process, the equilibrium modeling was carried out using the most fundamental models of Langmuir and Freundlich isotherms using the following equations. The main consideration of the Langmuir isotherm is sorption is monolayer and occurs at specific homogeneous sites of the sorbent **[288]**. Q_0 and b is Langmuir constants related to adsorption capacity and rate of adsorption, respectively. The Freundlich adsorption isotherm, which refers to multilayer sorption on heterogeneous surface, is based on the assumption that the adsorption sites are distributed exponentially with respect to the heat of sorption **[290]**. The equilibrium modeling for our sonochemically synthesized SrW, SrM, YW and YM samples indicated that the experimental values do not fit into the Langmuir model (results not shown). However, the sorption data fitted well to the Freundlich model and the corresponding data as well as the plots are given in **Table 6.4** and **Fig. 6.9**, respectively.

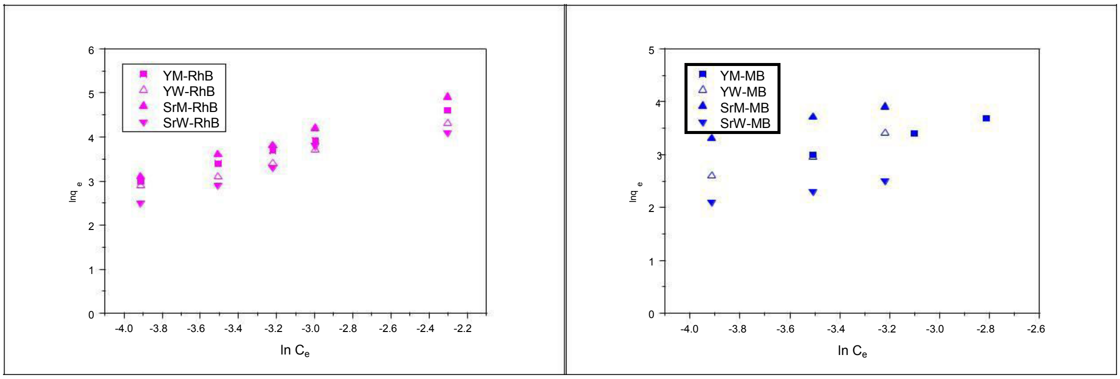

Fig. 6.9: Freundlich isotherm for (a) RhB and (b) MB sorption by $SrWO_4$, $SrMoO_4$, Y_2WO_6 and $Y_2Mo_3O_{12}$ nanosorbents

The calculated value of n for all the samples is mostly in the range of 1 – 2 suggesting that the sorption of the dyes is a favored process in almost all the systems **[288]**. Since the sorption data do not fit into the Langmuir model, it cannot be used to compute the maximum theoretical sorption capacity. Therefore the experimentally obtained values can be considered for practical applications.

Table 6.4: **Freundlich isotherm constants and correlation coefficients of $SrWO_4$, $SrMoO_4$, Y_2WO_6 and $Y_2(MoO_4)_3$ nanoparticles for RhB and MB dyes**

Sample	Dye solution	Freundlich		
		K_F	n	R^2
$SrWO_4$	RhB	770.369 ± 0.005	0.969 ± 0.001	0.986
	MB	73.699 ± 0.011	1.742 ± 0.003	0.981
$SrMoO_4$	RhB	965.069 ± 0.005	0.918 ± 0.005	0.972
	MG	812.405 ± 0.004	1.140 ± 0.001	0.983
Y_2WO_6	RhB	583.019 ± 0.012	1.100 ± 0.001	0.979
	MG	1096.633 ± 0.019	0.899 ± 0.002	0.943
$Y_2(MoO_4)_3$	RhB	998.995± 0.003	1.000 ± 0.001	1.000
	MG	665.141 ± 0.002	1.000 ± 0.001	1.000

6.4.6 Kinetic modeling

The sorption data were fitted to kinetic modeling. However, the fast kinetics of sorption exhibited by $SrMoO_4$ for both RhB and MB hinders the collection of sufficient data for kinetic modeling within the short time period (3 min). $SrWO_4$ has comparatively slower sorption kinetics and hence the sorption kinetic data for both the dyes has been analyzed using Lagergren's first order and pseudo-second order models as shown below, where k_1 and k_2 represents the first order adsorption rate constant (min^{-1}) and pseudo-second-order adsorption rate constant (g/mg/min), respectively **[310,311]**. It is to be noted that qt and qe represent the amount of dye adsorbed (mg/g) at any time t and at equilibrium time, respectively. The parameters obtained in case of $SrWO_4$ nanoparticles for RhB and MB sorption have been listed in **Table 6.5**.

Table 6.5: Pseudo-first order and Pseudo-second order kinetic models for dye sorption on $SrWO_4$ and Y_2WO_6 nano particles (10 mg sorbent, pH 2)

Sorbent	Dye	$q_{e,\,exp}$ (mg/g)	Pseudo-first order kinetic model			Pseudo-second order kinetic model		
			$q_{e,\,cal}$ (mg/g)	k_1 (min^{-1})	R^2	$q_{e,\,cal}$ (mg/g)	k_2 (g/mgmin)	R^2
$SrWO_4$	RhB	30	39	0.005	0.5244	30.3	$6x\ 10^{-3}$	0.9993
	MB	50	80.9	0.138	0.7788	56	$1.71x\ 10^{-3}$	0.9866
Y_2WO_6	RhB	100	64	0.07	0.7963	111	$8\ x\ 10^{-3}$	0.9883

The higher R^2 values indicate that the pseudo-second order kinetic model fit quite well with the experimental data and moreover the calculated and experimentally obtained qe values show a better match in this case [**312,313**]. Similarly, from kinetic modeling it could be deduced that RhB sorption on Y_2WO_6 nanoparticles follow pseudo second order kinetics, which indicates the possibility of chemisorptions as the rate limiting step [**289**].In order to understand the complex process of adsorption as well as the time dependent diffusion mechanism, the kinetic results were further analyzed by fitting them into the Weber and Morris intraparticle diffusion model as shown below **[314].**Here k_{id} (mol g^{-1} $min^{-0.5}$) is the rate constant for intraparticle diffusion and C is the intercept. The plot obtained for RhB sorption on Y_2WO_6 is shown in **Fig. 6.10a.**

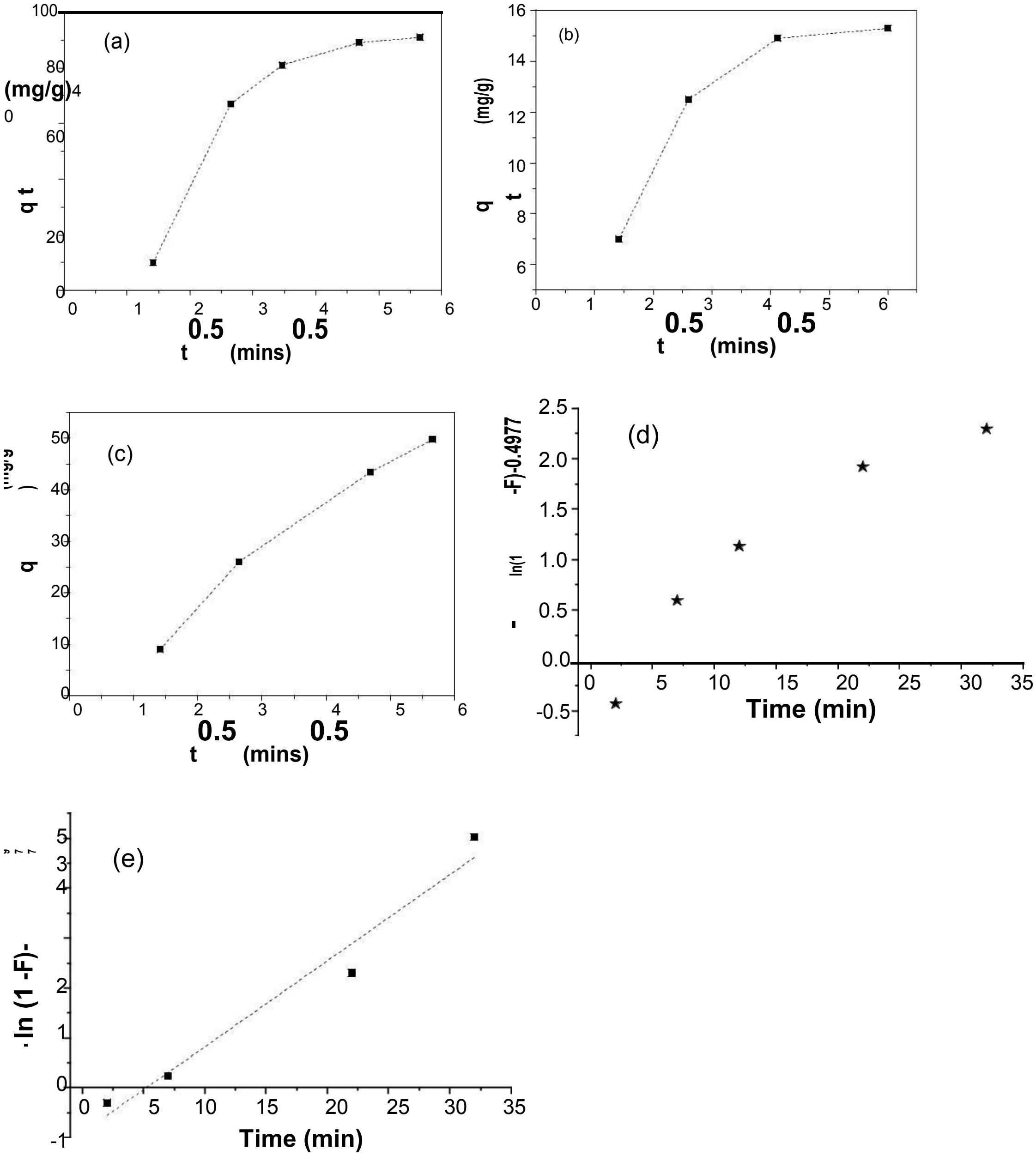

Fig. 6.10: **Webber Morris plot for (a) RhB sorption on Y_2WO_6, (b) RhB sorption on $SrWO_4$ and (c) MB sorption on $SrWO_4$. Also Boyd plot for (d) RhB sorption on Y_2WO_6 and (e) MB sorption on $SrWO_4$**

Piecewise linear regression of the data showed that the plot has three distinct regions. The first linear portion included the sorption period of 0−7 min, which represents external mass transfer and this has slope of 46 mg/g/min$^{0.5}$. The second linear portion included the sorption period of 7-22 min, representing intraparticle diffusion with a slope of 10.42mg/g/min$^{0.5}$. The third linear portion included the time period of 22 -32 min, which indicated adsorption−desorption equilibrium with a slope of 2.06 mg/g/min$^{0.5}$. As the plots do not cross the origin it is possible that both intraparticle diffusion and external mass transfer occur simultaneously. However, the ratio of the rate constants of external mass transfer to intraparticle diffusion was about 4:1. So, the overall sorption process was controlled by external mass transfer rather than intraparticle diffusion. Similarly, the Webber Morris plot obtained for RhB sorption on $SrWO_4$ also shows three distinct regions with slopes of 4.6 mg/g/min$^{0.5}$, 1.62 mg/g/min$^{0.5}$ and 0.2 mg/g/min$^{0.5}$ representing external mass transfer, intraparticle diffusion and adsorption−desorption equilibrium, respectively (**Fig. 6.10b**). In this case, also the plot indicates that both intraparticle diffusion and external mass transfer occur simultaneously. The overall sorption process was controlled by external mass transfer since the ratio of the rate constants of external mass transfer to intraparticle diffusion is about 3:1. In case of MB sorption on $SrWO_4$, the Webber Morris plot shows three distinct regions (**Fig. 6.10c**) with slopes of 13.1 mg/g/min $^{0.5}$, 8.5 mg/g/min$^{0.5}$ and 6.6 mg/g/min$^{0.5}$ and do not pass through the origin. However, the ratio of the rate constants of external mass transfer to intraparticle diffusion was about 1:1, which indicates that the overall sorption process was controlled by both external mass transfer and intraparticle diffusion. Efforts have been made to identify the slowest step in the adsorption process by using the Boyd plot.

Here F represents the fraction of solute adsorbed at any time, t (min), as calculated from $F = q_t/q_0$. The Boyd plot obtained for RhB sorption on Y_2WO_6 is shown in **Fig. 6.10d**. The Boyd plots do not pass through the origin, confirming the involvement of external mass transfer in the entire adsorption process. This result again confirmed the rate controlling mechanism of adsorption stated in Weber −Morris kinetic model study. The value of B_t calculated from slope is found to be 0.0085 min^{-1}. From the values of the r obtained from the size of the particles of Y_2WO_6, the diffusion coefficient (D_i) calculated was around 1.1x 10^{-8} $cm^2 s^{-1}$. From literature it is known that if external mass transfer of adsorbate across the liquid film to the adsorbent exterior surface is to be the rate-controlling step, the value of D_i should be in the range of $10^{-6}-10^{-8}$ $cm^2 s^{-1}$, and if intraparticle diffusion is the rate limiting step, the D_i value should be in the range of $10^{-11}-10^{-13}$ $cm^2 s^{-1}$**[315]**. In the sorption studies of RhB by Y_2WO_6, the calculated values of D_i is corresponding to that reported for the external mass transfer process which is in accordance with the Webber Morris Model (**Fig. 6.10a**).**Fig. 6.10e** shows the Boyd plot obtained for MB sorption on $SrWO_4$. The major role played by external mass transfer in the entire adsorption process is confirmed since the plot does not pass through the origin. From the graph, the value of B_t and D_i was found to be 0.1724 min^{-1} and 1.21x 10^{-9} $cm^2 s^{-1}$, respectively. Since the Di values do not fit in any of the two ranges given above, it can be inferred that in this case, both external mass transfer process and intraparticle diffusion is playing a role. This is in accordance with the Webber Morris Model as shown in **Fig. 6.10c.**

6.4.7 Insight of sorption mechanism based on sorbent structure

An idea about the sorption mechanism of RhB and MB dyes on the SrW, SrM, YW and YM nanoparticles could be deduced from the zeta potential measurements which indicates that the negative surface charge on the tungstates and molybdates acts as an attractive force for these cationic dyes. The different rates of sorption for RhB and MB exhibited by YM highlight that high surface area of the nanostructures is not playing a major role in the sorption process. From Figure 6.2a and 6.2b, more efficient sorption of both dyes is seen on SrM compared to SrW. The kinetic data modeling on SrW indicates a pseudo second order process which points towards chemisorptions. Both SrW and SrM have scheelite type tetragonal structures with [WO_4]/ [MoO_4] tetrahedral and [SrO_8] bisdisphenoids building blocks where the bonds between O-W-O/O-Mo-O and O-Sr-O atoms projects out of the unit cell **[316,317].** The greater attraction of SrM for the cationic dyes can be attributed to the lower electro negativity of Mo^{+6} compared to W^{+6} which renders higher electron density on the oxygen atom of the Mo-O bond. **Fig. 6.2a** also indicates the higher sorption affinity of YM for RhB dye compared to YW. Monoclinic YW has three non equivalent Y^{3+} lattice sites with two [YO$_8$] and one [YO$_7$] units linked via [WO$_6$] octahedral **[318]**. In case of YM, the unit cell comprises of two crystallographically independent Y^{3+} cations as well as three ortho- oxomolybdate (VI) tetrahedral [MoO$_4$]$^{2-}$ units. In the YM polyhedral, the [Y$_4$Mo$_4$O$_{12}$]$^{12+}$ units are arranged in sheets parallel to (001) and separated by the remaining [MoO$_4$]$^{2-}$ groups **[319]**. The larger incidence of [MoO$_4$]$^{2-}$ groups on the unit cell surface in case YM compared to YW, provides higher number of binding sites for the RhB dye. Analysis of the structures of RhB and MB dyes (**Fig. 6.11 (a-b)** indicates that additional binding to the YM surface is possible in case of RhB via hydrogen bond formation utilizing the –COOH group **[320]**. Hence YM shows a higher sorption affinity for RhB compared to MB dye. This has been confirmed by recording the FTIR spectra of pure YM and 100 ppm RhB adsorbed YM sample (**Fig. 6.11c**).

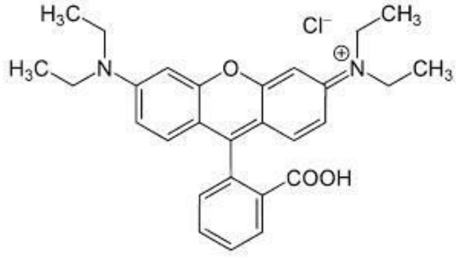

Rhodamine B

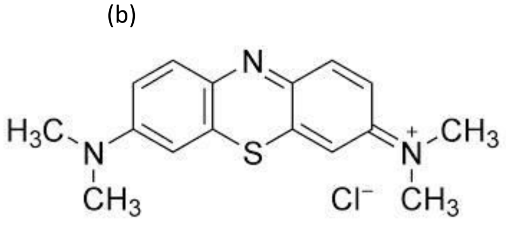

Methylene blue

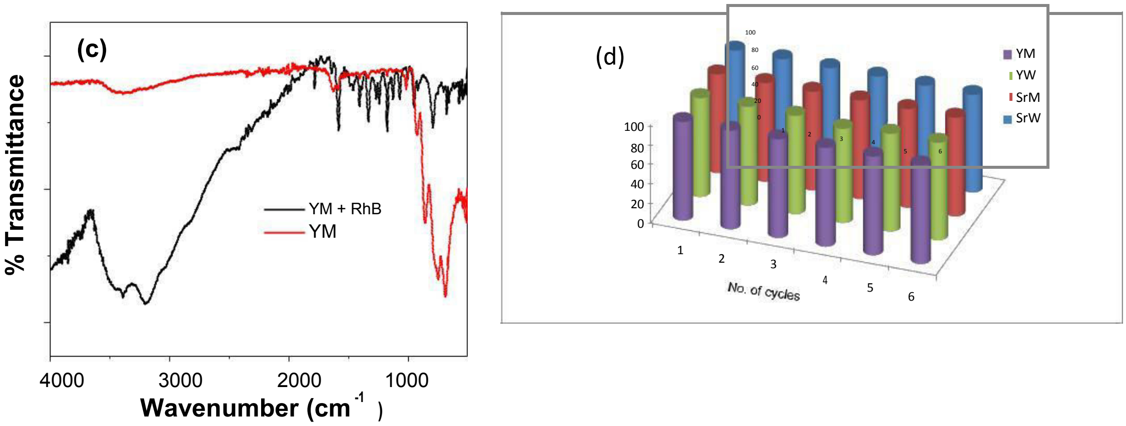

Fig. 6.11: Structure of (a) Rhodamine B, (b) Methylene blue, (c) FTIR of unloaded $Y_2Mo_3O_{12}$ and RhB loaded $Y_2Mo_3O_{12}$ and (d) regeneration efficiency of all four sorbents for 20ppm RhB sorption

The broad band between 950-600 cm^{-1} observed for pure YM can be assigned to the various Mo-O, O-Mo-O and Mo-O-Mo symmetric and asymmetric stretching vibrations present in the MoO_4 tetrahedra **[321]**. For the solid RhB dye, peaks at 1710 cm^{-1} , 3420 cm^{-1} ,1340 cm^{-1} and 1645 cm^{-1}has been assigned to C=O,O-H (adsorbed water),N-aryl and C N stretching, respectively **[322].** In case of present case RhB adsorbed YM sample, the C=O stretching appears as a broad peak centered at 1705 cm^{-1} and is very much weakened compared to that of the benzene ring at 1589 cm^{-1}, indicating the involvement of the C=O group in hydrogen bond formation during the sorption process **[323,324]**. From the tabulated values(**Table 6.2**), it can be inferred that the strontium/yttrium tungstates/molybdates exhibit much faster kinetics compared to CAC with lower amount of sorbent and mostly higher optimum concentration of dyes. The best results have been obtained for the sorption of MB/RhB by $SrMoO_4$ and RhB by $Y_2Mo_3O_{12}$ samples.

6.4.8 Regeneration of sorbents

For practical applicability of the sorbents, it is essential to check their multicyclic sorption properties. The thermal regeneration studies on our sonochemically synthesized SrW, SrM, YW and YM nanoparticles have been carried by heating the freeze-dried dye sorbed nanoparticles in a tubular furnace flushed with air. Complete removal of the dye was observed by heating the samples at 250°C for 15min. The heat treated sorbents were further used for sorption studies using 20ppm RhB solution. The process was repeated for six cycles and the results are shown in **Fig. 6.11d**. The efficiency of sorption remains almost unaffected after six cycles for all the four sorbents indicating their stability. Hence though the sorption process points towards chemisorptions, it can be inferred that the bonds formed are not very strong since regeneration of the sorbents is possible by mild heat treatment.

6.5. Conclusions

A facile route to synthesize tungstates and molybdates of strontium/yttrium has been established. The morphology of the samples has been analyzed using TEM and formation of nanospindles and nano spherical particles were seen in case of strontium and yttrium tungstates/molybdates, respectively. The highest surface area of 77.2(±1.5) m^2g^{-1} was obtained in case of $Y_2Mo_3O_{12}$ nanoparticles. The negative surface charge on the nanoparticles at pH 2-3 could be confirmed from zeta potential measurements. The sorption behavior of all the four samples for cationic dyes (RhB and MB) has been studied and it was observed that $Y_2Mo_3O_{12}$ and $SrMoO_4$ showed highest sorption capacity for RhB dye. In case of $Y_2Mo_3O_{12}$, the higher affinity for RhB uptake compared to MB in acidic pH has been attributed to additional binding of RhB to the nanoparticle surface via hydrogen bond formation. Though the tungstates have relatively less sorption capacity compared to molybdates, Y_2WO_6 exhibits better affinity for both dyes compared to $SrWO_4$. The preferential sorption of RhB compared to MB exhibited by $SrWO_4$ has been exploited and its selective sorption of RhB from a 30ppm mixture of RhB and MB dye has been demonstrated. The sorbents could be regenerated by heat treatment at 250°C for 15min and reused with no loss in sorption efficiency for six cycles. The molybdates of strontium and yttrium also exhibit good sorption of Cu(II) ions at acidic pH of 3. $Y_2Mo_3O_{12}$ shows the highest uptake with 98% removal of 100ppm Cu(II) ions within 150 min. Both $Y_2Mo_3O_{12}$ and Y_2WO_6 shows good uptake of ^{137}Cs at acidic pH indicating that the surface charge plays a crucial role in the sorption process. From the above observations, it can be concluded that among the four samples, sonochemically synthesized $Y_2Mo_3O_{12}$ nanoparticles exhibits superior sorption characteristics for uptake of dyes, heavy metal ions like Cu(II) and radioactive ^{137}Cs.

Chapter 7

Summary and future scope

In this dissertation work, synthesis, characterization of several nanomaterials and subsequent uptake studies for radionuclide specifically U(VI),Cs(I),Sr(II) and heavy metal ions such as Cr(VI)), Cu(II), Ni(II), Zn(II), Co(II), Fe(II) etc. have been performed by using batch sorption method. In the beginning the introduction chapter gives brief description regarding nanomaterial's application as sorbent and earlier workers experimental finding with advantage and disadvantages as a part of literature survey. Physical and chemical properties of Radionuclide and heavy metal ions special mention to U(VI), Cs(I), Sr(II) and Cr(VI), Cu(II) have been given. Their impact on human and environment has also been discussed in detail.

Various synthesis method for preparing nanomaterials and their property evaluation for characterization using different techniques has been elaborated in chapter 2. Suitable convenient bottom-up methods such as combustion, co-precipitation, and sonochemical method were employed for synthesis of various nanomaterials in the present study. However, other method of synthesis can also be used for a better size tuning properties. The powder form can be further modified to an extent so that it can be used in column experiment under dynamic conditions with a varied range of pH.

The next four chapters give an account of uptake studies using these synthesized nanomaterials as potential sorbents for radionuclide and heavy metal ions uptake. Uranium(VI), radioactive cesium(I) and strontium(II), hexavalent chromium and copper(II) removal from synthetic low level liquid waste were carried by a series of nanomaterials such as manganese dioxide, nano molybdate and tungstate of strontium and yttrium, bare magnetite, oleic acid coated magnetite, and silica coated magnetite**. The major findings and conclusions from this work are summarized as follows:**

(i) Nano crystalline manganese oxide was prepared by the hydrolysis of $KMnO_4$ and it was found to have a size of 8 nm and surface area of 145 m^2g^{-1}. Due to the high surface area, the sorption property of the nano manganese oxide was found to be excellent. It was found that the sorption was achieved at different pH values and with varying time of equilibration. Thus it is seen that the kinetics was an important aspect for the possible separation of metal ions. However, it was seen that the interferences was severe when metal ions were in low trace levels. Thus nano manganese oxide was found to be a good room temperature sorbent. The present study showed that the kinetics of sorption are different and hence there is a possibility of removing the transition metal ions from a solution mixture containing these along with uranium, thus leaving behind a nearly pure uranyl ion solution. Thus the favored sorption properties of the nano manganese oxide with respect to the transition metal ions can be used for the purification of mixture of ions. It is to be noted that the manganese oxide used in the present study has been used as such without any modification. The maximum capacity obtained in the present study is comparable to mesoporous silica sorbents but is less compared to polyacrylic ester resins. However, the main aspect of these results showed that there is a possibility of using the nano manganese oxide as room temperature sorbent for separation.

(ii) Nano magnetite and nano magnetite-haematite composite samples have been prepared for cesium(I) and strontium(II) uptake studies. Low concentration of up to 100 ppm of cesium and strontium solution and 0.1 g of nano-composite material for a maximum contact time of 1 h ensures nearly 100 percent removal of cesium and strontium. In order to prevent nano-aggregate and to minimize iron leaching in the filtrate, coating was done on magnetic samples by a long chain fatty acid like oleic acid and silica. The magnetic property study shows the presence of super-paramagnetism in these samples which is very effective in environmental concern as because the separation of material is very quick through an external magnet. The point of zero charge for nano magnetite was at pH 7.2 and for the nano-composite magnetite-haematite was at pH 2.7 and at pH 6.9, attributed to biphasic nature of this sample. This biphasic condition helps the sorption efficiency in the alkaline condition. It appears that RP, Sips model and Freundlich isotherm models dominate, for all the error function selection methods. The comparison table shows that for cesium sorption onto magnetite is better explained by RP models than Freundlich model which was best fit by linear regression method. For oleic acid coated magnetite, RP and Sips model dominate the better suitability, whereas DR model has been best fit by linear regression. This change is also seen in silica coated magnetite case, where both RP and Freundlich models were favored than the other model. Thus linear regression and the non-linear regression analytical results give two different models as the best-fitting isotherm for the given set of data. This indicates a surprising difference between the analytical methods. For the simplicity of linear regression sometimes chemical analysis leads to inaccurate results which are not good for design and development of sorption system.

(iii) The potential of as prepared nano manganese oxide has also been established for uptake of Cs(I),Sr(II) and Cr(VI) ions from simulated waste water. The sorption isotherm mainly follows Langmuir isotherm and the kinetics follows pseudo second order model for all the metal ion sorption. Intraparticle diffusion model may have a role in Sr(II) sorption also. Although the temperature effect has not been studied but it can be inferred from isotherm studies that the sorption may occurs via chemisorptions. In a very low metal ion concentration this nano MnO_2 can be used for effective removal of specific contaminants like Cs(I),Sr(II) from Low level environmental radioactive solutions and Cr (VI) solution from industrial effluent.

(iv) A facile route to synthesize tungstates and molybdates of strontium/yttrium has been established. The morphology of the samples has been analyzed using TEM and formation of nano spindles and nano spherical particles were seen in case of strontium and yttrium tungstates/molybdates, respectively. The highest surface area of $77.2 m^2 g^{-1}$ was obtained in case of $Y_2Mo_3O_{12}$ nanoparticles. The negative surface charge on the nanoparticles at pH 2-3 could be confirmed from zeta potential measurements. The molybdates of strontium and yttrium exhibit good sorption of Cu (II) ions at acidic pH of 3. $Y_2Mo_3O_{12}$ shows the highest uptake with 98% removal of 100ppm Cu (II) ions within 150 min. Both $Y_2Mo_3O_{12}$ and Y_2WO_6shows good uptake of ^{137}Cs at acidic pH indicating that the surface charge plays a crucial role in the sorption process. The sorption behavior of all the four samples has been extended for cationic dyes (RhB and MB) and it was observed that $Y_2Mo_3O_{12}$ and $SrMoO_4$ showed highest sorption capacity for RhB dye. In case of $Y_2Mo_3O_{12}$, the higher affinity for RhB uptake compared to MB in acidic pH has been attributed to additional binding of RhB to the nanoparticle surface via hydrogen bond formation. Though the tungstates have relatively less sorption capacity compared to molybdates, Y_2WO_6 exhibits better affinity for both dyes compared to $SrWO_4$. The preferential sorption of RhB compared to MB exhibited by $SrWO_4$ has been exploited and its selective sorption of RhB from a 30ppm mixture of RhB and MB dye has been demonstrated. The sorbents could be regenerated by heat treatment at 250°C for 15min and reused with no loss in sorption efficiency for six cycles. From the above observations, it can be concluded that among the four samples, sonochemically synthesized $Y_2Mo_3O_{12}$ nanoparticles exhibits superior sorption characteristics for uptake of dyes, heavy metal ions like Cu (II) and radioactive ^{137}Cs.

In future these nano materials such as nano MnO_2, bare magnetite, coated magnetites can be a potential candidate to be used as a deep geological repository material for U(VI),Cs(I) and Sr(II) ions retention. The potential for these materials of an engineering scale needs to be evaluated. Their beads with suitable polymers need to be prepared and evaluated for column experiments under dynamic conditions.

References

1. Book entitled as “Introduction to Water Resources and Environmental Issues ’’ 1st Edition, Pennington & Cech (2010)
2. Igor A. Shiklomanov, USGS Report on How much water is there on, in, and above the Earth? (2013)
3. United Nations Educational, Scientific and Cultural Organization (UNESCO) Report, (2013)
4. Thesis of Ryan Yin Wai Liu, Types of Water Sources, Department of Civil and Environmental Engineering Imperial College London, London (2013)
5. Roy and S. Pal, Current Opinion in Environmental Sustainability 1 (2009) 192
6. Document on Groundwater quality series: GWQS/ 09/2006-2007 CPCB
7. World Health Organization, Guidelines for drinking-water quality (2006)
8. World Nuclear Association (WANO) Report (March 2017)
9. Y. Park, Y-C. Lee, W. S. Shin, S-J. Choi, Chem. Eng. J.162 (2010) 685
10. Ritu Ambasta, Mika E Sillanpaa, J. of Environ. Radioactivity 105(2012) 76
11. G. Zakrzewska-Trznadel, Nukleonika 51(2006)101
12. International Atomic Energy Agency TECDOC-1086 (1999)
13. International Atomic Energy Agency TECDOC-1336 (2003)
14. International Atomic Energy Agency TECDOC-1492 (2006)
15. http://www.world-nuclear.org/information-library/nuclear-fuel-cycle/nuclear-wastes/radioactive-waste-management.asp
16. International Atomic Energy Agency Technical Report Series No 101 (1970)

17. T.P.Valsala, M.S. Sonavane, S.G. Kore, N.L. Sonar, Vaishali De, Y. Raghavendra, S.Chattopadhyaya, U. Dani, Y. Kulkarni, R.D.Changrani, J. Hazard. Mater.196(2011) 22

18. International Atomic Energy Agency Safety Series 111-F (1995)

19. A. Ahmadpoura, M. Zabihia, M. Tahmasbib, T. Rohani Bastami, J. Hazard. Mater.182 (2010) 552

20. http://cfpub.epa.gov/ncer_abstracts/index.cfm/fuseaction.display.abstractDetail/abstract/5775.report/F

21. Limson Zamora, M.Tracy, B. L. Zielinski, J.M. Meyerhof, D.P. Moss, Toxicol. Sci. 43 (1998) 68

22. J. I. Rodriguez Silva, A. C. De Melo Ferreira, A. C. A. Da Costa, J. Radioanal. Nucl. Chem 27 (2009) 909

23. Document of World Health Organization on “Uranium in Drinking Water” (2004)

24. Document of US EPA on “Basic Information about Radionuclides in Drinking Water” (September 17, 2013)

25. T. S. Anirudhan, C. D. Bringle, S. Rijith, Environ. Radioact. 101(2010) 267

26. A. Abdelouas, W. Lutze, H.E. Nuttall, Reviews in Mineralogy 38 (1999) 433

27. N.N. Greenwood, A. Earnshaw, Chemistry of the Elements. London: Pergamon Press (1984) 1542

28. Ajay Kumar,R. K. Singhal,Sabyasachi Rout,Usha Narayanan,Rupali Karpe,P. M. Ravi,J.Radioanal. Nucl. Chem. 295(2013) 649

29. K. Müller, V. Brendler and H. Foerstendorf, Inorg. Chem. 47 (2008) 10127

30. L. Zavodska, E. Kosorinova, L. Scerbakova, Lesny, Hungarian Electronic Journal of Sciences (2008)1

31. P. C. Burns, R. Finch, Reviews in Mineralogy 38, Washington: Mineralogical Society of America, (1999) i-xvi + 679 pages. ISBN 0-939950-50-2; ISBN13 78-0-939950-50-8

32. Documents of World nuclear organization (WANO) on Three Mile Island Accidents(March 2001)

33. A. V. Yablokov, V. B. Nesterenko, A. V. Nesterenko, J. D. Book on Chernobyl: Consequences of the Catastrophe for People and the Environment edited by herman-Novinger, Ann. NY Acad. Sci., Published by Wiley-Blackwell 181 (2009)

34. Durga Parajuli, Hisashi Tanaka, Yukiya Hakuta, Kimitaka Minami, Shigeharu Fukuda, Kuniyoshi Umeoka, Ryuichi Kamimura, Yukie Hayashi, Masatoshi Ouchi, and Tohru Kawamoto, Environ.Sci.technol. 47 (2013) 3800

35. Mc. Geoghegan, D.Whaley, S. Binks, K. Gillies, M.Thompson, K. McElvenny, J.Radiological Protection. 30 (2010) 407

36. S. Staunton, C. Dumat and Z. Solnay, J. Environ. Radioact. 58 (2002)163

37. Md.Rabiul Awual, Tsuyoshi Yaita, Yuji Miyazaki, Daiju Matsumura, Shiwaku &Tomitsugu Taguchi, Sci Rep 6 (2016) 19937

38. Document of EPA on “A Regulators’ Guide to the Management of Radioactive Residuals from Drinking Water Treatment Technologies” (July 2005)

39. Charu Dwivedi, PhD Thesis, HBNI, Mumbai, (August 2012)

40. B. J. Howard, N. A. Beresford and K. Hove, Health Physics 61 (1991) 715

41. W. L. Robison and E. L. Stone, Health Physics 62(1992) 496

42. K. Stark and H. B. L. Patterson, Radiation and Environmental Biophysics 47 (2008) 481

43. S. C. Jang , S.B. Hong , H.M. Yang , K.W. Lee , J.K. Moon , B.K. Seo , Y.S. Huh , C. Roh , Nano Materials 4 (2014) 894

44. B. Rosoff, S.H. Cohn, H. Spencer, Radiat Res 19 (1963) 643

45. M. R. Awual, S. Suzuki, T. Taguchi, H. Shiwaka, Yokamoto, T. Yaita, Chem Eng .J. 242 (2014) 127

46. Book on "Tables of isotopes" written by C M Lederer and V S Shirley, 7th Edition, Wiley-Interscience, New York (1978)

47. Document of USEPA on radionuclide Sr^{90} (April 2017)

48. E. Wieland, J. Tits, D. Kunz, R. Dahn, Environ. Sci. Technol. 42 (2008) 403

49. Drinking water and health, Volume 4, Safe Drinking Water Committee; Board on Toxicology and Environmental Health Hazards; National Research Council, ISBN: 0-309-55424-1(1982)

50. E. A. Martell, Science 129 (1959) 1197

51. Document of Agency for Toxic Substances and Disease Registry (ATSDR) on Toxicological profile for Strontium. Atlanta, GA: U.S. Department of Health and Human Services, Public Health Service (2004)

52. R. Yavari, D. Huang, A Mostofizadeh, J. Radioanal. Nucl. Chem. 285 (2010) 703

53. R.Yavari, D. Y. Huang, S. J. Ahmadi, G. Bagheri, J. Radioanal. Nucl. Chem. 286 (2010) 223

54. H. Nishioka, Y. Kato, Y. Nishiwaki, J. Radiat. Res. 3 (1962) 170

55. Wang Min, Ling. Zu, Peng Jing, Zhai Mao-lin, Li Jiu – qiang, Wei Gen-shuan J. Hazard. Mater. 171 (2009) 820

56. Lalhmunsiama, Diwakar Tiwari, Seung-MokLee, J. Environ. Radioact. 147 (2015) 76

57. J. Pan, X. Zou, Y. Yan, X. Wang, W. Guan, J .Han, X. Wu, Appl. Clay Sci. 50 (2010) 260

58. Q. Dai, W. Zhang, F. Dong, Z. Yulian, X. Wu, Chem. Eng. J. 249 (2014) 226

59. S. H. Wallace, S. Shaw, K. Morris, J. S. Small, A. J. Fuller, I.T. Burke, Appl. Geochem, 27 (2012) 1482

60. C. F. V. Mason, N. Lu and J. Conca, Characterization, Transport and Remedial Options for Radioactive Strontium and Cesium Contaminated Sites, Los Alamos National Laboratory, Los Alamos, New Mexico 87545, U.S.A (2000)

61. F. A. Cotton, and G. Wilkinson (Eds).Advanced Inorganic Chemistry: A Comprehensive Text, John Wiley & Sons, New York, USA (1980)

62. S. G. Hibbins, J. I. In Kroschwitz, M. Howe-Grant, Kirk-Othmer. Book on Strontium and Strontium Compounds. Encyclopedia of Chemical Technology, Volume 22. John Wiley & Sons, New York, USA. (1997) 947

63. A. Zhang, C. Chen, E. Kuraoka, M. Kumagai, Sep.Purif. Technol. 62, (2008) 407

64. H. J. Wang, A. L. Wang, F. Zhou, H. Peng, J. Yu Yang, J. Colloid Interface Sci. 316 (2007) 277

65. P G &E Hinkley, Chromium Cleanup California Environmental Protection Agency (9/10/08)

66. Schwartz, Naoki The Boston Globe (Dec 13, 2010)

67. M. A. Hashim, Soumyadeep Mukhopadhyay, Jaya Narayan Sahu and Bhaskar Sengupta, J. Environ. Manage. 92 (2011) 2355

68. N. K. Srivastava, C. B. Majumder, J. Hazard. Mater. 151(2008) 1

69. M. Jamil, M. S. Zia, M. Qasim, J. Chem. Soc. Pak. 32 (2010) 370

70. S. Khan, Q. Cao, Y.M. Zheng, Y.Z. Huang, Y.G. Zhu, China, Environ. Pollut. 152 (2008) 686

71. A. Singh, R. K. Sharma, M. Agrawal, F. M. Marshall, Food Chem. Toxicol. 48 (2010) 611

72. Khezami and Capart, J. Hazard. Mater. 123 (2005) 223

73. D. W. O'Connell, C. Birkinshaw, T. F. O'Dwyer, Bioresour. Technol. 99 (2008) 6709

74. T. A. Kurniawan, G. Y. S. Chan, W. H. Lo, S. Babel, Chem. Eng. J. 118 (2006) 83

75. N. Galil, M. Rebhun, Water Sci. Technol. 22 (1990) 203

76. B. J. Pan, B. C. Pan, W. M. Zhang, L. Lv, Q. X. Zhang, S. R. Zheng, Chem. Eng. J. 151 (2009) 19

77. S.P. Mishra, V.K. Singh, D. Tiwari, Appl. Radiat. Isot. 47 (1996) 15

78. M.D. La Grega, P.L. Buckingham, and J.C. Evans, Hazardous Waste Management, 79 (1994) 641

79. US-EPA-Basic-Information-about-Copper-in-Drinking-Water (April 2017)

80. Environmental and Ecological chemistry, Vol. III Remediation of Groundwater Contaminated with Radioactive Compounds - K. Thomas Klasson and Paul A. Taylor (2010)

81. N. Madane, G. Nikam, K. Mahanwar, and B. Mohite, J. Radioanal. Nucl. Chem. 288 (2011) 285

82. Jyothi Kumar, Joon-Soo Kim, Jin-Young Lee, and Ho-Sung Yoon, J. Radioanal. Nucl. Chem. 285 (2010) 301

83. Sevda Ayata and Melek Merdivan, J. Radioanal. Nucl. Chem.283 (2010)603

84. Xiao lei Qu, Pedro J. J. Alvarez, Qulin Li, Water Research 47 (2013) 3931

85. Book entitled as Nanomaterials – B. Viswanathan, Published by Narosa Publishing House ISBN: 978-81-7319-936-3 (2014)

86. The world of oxide nano materials (Book), Synthesis, properties and application of oxide nano materials, Edited by Jose A Rodriquez and Marcos Fernandez-Garcia, Copyright © 2007 John Wiley & Sons, Inc (2007)

87. M. Fernandez-Garcia, A. Martinez Arias, J. C. Hanson, Rodriguez, J. Amer. Chem. Soc.104 (2004) 4063

88. W. J. Weber , R. C. Ewing , C. R. A. Catlow , T. Diaz de la Rubia , J.Mater.Res.13 (19C8) 1434

89. W. L. Gong, W. Lutze, R.C. Ewing, J. Nucl.Mater.277 (2000) 239

90. W. Adelhelm Lutze, R C Ewing, Book entitled as In radioactive waste forms for the future; Eds, Elsevier NY (1988) 393

91. Maryline CheeKimling, Nicholas Scales, L Tracey. Hanley, and A. Rachel Caruso, Environ. Sci. Technol. 46 (2012) 7913

92. Simona Regenspurg, Dieter Schild, Thorsten Schäfer, Florian Huber, Maria E. 9Malmström, Appl. Geochemistry 24 (2009) 1617

93. Susan Sadeghia, Hoda Azhdaria, Hadi Arabib, Ali Zeraatkar Moghaddama, J. Radiation Hazards, 215-216 (2012) 208

94. T. A. Todd, T. A. Batcheller, J. D. Law, R. S. Herbst, Cesium and Strontium Separation Technologies Literature Review, INEEL/EXT-04-01895

95. J. Rydberg, G.R. Choppin, C. Musikas, T. Sekine, Book on Solvent extraction equilibria, Solvent Extraction Principles and Practice, Marcel Dekker, Inc. New York (2004)

96. J. Van R. Smit et al, Indust. & Eng. Chem. 5 (1966)117

97. E. H. Borai, R. Harjula, L. Malinen and Paajanen, J. Hazard. Mater. 172 (2009) 416

98. J. L. Collins, K. K. Anderson, Development of Spheroid Inorganic Sorbents for Treatment of Acidic Salt-Bearing Liquid Waste, ORNL/TM-2000/367 (2000)

99. R. D. Ambashta, P. K. Wattal, S. Singh, D. Bahadur, J Magnetism Magnetic Materials 267(2003) 335

100. I. J. Singh, M Ramaswamy, BARC Report No. BARC/1991/E/022

101. Diana Cuc, Sabine Bouguet-Bonnet, Nicole Morel-Desrosiers, Jean-Pierre Morel, Pierre Mutzenhardt and Daniel Canet, J. Phys. Chem. B 113 (2009) 10800

102. J. F. Dozol et al Application of Crown-Ethers to Caesium and Strontium Removal from Marcoule Reprocessing Concentrate, (Book chapter) New Separation Chemistry Techniques for Radioactive Waste and Other Specific Applications , 173

103. Yan Wu, Yuezhou Wei, Energy Procedia, 39 (2013) 319

104. S. Shylesh, V. Schunemann, WR.Thiel, Angew. Chem. Int .Ed. 49 (2010) 3428

105. Slavica Stankic, Sneha Suman, Francia Haque, and Jasmina Vidic, J Nanobiotechnology, 14 (2016) 73

106. Sung-Chan Jang et al, Nano Materials 4 (2014) 894

107. R. R. Sheha, E. Metwally, J. Hazard. Mater. 143 (2007) 354

108. Y. Namiki, T. Namiki , Y. Ishii , S. Koido , Y. Nagase , A.. Tsubota , N Tada , Y. Kitamoto, Pharm. Res., 29 (2012) 1404

109. Yoshihisa Namiki, Toshihiko Ueyama, Takayuki Yoshida, Ryoei Watanabe, Shigeo Koido and Tamami Namiki ,Scientific Reports, 6 (2016) 19937

110. Dai Daizo Yamaguchi, Kazumi Furukawa, Masaya Takasugaand Koki Watanabe Scientific Reports, 4 (2014) 6053

111. R. O. Abdel Rahman, H. A. Ibrahim and Yung-Tse Hung, Water 3 (2011) 551

112. H. D. Liu, F. Z. Li, X. Zhao, Chin. J. Inorg. Chem. 24 (2008) 1657
113. International Atomic Energy Agency, Handling and Processing of Radioactive Waste from Nuclear Applications; TRS No. 402, Vienna, Austria (2001)
114. An Yu Zhang, Takaya Akashi, Bo Ping Zhang and Takashi Goto, Materials Letters 60 (2006) 2834
115. S. P. Mishra, D. Tiwary, Appl Radiat Isot.51 (1999) 315
116. Y.Cho, S.Komarneni, Appl Clay Sci.44 (2009) 15
117. S. Rao, Biplob Paul, K. Lal, S. V. Narasimhan, Jaleel Ahmed, J. Radioanal and Nucl. Chem 246 (2000) 413
118. N. Rawat, P. K. Mohapatra, D. S. Laxmi, A. Bhattacharya, V. K. Manchanda, J. Membr. Sci. 275 (2006) 82
119. D. R. Raut, P. K. Mohapatra, V. K. Manchanda, J. Membr. Sci. 390-391 (2012) 76
120. Z. V. P. Murthy, Snehal Parmar, Desalination 282 (2011) 63
121. V. Nora and C.-K. Kim, Appl. Radiat. Isot. 68 (2010) 2306
122. Dmitry V. Marinin, Garrett N. Brown, Waste Management 20 (2000) 545553
123. S. Chegrouche, A. Mellah, M. Barkat, Desalination 235 (2009) 306
124. C. Chen, J. Hu, D. Shao, J. Li, X. Wang, J. Hazard. Mater.164 (2009) 923
125. M. J. Manos, N. Ding and M.G. Kanatzidis, Proc. National Acad. Sci. 105 (2008) 3696
126. Z. Cheng, Z. Gao , W. Ma , Q. Sun , B. Wang , X. Wang, Chem. Eng. J. 209 (2012) 451
127. Chen Yuwei, Wang Jianlong ,Nuclear Engineering and Design 242 (2012) 445
128. F. L. Fu, Q. Wang, J. Environ. Manage. 92 (2011) 407
129. Y. H. Wang, S. H. Lin, R. S. Juang, J. Hazard. Mater. 102 (2003) 291
130. T. A. Kurniawan, G. Y. S. Chan, W.H.Lo, S. Babel, Chem. Eng. J. 118 (2006) 83

131. P. Chandra Mouli, S. Venkata Mohan and S. Jayarama Reddy, J. Scientific and Industrial research 63 (2004) 11
132. J. A. Coston, C. C. Fuller, J. A. Davis, Geochim. Cosmochim. Acta 59 (1995) 3535
133. P. Liang, T. Q. Shi, J. Li, Int. J. Environ. Anal. Chem. 84 (2004) 315
134. A. Agrawal and K. K. Sahu, J. Hazard. Mater. 137 (2006) 915
135. N.C. Strandwitz, G.D. Stucky, Chem. Mater. 21 (2009) 45
136. J.E.Vanbenschoten, B.E. Reed, M.R. Matsumoto, P. J. Mc Garvey, Water Environ. Res. 66 (1994) 168
137. K. M Joshi, V. S Shrivastava., Appl. Nanosci. 1 (2011) 147
138. H. I Adegoke, F. A Adekola, Colloid Journal 74 (2012) 420
139. S. Recillas, J. Colon, E. Casals, E. Gonzalez, V. Puntes, A. Sanchez, X. Font, J. Hazard. Mater. 184 (2010) 425
140. C.Y. Cao, Z.M. Cui, C.Q. Chen, W.G. Song, W. Cai, J. Phys. Chem. C 114 (2010) 9865
141. S. Mallick, S. S. Dash, J. Colloid Interface Science 297(2006) 419
142. K Gupta, S Bhattacharya, D Chattopadhyay, A .Mukhopadhyay and Biswas, Chem. Eng. J. 172(2011) 219
143. G. R. Calle, I. T. Vargas, M. A. Alsina, P. A. Pastén, and G. E. Pizarro, Env. Sci. Tech. 41 (2007) 7430
144. A. R. West, Solid State Chemistry and its Applications, John Wiley & Sons, New York (1984)
145. A. K. Tyagi, Bull. Soc. Mater. Chem. 2 (2011) 1
146. Jayshree Ramkumar, R Shukla, S Chandramouleeswaran, T Mukherjee, A.K. Tyagi, Nanosci. Nanotechnol. Lett. 4 (2012) 15

147. Sophie Laurent, Delphine Forge, Marc Port, Alain Roch, Caroline Robic, Luce Vander Elst and Robert N. Muller, Chem. Rev.108(2008)2064

148. Werner Stober, Arthur Finka and D Ernst Bohn, J. Colloid Interface Sci. 26(1968) 62

149. Yong-Hui Deng, Chang-Chun Wang, Jian-Hua Hu, Wu-Li Yang, Shou-Kuan Fu, A: Physicochem. Eng. Aspects 262 (2005) 87

150. H Xu, BW Zeiger and K .S Suslick, Chem. Soc. Rev. 42(2013)2555

151. K. S. Suslick, S.-B. Choe, A.A. Cichowlas, M.W. Grinstaff, Nature 353(1991) 414

152. Alireza Aslani, Alireza Bazmandegan-Shamili, Karim Kaviani, Physica B 405 (2010) 3972

153. B. Fultz, J. Howe, Transmission Electron Microscopy and Diffractometry of Materials, Graduate Texts in Physics, © Springer-Verlag Berlin Heidelberg (2013)

154. H. P. Klug and L. E. Alexander, X-ray Diffraction Procedures, Wiley-Interscience Publication, New York (1974)

155. www.icdd.com (The International Centre for Diffraction Data)

156. B. D. Cullity, Elements of X-ray Diffraction, Addison-Wilson Publishing Comp. Inc. USA (1959)

157. A. Guinier and G. Fournier, “Small-Angle Scattering of X-Rays,” Wiley, New York (1955)

158. Thesis of Jerina M Majeed, Nanostructures for bio-application and toxic species remediation, HBNI, Mumbai (2016)

159. R Leo, William, Book on Techniques for Nuclear and Particle Physics Experiments A How-to Approach. Springer-Verlag Berlin Heidelberg (1994)

160. D. Beaty Richard and Jack D. Kerber, Concepts, Instrumentation and Techniques in Atomic Absorption Spectrophotometry, Second Edition The perkin- Elmer Corporation (1993)

161. I. Langmuir J. Am. Chem. Soc 40(1918) 1361

162. H. M. F. Freundlich J. Phys. Chem 57(1906) 385

163. M. I. Tempkin, Pyzhev, Acta Physico-Chimica Sinica USSR 12 (1940) 327

164. M. M. Dubinin, Chem. Rev. 60(1960) 235

165. O. Redlich, D. L. Peterson, J. Phys. Chem. 63 (1959) 1024

166. R. J. Sips, Chem. Phys. 16 (1948) 490

167. S. Lagergren, Kungliga Svenska Vetenskapsakademiens Handlingar 24 (1898)

168. Y. S. Ho and G. McKay, Proc. Safety Environ. Protect. 76 (1998) 183

169. C. Aharoni and F.C. Tempkins Kinetics of adsorption and desorption and the Elovich equation D.D. Eley, H. Pines, P.B. Weisz (Eds.), Advances in Catalysis and Related Subjects, 21, Academic Press, New York (1970) 1

170. G. E. Boyd, A. W. Adamson and L. S. Myers Jr, J. Am. Chem. Soc. 69 (1947) 2836

171. K. Y. Foo, B H. Hameed, Chem. Eng. J. 156 (2010) 2

172. K. V. Kumar. J. Hazard. Mater. B137 (2006) 197

173. K. Bhagyashree, R. K. Mishra, R. Shukla, S. Kasar, A. Kar, S. Kumar, C.P.Kaushik, A. K. Tyagi, B. S.Tomar, J. Radioanal. Nucl. Chem. 295 (2013) 1561

174. C. Ozeroglu, N. Metin, J. Radioanal. Nucl. Chem. 292 (2012) 923

175. D. L. Zhao, S. B. Yang, S. H. Chen, Z. Q. Guo, X .Yang J. Radioanal. Nucl. Chem. 287 (2011) 557

176. N. Kamei-Ishikawa, K. Tagami, S .Uchida, J. Radioanal. Nucl. Chem. 274 (2007) 5551

177. S. L. G. Petroni, M. A. F. Pires, C. S. Munita, J. Radioanal. Nucl. Chem. 259 (2004) 239

178. M. Sadeghi, P. Sarabadani, H. Karami, J. Radioanal. Nucl. Chem. 283(2010) 297

179. M. Sadeghi, H. Karami, P. Sarabadani, F. Bolourinovin, J. Radioanal. Nucl. Chem. 281 (2009) 619

180. P. C. R. Varma, R.S. Manna, D. Banerjee, M. R. Varma, K.G. Suresh, A. K. Nigam, J. Alloys. Compd. 453 (2008) 298

181. W. Dong, S. Wu, D. Chen, X. Jiang, C. Zhu, Chem. Lett. 5 (2000) 496

182. C. Baratto, P.P. Lottici, D. Bersani, G. Antonioli, G .Gnappi, A Montenero ,J. Sol–Gel Sci. Technol. 13 (1998) 667

183. C. Albertina, P. Martyn, J. Mater. Sci, 11 (2001) 1408

184. S. Grimm, M. Schultz, S. Barth, R. Muller, J. Mater. Sci. 32 (1997) 1083

185. O. Fukumasa, T. Fujiwara, Thin Solid Films, 435 (2003) 33

186. S. Y. Zhao, D. K. Lee, C. W. Kim, H. G. Cha, Y. H. Kim, Y. H. Kang , Bull. Korean Chem. Soc. 27 (2006) 237

187. V. V. Paike, P. S. Niphadkar, V. V. Bokade, P. N. Joshi, J. Am. Ceram. Soc. 90 (2007) 3009

188. A. Falqui, A. Musinu, C. Cannas, D. Peddis, G. Piccaluga, J. Nanopart. Res. 8 (2006) 255

189. S. Bhaduri, S.B. Bhaduri, Ceram. Int. 28 (2008) 153

190. J. Yuan, K. Laubernds, J. Villegas, S. Gomez, S.L. Suib, Adv. Mater.16 (2004) 1729

191. S. L. Brock, M. Sanabria, S.L. Suib, V. Urban, P. Thiyagarajan, D.I. Potter, J. Phys. Chem. B 103(1999) 7416

192. S. L. Brock, N.G. Duan, ZR Tian, O. Giraldo, H. Zhou, S.L. Suib, Chem. Mater. 10 (1998) 2619

193. Li Qin, L. Yunhai, C. Xiaohong, P. Cui, J. Radioanal. Nucl. Chem. 293 (2012) 67

194. Y. Zheng-ji and Y. Jun, J. Radioanal. Nucl. Chem. 293 (2012) 907

195. H. Faghihian, S. Peyvandi, J. Radioanal. Nucl. Chem. 293 (2012) 783

196. W. Xiaoliang, P. Guowen, Y. Yan, Y. Wang, H. Tingting, J. Radioanal. Nucl. Chem. 291 (2012) 825

197. M. Konstantinou, I. Pashalidis, J. Radioanal. Nucl. Chem. 273 (2007) 549

198. Z. Hongxia, Y. Chao, T. Zuyi, J. Radioanal. Nucl. Chem. 279 (2007) 317

199. M. H. Baik, S.P. Hyun, P.S. Hahn, J. Radioanal. Nucl. Chem. 256 (2003) 11

200. S. Chandramouleeswaran, J. Ramkumar, V. Sudarsan, A.V.R. Reddy, J. Hazard. Mater. 198 (2011) 159

201. M.M. Saeed, A. Rusheed, N. Ahmed, J. Radioanal. Nucl. Chem. 211 (2005) 283

202. G. Atun, A. Kilislioglu, J. Radioanal. Nucl. Chem. 258 (2003) 605

203. K.M. Abd El-Rahman, A.M. El-Kamash, M.R. El-Sourougy, N.M. Abdel-Moniem , J. Radioanal. Nucl. Chem. 268 (2006) 221

204. D. Nayak, S. Lahiri, J. Radioanal. Nucl. Chem. 267(2006) 59

205. W.H. Zou, L. Zhao, L. Zhu, J. Radioanal. Nucl. Chem. 292(2012) 1303

206. J.C.Y. Ng, W.H. Cheung, G. McKay,J. Colloid. Interface. Sci. 255 (2002) 64

207. F.Gimbert, N. Morin-Crini, F Renault, P.M. Badot, G. Crini, J. Hazard. Mater. 157 (2008) 34

208. T. Shih-Chin, J. Kai-Wei, J. Radioanal. Nucl. Chem. 243 (2000) 741

209. M. I. Ojovan, W. E. Lee, An introduction to nuclear waste immobilization, Elsevier (2005) 315

210. M.I. Ojovan, W.E. Lee, New developments in glassy nuclear waste forms, Nova Science Pub Inc. (2007) 131

211. International Atomic Energy Agency, IAEA-TECDOC-1563 (2007) IAEA Vienna, 29

212. International Atomic Energy Agency, Technical Reports Series No. 339 (1992) 50

213. International Atomic Energy Agency, IAEA-TECDOC-1208 (2001) 25

214. P. Sengupta, C.P. Kaushik, G.K. Dey, Immobilization of High-level nuclear wastes: The Indian Scenario, On a Sustainable Future of the Earth's Natural Resources: Editor M. Ramkumar, Springer-Verlag (2013) 25

215. P. Sengupta, J. Hazard. Mater. 235-236 (2012) 17

216. P. Sengupta, S. Fanara, S. Chakraborty, J. Hazard. Mater. 190 (2011) 229

217. R.K. Mishra, P. Sengupta, C.P. Kaushik, A.K. Tyagi, G.B. Kale, K. Raj, J. Nucl. Mater. 360 (2007) 143

218. C.P. Kaushik, R.K. Mishra, P. Sengupta, A. Kumar, D. Das, G.B. Kale, K. Raj, J. Nucl. Mater. 358 (2006) 129

219. A.E. Ringwood, S.E. Kesson, N.G. Ware, W. Hibberson, A. Major, Nature 278 (1979) 219

220. I.W. Donald, B.L. Metcalfe, R.N.J. Taylor, J. Mater. Sci. 32 (1997) 5851

221. R.C. Ewing, L.M. Wang, Rev. Miner. Geochem. 48 (2002) 673

222. W.E. Lee, M.I. Ojovan, M.C. Stennett, Adv. Appl. Ceram. 105 (2006) 3

223. R.K. Mishra, V. Sudarsan, P. Sengupta, R.K. Vatsa, A.K. Tyagi, C.P. Kaushik, D. Das, K. Raj, J. Am. Ceram. Soc. 91 (2008) 3903

224. N. Das, P. Sengupta, S. Roychowdhury, G. Sharma, P.S. Gawde, A. Arya, V. Kain, U.D. Kulkarni, J.K. Chakravartty, G.K. Dey, J. Nucl. Mater. 420 (2012) 559

225. P. Sengupta, J. Nucl. Mater. 411 (2011) 181

226. P. Sengupta, P.S. Gawde, K. Bhanumurthy, G.B. Kale, J. Nucl. Mater. 325 (2004) 180

227. R.S. Dutta, C. Yusufali, B.Paul, S. Majumdar, P. Sengupta, R.K. Mishra, C.P. Kaushik, R.J. Kshirsagar, U.D. Kulkarni, G.K. Dey, J. Nucl. Mater. 432 (2013) 72

228. P. Sengupta, D. Rogalla, H.W. Becker, G.K. Dey, S. Chakraborty, J. Hazard. Mater. 208(2011)

229. P.S. Mahadik, P. Sengupta, R. Halder, G. Abraham, G.K. Dey, J. Hazard. Mater. 287 (2015) 207

230. N.P. Qafoku, O. Qafoku, C.C. Ainsworth, A. Dohnalkova, S.G. McKinley, Appl. Geochem. 22 (2007) 2054

231. T.J. Yasunari, A. Stohl, R.S. Hayano, J.F. Burkhart, S. Eckhardt, T. Yasunari Proc. Natl. Acad. Sci. USA 108(2011) 19530

232. K.O. Buesseler, S.R. Jayne, N.S. Fishr, II. Rypina, H. Baumann, Z. Baumann, C.F. Breier, E.M. Douglas, J. George, A.M. Macdonald, H. Miyamoto, J. Nishikawa, S.M. Pike, S. Yoshida Proc. Natl. Acad. Sci. USA 109 (2012) 5984

233. N. Krishna Rao, and G.V.U Rao, Journal of Geological Society of India, 21 (1980) 387

234. N. Krishna Rao, G.V.U. Rao, and S.K Aggarwal, Journal of Geological Society of India, 20 (1979) 124

235. C. Tournassat, C. Lerouge, P Blanc, J Brendle, J.M. Greneche, S. Touzelet, E.C. Gaucher, Appl. Geochemistry 23 (2008) 641

236. T.M. Petrova, L. Fachikov, J. Hristov, Inter. Rev. Chem. Engg. 3 (2011) 134

237. F. Huber, D. Schild, T. Vitova, J. Rothe, R Krisch, T. Schäfer, Geochim. Cosmochim. Acta. 96 (2012) 154

238. D. Das, M.K. Suresh Kumar, S. Koley, N. Mithal, C.G.S. Pillai, J. Radioanal. Nucl. Chem. 285 (2010) 447

239. A. D. Ebner, J.A. Ritter, J.D. Navratil, Ind. Eng. Chem. Res. 40 (2001) 1615

240. P. Thammawong, P. Opaprakasit, P.Tangboriboonrat, Sreearunothai, J. Nanopart. Res. 1516989(2013) 1

241. T.A. Marshall, K. Morris, G.T.W. Law, J.F.W. Mosselmans, P. Bots, S.A. Parry, S. Shaw, Environ. Sci. Technol. 48 (2014) 11853

242. J.D. Pablo, M. Rovira, J. Gimenez, I. Casas, F. Clarens, RW Grimes, J.W. Roberts, N.C. Hyatt, W.E. Lee, Book on Magnetite sorption capacity for strontium as function of pH, Scientific Basis for Nuclear Waste Management XXXI, Eds 1107 (2007)

243. Thorsten Schäfer, F Huber, H seher, T Missana, U Alonso, M. Kumke, S Eidner, F. Claret, F. Enzmann Appl. Geochemistry 27 (2012) 390

244. W. Wu, Q. He, C. Jiang, Nanoscale. Res. Lett. 3 (2008) 397

245. R Fu, X Jin, J Liang, W. Zheng, J Zhuang, W Yang, J. Mater. Chem. 21 (2011) 15352

246. W. Wu, Q. He, C. Jiang, Nanoscale. Res. Lett. 3 (2008) 397

247. S. Sun and H. Zeng, J. Am. Chem. Soc. 124 (2002) 8204

248. J. Teixeira, J. Appl. Cryst. 21 (1988) 781

249. O. Togawa, P.P. Povinec, H.B.L. Pettersson, Sci. Total Environ. 237/238 (1999) 241

250 Q. Qin, Q. Wang, D. Fu, & J. Ma, Chem. Eng. J. 172 (2011) 68

251. M. Hua, S. Zhang, B. Pan, W. Zhang, ,L. Lv & Q. Zhang, J. Hazard. Mater. 211–212(2012) 317

252. Vejsada, Appl. Radiat. Isotopes 64 (2006) 1538

253. T. Missana, M. Garcia-Gutierrez, U. Alonso, Phys. Chem. Earth 33 (2008) S156

254. N.V. Elizondo, E. Ballesteros, B.I. Kharisov, Appl. Radiat. Isot. 52 (2000) 27

255. Lalhmunsiama, C.Lalhriatpuia, , D.Tiwari, S.M. Lee, App. Surface Science 321 (2014) 275

256. Y.Park, W. S.Shin & S.-J.Choi, J. Radioanal. Nucl. Chem. 292 (2012) 837

257. Jamal AlAbdullah,Abdul G.Al Lafi ,Wafa'aAl Masri,Yusr Amin &Tasneem Alnama, Water Air Soil Pollut. 227 (2016) 241

258. D.Armin, James Ebner, A.Ritter and James D. Navratil, Ind. Eng. Chem. Res. 40 (2001) 1615

259. Jean-Philippe Bellenger, Siobhan Staunton, J. Environ. Radioact. 99 (2008) 831

260. O.I. Pendelyuk, T.V. Lisnycha, V.V. Strelko, S.A. Kirillov, Adsorption 11 (2005) 799

261. M. Cielslak-Golonka , Polyhedron, 15 (1995) 3667

262. Z. Kowalski, J. Hazard. Mater. 37(1994) 137

263. Document of USHHS (United States Department of Health and Human Services)(1991)

264. Document of USEPA (United States Environmental protection Agency) (2003)

265. B. A Shah, A. V. Shah, R. R. Singh Int. J. Environ. Sci. and Tech. 6 (2009) 77

266. S.Q. Zhao, L.J. Da, Z.Y. Tang, H.J. Fang, K. Song, J.Y. Fang, Frontier in Eco. Environ. 4 (2006) 341

267. R.L. Droste, Theory and practice of water and wastewater treatment ,John Wiley & Sons, New York (1997)

268. I. Ali, C.K. Jain, Water Encyclopedia: Domestic, municipal, and industrial water supply and waste disposal, ed. J. Lehr, John Wiley & Sons, New York (2005)

269. A. Nezamzadeh-Ejhieh, S. Hushmandrad, Appl. Catal. A: Gen. 388 (2010) 149

270. A. Nezamzadeh-Ejhieh, S. Hushmandrad, Appl. Catal. A: Gen. 477 (2014) 83

271. M. Karimi-Shamsabadi, A. Nezamzadeh-Ejhieh, J. Mol. Catal. A: Chem. 418 (2016) 103

272. A. Nezamzadeh-Ejhieh, M. Karimi-Shamsabadi, Chem. Eng. J. 228 (2013) 631

273. F.L. Slejko, Adsorption Technology, Marcel Dekker, New York, (1985)

274. I. Ali, V. K. Gupta, Nature Protocols 1 (2007) 2661

275. M. M. Rao, D. H. Reddy, P. Venkateswarlu, K. Seshaiah, J Environ. Manage. 90 (2009) 634

276. V. K. Gupta, Suhas. J, Environ. Manage. 90 (2009) 2313

277. M. Ahmaruzzaman, V. K. Gupta, Ind. Eng. Chem. Res. 50 (2011) 13589

278. G. Crini, Bioresource Tech. 97 (2006) 1061

279. S. M. Maliyekkal, A. K. Sharma, L. Philip, Water Res. 40 (2006) 3497

280. I. Ali, Chem. Rev. 112 (2012) 5073

281. S. Dashamiri, M. Ghaedi, K. Dashtian, M. R. Rahimi, A. Goudarzi, R. Jannesar, Ultrason. Sonochem. 31 (2016) 546

282. M. Jamshidi, M. Ghaedi, K. Dashtian, S. Hajati, A.A. Bazrafshan, Asson. Confirro. Sonochem 32 (2016) 119

283. F. Nasiri Azad, M. Ghaedi, K. Dashtian, S. Hajati, A. Goudarzi and M. Jamshidi, New J. Chem. 39 (2015) 7998

284. M. Roosta, M. Ghaedi, F. Yousefi, , RSC Adv. 5 (2015) 100129

285. A. A. Bazrafshan, S. Hajati and M. Ghaedi, RSC Adv. 5 (2015) 79119

286. D. P. Dutta, A. Mathur, J. Ramkumar, A. K. Tyagi, RSC Adv. 4 (2014) 37027

287. A. Singh, D. P. Dutta, J. Ramkumar, K. Bhattacharya, A. K. Tyagi, M. H. Fulekar, RSC Adv. 3 (2013) 22580

288. D. P. Dutta, A. Rathore, A. Ballal, A. K. Tyagi, RSC Adv. 5 (2015) 94866

289. J. H. Bi, L. Wu, Y. F. Zhang, Z. H. Li, J. Q. Li, X. Z. Fu, Appl. Catal. B Environ. 91 (2009) 135

290. M. Anicete-Santos, E. Orhan, M.A. de Maurera, L.G.P. Simões, A.G.Souza, P.S. Pizani, E.R. Leite, J.A.Varela, J. Andrés, A. Beltrán, E. Longo, Phys. Rev. B 75 (2007) 165105

291. Y. S. Luo, W. D. Zhang, X. J. Dai, Y. Yang, S. Y. Fu, J. Phys. Chem. C 113 (2009) 4856

292. J.C. Sczancoski, L.S. Cavalcante, M.R. Joya, J.A. Varela, P.S. Pizani, E. Longo, Chem. Eng. J. 140 (2008) 632

293. H. T. Shi, L. M. Qi, J. M. Ma, N. Z. Wu, Adv. Funct. Mater. 15 (2005) 442

294. J. C. Sharma, A. Vijay, S. Bhardwaj, World Appl. Sci. J. 23 (2013) 208

295. H. Lee, S. H. Park, Young-K. Park, B. H. Kim, Sun-J. Kim, Sang-C. Jung, Chem. Central J. 7 (2013) 156

296. M. Rafatullah, O. Sulaiman, R. Hashim, A. Ahmad, J. Hazard. Mater 177 (2010) 70

297. G. R. Calle, I. T. Vargas, M. A. Alsina, P. A. Pastén, and G. E. Pizarro, Env. Sci. Tech, 41 (2007) 7430

298. M. Manolopoulou, E. Vagena, S. Stoulos, A. Ioannodou, C. Papastefanou, J. Environ. Radioact. 102 (2011) 796

299. Liang-D. Feng, Xi-B. Chen, Chang-J. Mao, Mater. Lett. 64 (2010) 2420

300. Z. Xia, Q. Xue, K. Zhang, H. Zhang, T. He, J Mater. Sci. Mater Electron 26 (2015) 8078

301. Chang-J. Mao, J. Geng, Xing-C. Wu, Jun-J. Zhu, , J. Phys. Chem. C 114 (2010) 1982

302. J. Wang, Zhi-J. Zhang, Jing-T. Zhao, Hao-H. Chen, Xin-X. Yang, Y. Tao, Y. Huang, J. Mater. Chem. 20 (2010) 10894

303. A. M. Kaczmarek, K. Van Hecke, R. Van Deun, Inorg. Chem. 53 (2014) 9498

304. X. Liu, Y. Cheng, E. Liang, M. Chao, Phys. Chem. Chem. Phys. 16 (2014) 12848

305. S. Woislawski, J. Am. Chem. Soc. 75 (1953) 5201

306. R. W. Ramette, E. B. Sandell, Rhodamine B equilibria, J. Am. Chem. Soc. 78 (1956) 4872

307. S. Merouani, O. Hamdaoui, F. Saoudi, M. Chiha, Chem. Eng. J. 158 (2010) 550

308. A. K. Patra, A. Dutta, A. Bhaumik, J. Hazard. Mater. 201- 202 (2012) 170

309. A. S. Madden, M. F. Hochella, T. P. Luxton, Geochim. Cosmochim. Acta 70 (2006) 4095

310. J. Xia, L. X. Song, W. Liu, Y. Teng, Q. S. Wang, L. Zhao, M.M. Ruan, RSC Adv. 5 (2015) 12015

311. Y. S. Ho, J. Hazard. Mater. B136 (2006) 681

312. M. Heidari-Chaleshtori, A. Nezamzadeh-Ejhieh, New J. Chem. 39 (2015) 9396

313. M. Anari-Anaraki, A. Nezamzadeh-Ejhieh, J. Coll. Inter. Sci. 440 (2015) 272

314. W. J. Weber, J. C. Morris, J. Sanit. Eng. Div., Am. Soc. Civ. Eng. 89 (1963) 31

315. L. D. Michelson, P. G. Gideon, E. G. Pace, L. H .Kutal, US Department Industry, Water Res Tech Bull. 74 (1975)

316. L.S. Cavalcante, J.C. Sczancoski, N.C. Batista, E. Longo, J.A. Varela, M.O. Orlandi, Adv. Powder Tech. 24 (2013) 344

317. Chang-J. Mao, J. Geng, Xing-C. Wu, Jun-J. Zhu, J. Phys. Chem. C 114 (2010) 1982

318. R. V. Deun, D. Ndagsi, J. Liu, I. V. Driessche, K. V. Hecke, A. M. Kaczmarek, Dalton Trans. 44 (2015) 15022

319. S. Laufer, S. Strobel, T. Schleid, J. Cybinska, Anja-V. Mudring, I. Hartenbach, New J. Chem. 37 (2013) 1919

320. Y. Wan, X. Wang, Y. Gua, L. Guo, Z. Xu, Appl. Surf. Sci. 366 (2016) 59

321. J. J. Uhlrich, J. Sainio, Y. Lei, D. Edwards, R. Davies, M. Bowker, S. Shaikhutdinov, H.-Freund, Surf. Sci. 605 (2011) 1550

322. L. Pan, J. J. Zou, X. W. Zhang, L. Wang, J. Am. Chem. Soc. 133 (2011) 10000